Title	Pillar Design in Jointed Shallow Room-and-Pillar Hard Rock Mines
Author(s)	Dzimunya, Nevaid Zvikomborero
Degree Grantor	北海道大学
Degree Name	博士(工学)
Dissertation Number	甲第16355号
Issue Date	2025-03-25
DOI	https://doi.org/10.14943/doctoral.k16355
Doc URL	https://hdl.handle.net/2115/95081
Type	doctoral thesis
File Information	Nevaid_Zvikomborero_Dzimunya.pdf

Pillar Design in Jointed Shallow Room-and-Pillar Hard Rock Mines

A dissertation submitted in partial fulfillment of the requirements for the degree of
Doctor of Philosophy in Engineering

By

Nevaid Zvikomborero DZIMUNYA

Supervisor: Prof. Yoshiaki FUJII

Laboratory of Global Resources and Environmental Systems
Division of Sustainable Resources Engineering
Graduate School of Engineering
Hokkaido University

March 2025

ACKNOWLEDGEMENTS

I want to express my heartfelt gratitude to all those who have supported me throughout my PhD journey.

First and foremost, I would like to thank my main supervisor, Professor Yoshiaki FUJII, for his unwavering guidance, insightful feedback, and constant encouragement. Your expertise and dedication have been invaluable in shaping my research. This research would not have been successful without your immense knowledge and input, particularly the NUTEX numerical simulation code. I remain grateful to him.

I am also deeply grateful to Professor Junichi KODAMA for granting me access to essential software and for your invaluable feedback during evaluations. Your support during my field trip to Zimbabwe greatly enhanced my research experience, and I am thankful for the time we spent together in the field. My sincere appreciation goes to Professor Daisuke FUKUDA for your motivational words and encouragement. Your belief in my abilities inspired me to push through challenges.

I would like to extend my gratitude to the Japan International Cooperation Agency (JICA) under the Human Resources Development in the Mining Sector Program (KIZUNA program) for supporting this research and sponsoring my PhD studies at Hokkaido University. This opportunity has been transformative, and I am deeply appreciative of your support. I also express my deepest gratitude to the management of the hard rock PGM Mine in Zimbabwe for allowing their mine to be used as a research site.

To my colleagues in the Laboratory of Global Resources and Environmental Systems and the Rock Mechanics Laboratory, thank you for creating such a collaborative and inspiring research environment. Your camaraderie made the journey not only productive but also enjoyable.

To my family, thank you for your unwavering prayers and encouragement. To my wife, Lindy, and my children, Elisheba and Meek, your love and support have been my anchor throughout this journey. I could not have done this without you.

I would also like to thank Mr. O. Mapengo, Omberai Mandingaisa, Luke Mukomberi, Vincent Shamu, and Joseph Dzingirai for your special contributions to my success over the past three years. Your assistance and friendship have been pivotal.

Finally, I am grateful to the authors whose ideas have informed my work. Your research laid the groundwork for my own, and I am honoured to build upon your contributions.

Thank you all for being a part of this incredible journey.

ABSTRACT

This dissertation addressed three research gaps related to pillar stress estimation, pillar strength determination, and regional support design in shallow hard rock room-and-pillar mines. Firstly, a multi-layer perceptron neural network (MLPNN) was applied to predict the vertical loads of regular pillars more accurately. Hundreds of room-and-pillar mine layouts were modelled using a displacement discontinuity method (DDM), and a database of 2355 sampled pillar cases was compiled. The MLPNN was trained based on this database, and its prediction capabilities were further validated using simulations by a finite difference code (i.e., FLAC3D). The model predictions and the FLAC3D simulations reasonably agreed with a regression coefficient of 0.99. The model was also adapted for mine cases with evenly spaced barrier pillars, and its application to a real case study mine has shown to provide accurate pillar stress estimations; hence, this model is suitable for practical use at mines. Even though the MLPNN model cannot be universally applied to all mine situations, it appears to be a significant improvement over existing analytical techniques in terms of accounting for the influence of abutments on pillar stresses. Secondly, a framework was proposed to estimate pillar strength based on ongoing pillar mapping, risk management decision making, numerical modelling, and analytical hierarchy process. The framework has the potential to be universally applicable, user-friendly, and customisable for each mine's specific characteristics, allowing for ongoing monitoring. Lastly, guidelines for barrier pillars are limited and rely mainly on ambiguous rules of thumb. To improve this, the last part of the dissertation presents a new linear model for estimating the spacing of barrier pillars by using large-scale numerical simulations and multivariate regression analysis. The simple linear model, which depends on mining depth and extraction ratio, was confirmed using the case study of a hard rock room-and-pillar mine and an arbitrary hypothetical mine. Its application proved to provide adequate regional mine support and enhanced stiffness of the entire pillar systems. Additionally, the model was compared to the rules of thumb. This method is an improvement over the rules of thumb, which may result in ore sterilisation and unreliable designs in certain circumstances.

TABLE OF CONTENTS

LIST OF FIGURES

LIST OF TABLES

CHAPTER 1 INTRODUCTION

1.1 Background

Hard rock tabular ore bodies situated at depths of no more than 600 m are frequently mined using the room-and-pillar mining technique. The room-and-pillar mining method is one of the most vital underground ore extraction methods in practice today. In this method, non-yield pillars are systematically left in situ to support the overburden weight of the overlying rock mass. The need for using pillars is dictated by prevailing rock mechanics at shallow depths, such as the large tensile stresses in the hangingwall and geological weaknesses in the hangingwall rockmass (Ozbay et al., 1995).

Designing non-yield pillar systems for shallow hard rock room-and-pillar mines has always been a challenging task. If the rooms and pillars are not designed carefully, it can compromise safety or lead to sterilisation of the ore reserves. Therefore, pillar design optimises both the minimal ore left underground and the overall mine stability. Pillar instabilities pose significant threats to operating and abandoned mines. Despite the numerous research outcomes, pillar failures still occur in underground room-and-pillar mines. The literature contains documented examples of such failures and their consequences (Cui et al., 2014; Esterhuizen et al., 2006, 2019; Malan, 2012; Ozbay et al., 1995). Since this relates both to yields and safety, mine engineers and researchers have always seen this as a topic of prime interest.

The challenges associated with designing pillars, and the occurrence of local and large-scale pillar failures highlight the need for ongoing research. The design of room-and-pillar mines involves multiple aspects that can be examined. The present study focuses on addressing research gaps related to estimating pillar stress, determining pillar strength, and designing regional support. The background and the necessity for further research in each of these areas are discussed individually as follows:

Pillar stress

In pillar design, the factor of safety (FoS) is a routine indicator for assessing pillar stability. FoS is the ratio between the pillar strength and the vertical stress acting on that pillar. The calculation of

FoS implies that the average vertical pillar stress and pillar strength must be known. In room-and-pillar mines, pillar stress is customarily determined using the tributary area theory (TAT), pressure arch theory (PAT), or numerical modelling. Recently, a quadratic equation was also developed to estimate pillar stresses considering the relative extraction ratio (Hauquin et al., 2016). On the other hand, computing the actual pillar strength is also a challenging task due to scale effects and other influencing parameters such as in-situ stress, geometry of pillars, rock mass quality and variation in rock types (Wang & Cai, 2021).

TAT assumes that the overburden load is evenly distributed and equally shared among the pillars (Brady & Brown, 2004; Hedley & Grant, 1972; Salamon & Munro, 1967). This method does not consider the influence of nearby abutments, and it is well-known to overestimate pillar stresses, especially for narrow mine panel widths (Wagner, 1980; Wagner et al., 2016). PAT assumes that a pressure arch is formed between the abutments and that most of the pillar loads are carried by these abutments. The method uses an averaged extraction ratio over several pillars, and as a result, it generally underestimates pillar stresses around an average value (Hauquin et al., 2016). Applications and modifications of PAT are available (Abel, 1988; Poulsen, 2010), and the dependence of the method on a parameter called the load transfer distance makes its application uncertain in hard rocks because this parameter was calibrated in sedimentary coal seams.

On the other hand, the quadratic equation assumes that a portion of the overburden load is transferred to pillars and abutments that support the remainder. Despite the model's better performance over TAT and PAT in general mine conditions, it did not give accurate pillar stresses within approximately 72 m from the abutments, indicating the need for a method that captures the influence of abutments on pillar stresses.

Numerical modelling remains the only tool that can accurately evaluate the dependability of pillar stresses analytically. However, the main challenge of numerical tools is that they require significant time and expertise, which is generally not readily available at mines in practice (Potvin, 2017; Sweby et al., 2016). Furthermore, numerical modelling is not very convenient for routine stress analysis work in a typical mining environment where highly variable ground control districts (geotechnical zones) are regularly encountered, prompting frequent changes to extraction ratios and pillar outlines. As a result, design engineers at mine sites recurrently use the TAT despite the availability of numerical tools. However, this technique is conservative and cannot incorporate the influence of abutments into pillar stresses. Consequently, TAT remains the most used technique because it is simple, and it tends to make mine constructions safer by overestimating pillar stresses.

Pillar strength

Designing non-yield pillar systems for shallow hard rock room-and-pillar mines has always been a challenging task. It is important to know the stress distribution in the pillar and the strength of the pillar so that a sound design be produced. Due to the significance of these parameters, extensive research has been conducted on the strength of pillars in hard rocks.

For many years, the strength of pillars has been evaluated using empirical methods or numerical modelling. Empirical formulae are popular in the mining industry due to their simplicity. A series of historic pillar strength research studies and empirical formulae are summarised in Martin and Maybee (2000). Two classic pillar strength formulae used in hard rocks and metal mines are Hedley and Grant (1972), and Lunder and Pakalnis (1997). While empirical equations are typically used to estimate pillar strength, numerical methods are also preferred among practising rock engineers in the mining industry for pillar strength and stress estimation. Recently, several researchers have established that numerical methods are reliable techniques for estimating pillar strength in underground mines (Elmo et al., 2021; Jessu & Spearing, 2019; Monsalve et al., 2020; Rafiei-Renani & Martin, 2018). Numerical modelling has not only enabled more realistic estimates of pillar strength but has also allowed researchers to model complex pillar behaviours and compare the modelling capabilities of different constitutive relationships (Mortazavi et al., 2009; Sinha & Walton, 2018; Walton et al., 2015).

An acceptable estimation of pillar strength using the empirical and numerical methods previously mentioned is to ensure that this strength always exceeds the estimated pillar stress by an appropriate FoS. However, in a typical underground mine, many pillars are formed and variations in pillar strength are inevitable due to different geological and rock mass conditions inside the mining lease. The fact that pillars are usually not formed according to their design specifications due to the difficulties in controlling blasting further exacerbates this issue. As a result, the true characteristics of a given pillar can only be known when it has been formed. Even though the initial design using either numerical modelling or empirical formulae may predict stable pillars, uncertainties are always present and unstable pillars will be encountered in reality (Alejano et al., 2017). It is critical to also estimate the strength of a pillar after it has been excavated. In this regard, empirical methods are limited because they are derived from site-specific conditions and cannot be extrapolated beyond the range of the databases used to derive them. In practice, the strength of many pillars will have to be estimated. Numerical methods, despite their capabilities, may not be convenient in a typical mine environment where solutions are urgently demanded because of production pressures. As a result, additional tools that are easy to use are needed to complement numerical methods.

Alejano et al. (2017) mentioned that: "*Practical experience and recent literature, nevertheless, illustrate the shortcomings of empirical and numerical design approaches. Ongoing monitoring of pillars is therefore recommended to minimise the risk associated with these designs*." This underlines the need for complementary pillar strength estimation tools as previously mentioned. Ideally, such tools must be universally applicable by considering the site-specific characteristics of each mine. Jessu et al. (2022) proposed a methodology that begins with using a suitable empirical formula to estimate the strength of the pillar and adjusting it by applying corrections for pillar inclination, blast damage, and the presence of an adverse discontinuity. However, this methodology only considers three parameters for adjustment and, according to the authors, was developed using a limited range of pillar width-to-height (*w:h*) ratios.

Regional support

Instabilities of pillars in room-and-pillar mines, both active and abandoned, are a serious hazard. When pillars fail, the induced displacements of the rock mass can cause damage to mining operations or surface structures due to subsidence. Pillars can fail suddenly if their strength is exceeded by the stress imposed on them or they can fail slowly due to the creep effect that causes structural deterioration. In hard rock room-and-pillar mines, geological alterations and weak layers in the reef can cause large-scale pillar collapses (Couto & Malan, 2023b). These geological alterations have a damaging effect on the strength of pillars and the overall stability of the mines. Couto and Malan (2023a) documented large-scale pillar collapses caused by weak alterations in South African mines. Similarly, an extended collapse in a large-scale mine on the Great Dyke of Zimbabwe was caused by a sub-horizontal mylonitic shear structure with soft infilling that affected the entire failed region (Mushangwe, 2018). Case studies of large-scale pillar collapses have been extensively studied, and there are documented examples of such failures and their consequences as previously cited.

To enhance the strength of deteriorating pillars and prevent individual failures, strapping pillars with cables is a useful technique (Alejano et al., 2017). On the other hand, to prevent large-scale pillar failures, small in-panel pillars are combined with evenly spaced lines of bigger barrier pillars. Barrier pillars are essential for mitigating risks and improving the structural integrity of mining operations with geological difficulties such as shear zones or weak alteration layers.

Extensive research has been conducted on the design of in-panel pillars. While many studies have focused on designing the in-panel pillars, the barrier pillars are not universally used, and their design procedures are not clearly defined. Mine sites often rely on ambiguous rules of thumb to design barrier pillars (Ozbay et al., 1995; Ryder & Ozbay, 1990). When designing these pillars, it is essential to consider their strength and the distance between them, known — in this dissertation — as inter-barrier pillar spacing (*IBS*). Designing *IBS* involves understanding how abutments affect load transfer in the pillar system. Abel (1988) introduced a parameter called the load transfer distance, which is the maximum distance any stress can be laterally transferred. Poulsen (2010) presents further discussion and application of this parameter. Though this parameter was developed from a sedimentary rock database, its concepts are fundamental to understanding and improving the design of *IBS*.

Despite the availability and superiority of numerical modelling, mine sites predominantly rely on rules of thumb to estimate *IBS*. However, for simulating large-scale room-and-pillar outlines, the displacement discontinuity method (DDM) is the most convenient numerical modelling approach. DDM, originally developed by Crouch (1976), is a kind of boundary element method (BEM) solving displacement discontinuity of elements under suitable boundary conditions. Several studies have successfully simulated large-scale pillar outlines using DDM (Couto & Malan, 2023b; Napier & Malan, 2021, 2023; Tuncay et al., 2021).

The ultimate choice of an optimum *IBS* can be guided by numerical modelling. However, according to Ozbay et al. (1995), the procedure requires modifications of the numerical models to iterate the *IBS*. This must be repeated several times until the optimum *IBS* is obtained. Thus, numerical modelling does not offer simple procedures for designing *IBS* at mine sites where quick solutions are often demanded. Additionally, local geological conditions constantly change resulting in alterations to extraction ratios, and consequently, *IBS* may need continuous updating.

1.2 Problem statement

The current analytical methods for estimating pillar stress in room-and-pillar mining operations often do not adequately consider the influence of abutments. Additionally, there is a lack of universally applicable and user-friendly procedures for estimating pillar strength, which can be customised to the specific characteristics of each mine and used for ongoing monitoring. Furthermore, the reliance on ambiguous rules of thumb for the design of barrier pillar support results in inconsistent practices that may not align with the unique geological and geometrical characteristics of individual mines. This dissertation addresses these gaps by developing techniques for estimating pillar stress and strength, along with designing regional support spacing for room-and-pillar hard rock mines.

1.3 Objectives

The objectives of this research are as follows:

1. To critically appraise the current pillar design procedures referring to room-and-pillar mines operating on the Great Dyke of Zimbabwe.
2. To establish a machine learning model that can integrate the influence of abutments into estimating pillar stress.
3. To propose a universally applicable and user-friendly framework for estimating pillar strength, which can be customised to the specific characteristics of each mine and used for ongoing monitoring.
4. To develop a simple linear model for estimating the spacing of barrier pillars in room-and-pillar design.

1.4 Research outline

Chapter 1 is the introduction and outlines the background information, problem statement, and objectives of the dissertation. Chapter 2 provides a critical presentation of rock mass conditions and pillar design methodologies in Zimbabwe. General principles of pillar design and a discussion to offer better insights into the limitations of current methods and directions for future research are described. In Chapter 3, an artificial neural network (ANN) model for estimating pillar stress is presented. Chapter 4 describes a framework for estimating pillar strength which can be customised to the specific characteristics of each mine and used for ongoing monitoring. Chapter 5 outlines the development of a simple linear model for estimating the spacing of barrier pillars in room-and-pillar mining design. Finally, Chapter 6 is the conclusions. The findings obtained by the research are summarised and the recommendations for future research are proposed.

CHAPTER 2 OVERVIEW OF HARD ROCK PILLAR DESIGN: AN EMPHASIS ON MINES ALONG THE GREAT DYKE OF ZIMBABWE

2.1 Introduction

Mining methods, such as room and pillar, require that pillars be left to act as primary support. This maintains stability as mining proceeds. This method results in permanent or temporary sterilisation of valuable mining ore reserves in the pillars. An economically viable design of the pillars requires minimising the ore left in the pillars. This must be achieved without compromising the requirement of guaranteeing the overall stability of the mine. Therefore, a thorough understanding of the behaviour of pillars and pillar systems is crucial for mine layout design to achieve an orebody's maximum safe and economic potential.

The design of stable pillars in mining is fundamental, not only in the hard rock platinum mines along the Great Dyke of Zimbabwe but throughout the mining industry. It is necessary to predict the behaviour of these underground hard rock pillars, i.e., whether they will remain stable, yield, or burst. Various authors have indicated that the current pillar design methods still have major deficiencies. As a result of these shortcomings, design engineers have largely been conservative when estimating the pillar strength and stress. The consequence of this approach is that valuable ore will be sterilised and become unavailable for production in the future (Kersten, 2019).

The estimation of the strength of hard rock pillars is essential for the success of any room and pillar mining operation. It is nevertheless a challenging task because many factors influence the performance and behaviour of these pillars (Wang & Cai, 2021). These factors include pillar geometry, mining depth, mine geometry, blasting, geology, and rock mass quality. Most empirical equations currently available do not incorporate all these parameters. The Hedley and Grant (1972) equation is the most used formula to estimate pillar strength in Zimbabwe. Pillar stress is typically estimated using TAT.

A large number of research publications and practices on pillar design can be found in the literature. However, this Chapter aims to provide a concise literature review on pillar design and highlight the challenges associated with hard rock pillar design, using mines in Zimbabwe as case studies. The Chapter includes a description of rock mass conditions and pillar design methodologies in Zimbabwe along with the general principles of pillar design. Furthermore, a discussion to offer better insights into the limitations of current methods and future research directions is presented.

2.2 Pillar design approaches and rock mass conditions in Zimbabwe

2.2.1 Pillar design

The Great Dyke is a platinum group metals (PGM) bearing geological feature that runs from north to south direction of Zimbabwe. It is a lopolith made up of mafic and ultramafic rocks. This geological feature is roughly 550 km long and up to 11 km wide and it is second to the Bushveld Complex of South Africa in terms of its PGM resource base. The room-and-pillar mining method is used to extract the shallow-seated tabular deposits. The exploitable reef is universally called the Main Sulphide Zone (MSZ).

To ensure the stability and sustainability of these mining operations, pillar design is a critical step in the operation of the mines. The regional stability of any room-and-pillar mine employing a solid pillar system depends on the principle of each pillar carrying its portion of the overburden weight without failing. The design of these pillars relies on a calculation of the pillar FoS. The principle of the FoS relies on four factors:

- Approximating the vertical stress to be carried by each pillar.
- Correctly estimating the strength of the pillar.
- Incorporating an adequate FoS or probability of failure (Griffiths et al., 2002) into the design. The generally accepted minimum is 1.6 for hard rock mines in Zimbabwe. The choice of a FoS of 1.6 is based on its standard use in South African coal-mine rock engineering and hard-rock mining, as noted by Ozbay et al. (1995). Additionally, Hedley and Grant (1972) recommended a FoS of 1.5 based on their back analysis and pillar performance observations from the Elliot Lake Quirke Mine. Conversely, Ryder and Ozbay (1990) indicated that the FoS in hard rock mines should be selected on a case-by-case basis, advising that values below 1.3 should be avoided unless regional stability requirements are

appropriately established. Given these recommendations and research findings, a FoS of 1.6 or higher is commonly applied in Zimbabwe.

- Monitoring the behaviour of pillars to ensure that they are performing as anticipated, and are carrying the load without spalling, yielding, or failing.

While this writing's nuclei are on pillar design in hard rock mines, it is valuable to scrutinise the development of hard rock pillar design in Zimbabwe. This will highlight the noticeable deficiency of appropriate pillar design techniques for shallow hard rock mines.

Estimating the average pillar stress in Zimbabwe has mostly been done using TAT. Although TAT has been used successfully in these operations, it must be noted that this method gives the upper limit of pillar stress making the designs more conservative. Calculating the pillar strength is the other difficult and complex aspect of pillar design. Pillar strength computations in Zimbabwe have used the same approaches as for mines in South Africa. Following the success of the Salamon and Munro (1967) power-law strength formula for South African coal mines, the shallow hard rock mines in South Africa and Zimbabwe effortlessly embraced a similar power-law formula. Instead of researching to develop a suitable hard rock pillar strength formula, the Headly and Grant (1972) power-law equation was adopted. A reason for the absence of this research at that moment could be attributed to the lack of datasets comprising failed pillar cases from which back analysis studies to develop the equations can be performed. Therefore, in Zimbabwe, the only changes made to this formula were the *K* value to incorporate local rock mass strength conditions. In comparison, commendable efforts to improve the calculation of pillar strength in South African hard rock mines can be seen in several studies (Oates & Malan, 2023; Watson et al., 2021a; Watson et al., 2021b).

The general form of the Hedley and Grant pillar strength formula used in Zimbabwe is illustrated in Eq. 2.1:

$$P_s = K\left(\frac{w^{0.5}}{h^{0.75}}\right), \tag{2.1}$$

where P_s is the pillar strength, *w* is pillar width (m), *h* is the height (m), and *K* is the design rock mass strength which ranges from 20 to 50% of uniaxial compressive strength (UCS) (Stacey & Swart, 2001). Generally, 33% is used in Zimbabwe and UCS values for the mines range between 160 – 220 MPa.

It is prudent to note that empirical design methods are formulated from the statistical evaluation of actual observations. The direct application of these techniques is limited to rock mass conditions similar to the database used to develop the empirical method. Equation 2.1 was originally developed for uranium mines in Canada. The rock mass and pillar conditions within these mines are not like those encountered in Zimbabwe. However, it is common practice in rock engineering design to adopt design criteria, specifically formulated for a particular case, into a unique rock mass condition without questioning the original assumptions. Malan (2012) stated: "*Over time, initial assumptions and interim solutions get entrenched as common practice and the original assumptions are rarely revisited or questioned.*" A critical appraisal of the assumptions made in the original paper by Hedley and Grant was performed by Malan (2012) and is summarised in the following paragraphs to illuminate the point that additional research is required for pillar design.

The original Hedley and Grant equation was developed for slender pillars. This is because the pillars that formed the database were typically 3 – 6 m wide and 2.5 – 6 m high giving *w:h* ratios close to 1 for most of the pillars and only a few pillars (three in the dataset) had a *w:h* ratio of 2.5. It is questionable whether this equation applies to squat pillars with *w:h* ratios greater than 2.5 as in the case of Zimbabwe hard rock mines. The dataset used was very small comprising twenty-eight pillar cases with only five pillars as crushed or partially crashed. The entire process of formulating the Hedley and Grant formula was based on many assumptions, especially the derivation of powers 0.5 and 0.75.

Despite the questionable applicability of the Hedley and Grant formula, this equation has been used in all the platinum mines along the Great Dyke and South African mines (Malan, 2012). In Zimbabwe, no stress-induced pillar collapses have been experienced except for cases in which shear zones existed or other isolated cases of persistent geological structures such as a fault intersecting the pillar.

González-Nicieza et al. (2006) compared several hard rock pillar strength estimation formulae considering a specific case of a 10 m square pillar. In their comparison, pillar strength was illustrated as a function of pillar height for all the formulae. Hedley and Grant's formula furnished average values of pillar strengths considering those calculated by the other formulae. This may be why this equation is popular for calculating pillar strength. Additionally, it is generally understood that the estimates derived from Eq. 2.1 are conservative and design engineers prefer this option as it poses no significant geotechnical risks to their operations. It is also necessary to note that while this equation has been used in Zimbabwe and elsewhere for most pillar designs, several numerical tools have been developed in the same period. Also, suitable failure criteria have been developed and continuously updated but, though being the most reliable, these tools have seldom been used at mine sites (Kersten, 2019; Potvin, 2017; Sweby et al., 2016). This is because numerical tools require time and skill and are not convenient for mine sites where quick solutions are needed to meet ore production targets.

Similar studies have also noted the concerns echoed in this Chapter (Zvarivadza & van der Merwe, 2017). During a feasibility study of a greenfield project along the Great Dyke, the authors utilised several empirical equations to determine the width of square pillars assuming different mining depths. A constant FoS was used, but different results were obtained. The calculations were done to clarify the uncertainties presented using different formulae when designing pillars in narrow reef mines.

A careful and critical study of recent literature on pillar design principles was undertaken in this Chapter. This enabled outstanding gaps to be identified, the details of which will be addressed in Chapters 3 to 5. Additionally, the following Sections illustrate the different rock conditions and geological structures within the PGM mines in Zimbabwe. Numerous geological structures are encountered during mining, and the work presented here is intended to emphasise that an integrated approach is necessary during pillar design in shallow hard rock mines.

2.2.2 Rock mass conditions

Several mines are in operation along the Great Dyke (Fig 2.1). Different geological structures are encountered within the mines. The descriptions below are not exhaustive but were selected to illustrate the typical conditions encountered by these mining operations. Generally, several major geological structures are known to exist in these mines, although these vary from operation to operation. The discussion mainly focuses on a case study mine — the name is withheld to maintain confidentiality — and then concludes with general comments on the remaining mining operations.

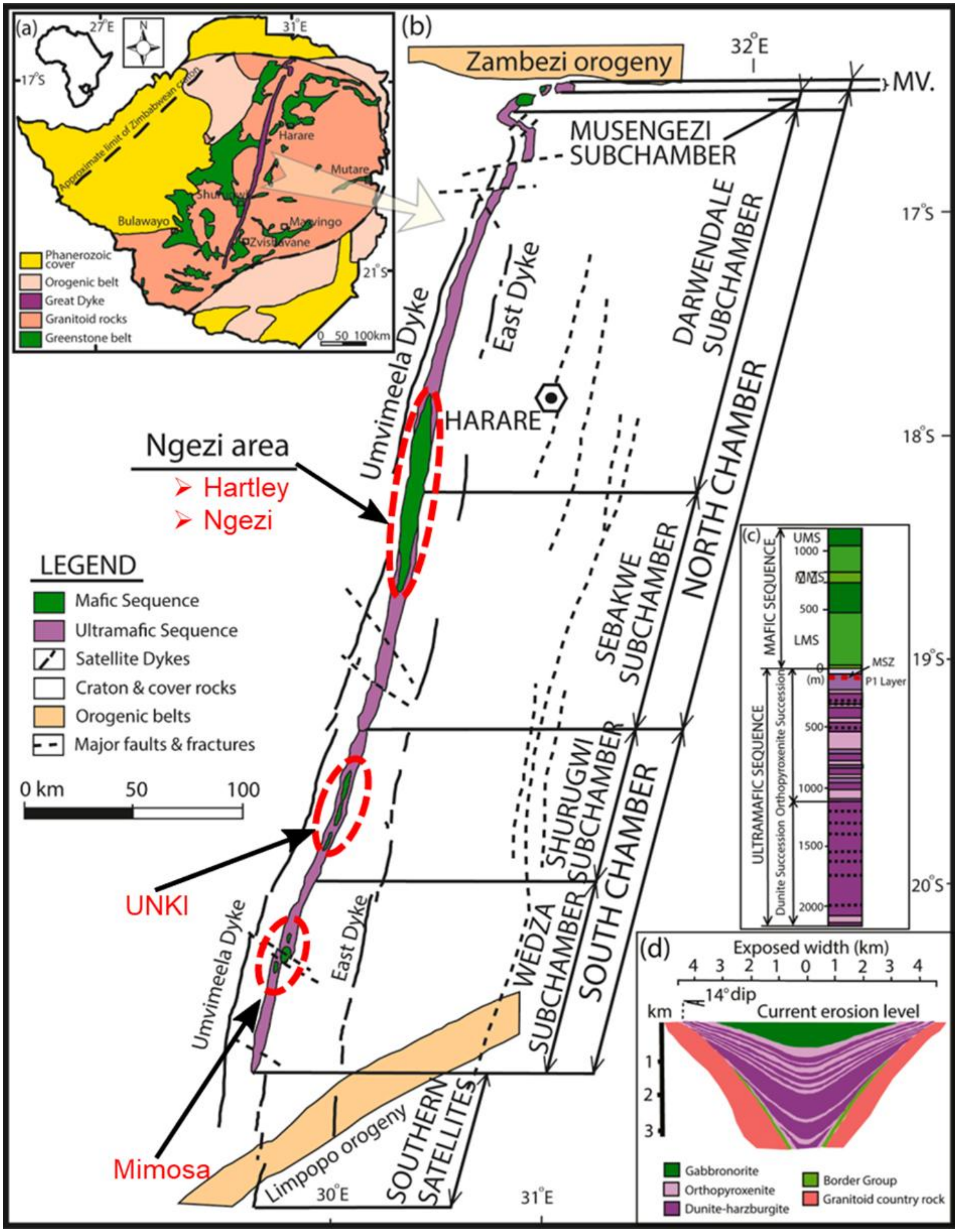

Fig. 2.1 (a) A simplified geology map of Zimbabwe indicating the Zimbabwean Archean craton that was intruded by the Great Dyke, (b) the length and subdivision of the Dyke into chambers and

subchambers, and the position of various mines on the Great Dyke. (c) Vertical section of the Great Dyke into Mafic and Ultramafic sequences, and (d) cross-section of the Great Dyke showing the layering of the synclinal nature of the individual layers of the Ultramafic Sequence and the overlying Mafic Sequence (After Wilson and Prendergast (1989) and extracted from Chaumba (2022)).

Case study mine

The orebody at the case study mine and other mining operations forms a syncline that outcrops on the western and eastern sides of the Great Dyke (Fig. 2.2). At the outcrops, the maximum dip of the orebody is approximately 15° and becomes flat (0°) around the centre of the syncline.

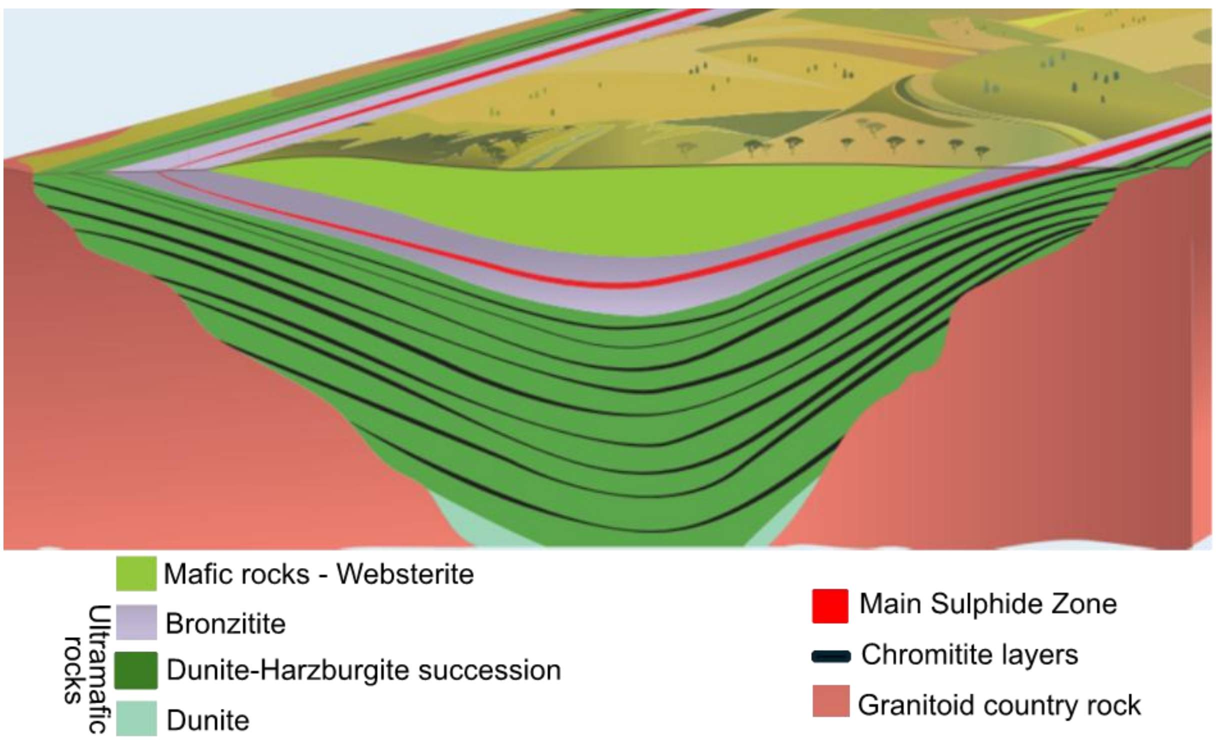

Fig. 2.2 Schematic diagram of the northern portion of the Great Dyke indicating the syncline nature of the orebody (IMPLATS, 2019).

Additionally, the orebody is bound by major normal faults, vertical faults, hanging wall faults and the footwall fault (FwF). These structures produce discontinuities in their vicinity rendering the geology unpredictable and complex. The hanging wall faults usually affect the roof of the stopes, and the FwF is of specific concern to pillar stability. This FwF runs parallel and is in the footwall of the reef. According to the mine reports, this structure is less than 0.75 m thick and occurs roughly between 0.6 and 2.9 m below the base of the MSZ — an arbitrary reference marker horizon of the reef. It is understood that this fault does not cross the base of the MSZ and is a localised feature that only affects the eastern portion of the immediate mining area. However, it is associated with sympathetic faulting and jointing that result in challenging ground conditions particularly where these structures expand into the hanging wall or traverse the pillars (Mandingaisa, 2018). The structure of the FwF consists of highly altered, brecciated and mylonitic plagioclase pyroxenite. Figure 2.3 indicates the position of the FwF relative to the base of the MSZ. Consequently, some pillars at the mine are partly composed of the FwF, jeopardising their strength.

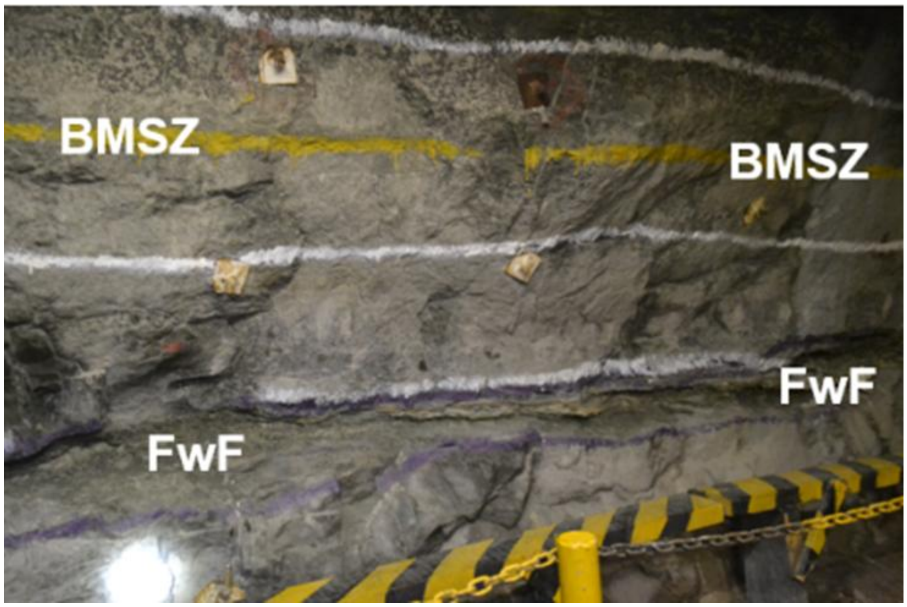

Fig. 2.3 Position of FwF relative to the base of MSZ (Mandingaisa, 2018).

The UCS of the pyroxenite laboratory specimens is high and an average value of 205 MPa is reported and used for design purposes at the mine. Despite this high UCS at the mine, underground observations indicate that the behaviour of pillars is dominated by the geological structures present. Joint sets and spacing are critical in pillar stability at the mine. The rock mass near the reef contains four joint sets (J1, J2, J3, and J4) and other random joints. Most deteriorating pillars at the mine are associated with joint set J1, which consists of low-angled joints with an average dip of 39°. The mine uses the rock mass rating (RMR) system for rock mass characterisation. The rock mass at the mine is of fair to good quality.

To design the pillars at the mine, Eq. 2.1 with a rock mass strength parameter of $K = 0.33 \times UCS$ is used. The mining recovery ratio aims to extract a stope height of 1.9 m and achieve a pillar *w:h* ratio of 3. However, according to the mine reports, the target *w:h* ratio has never been attained due to inherent difficulties in controlling blasting activities, and pillar heights are typically cut over 2 m.

The variation in rock mass quality, pillar geometry, and geological conditions automatically introduces variability in pillar strengths at the mine. The following visuals (extracted from mine reports) show variations in conditions of different pillars at the mine. The strength of these pillars will vary. Figure 2.4 shows examples of pillar cases at the mine. The hybrid pillar conditions depicted in Fig. 2.4 and encountered at the mine pose instability risks. Thus, a robust pillar layout system involving in-panel pillars and evenly spaced barrier pillars is used at the mine to ensure adequate local and regional stability.

Figure 2.4a illustrates an intact pillar with minimum visible discontinuities or adverse geological structures. The previous discussion highlighted an unfavourable J1 joint set observed to significantly weaken pillars. Figure 2.4b is an illustration of a pillar that is affected by this joint set and dip of the reef. Figure 2.4c shows a pillar with FwF almost constituting more than 25% of the pillar. Figure 2.4d also shows a pillar with the FwF material. However, in this illustration, the FwF fault gouge is softer and prone to squeezing. Notably, the conditions depicted in Fig. 2.4 of the FwF in the pillars are exceptions rather than the norm.

Other structural and general rock mass conditions

In some of the other mining operations, muddy infills (up to 40 mm thick) are observed at the roof-pillar contacts. These structures are said to occur in localised faulted areas in some mines along the Great Dyke. The muddy fills generally occur at variable distances from the roof into the hanging wall. They are exposed if they occur at pillar-roof contact and weak material like talc forms part of the infill. When the muddy fill is dry and ground, its texture is soil-like with a slippery feel. This infill material is usually part of flexural slip faults, and its existence is understood to undermine the strength of pillars in South Africa’s Bushveld mines (Malan, 2012). Poor ground conditions are prevalent within the shallowest portions of the deposits. These portions have the steepest dips, and the pillars designed in these areas pose the most stability challenges.

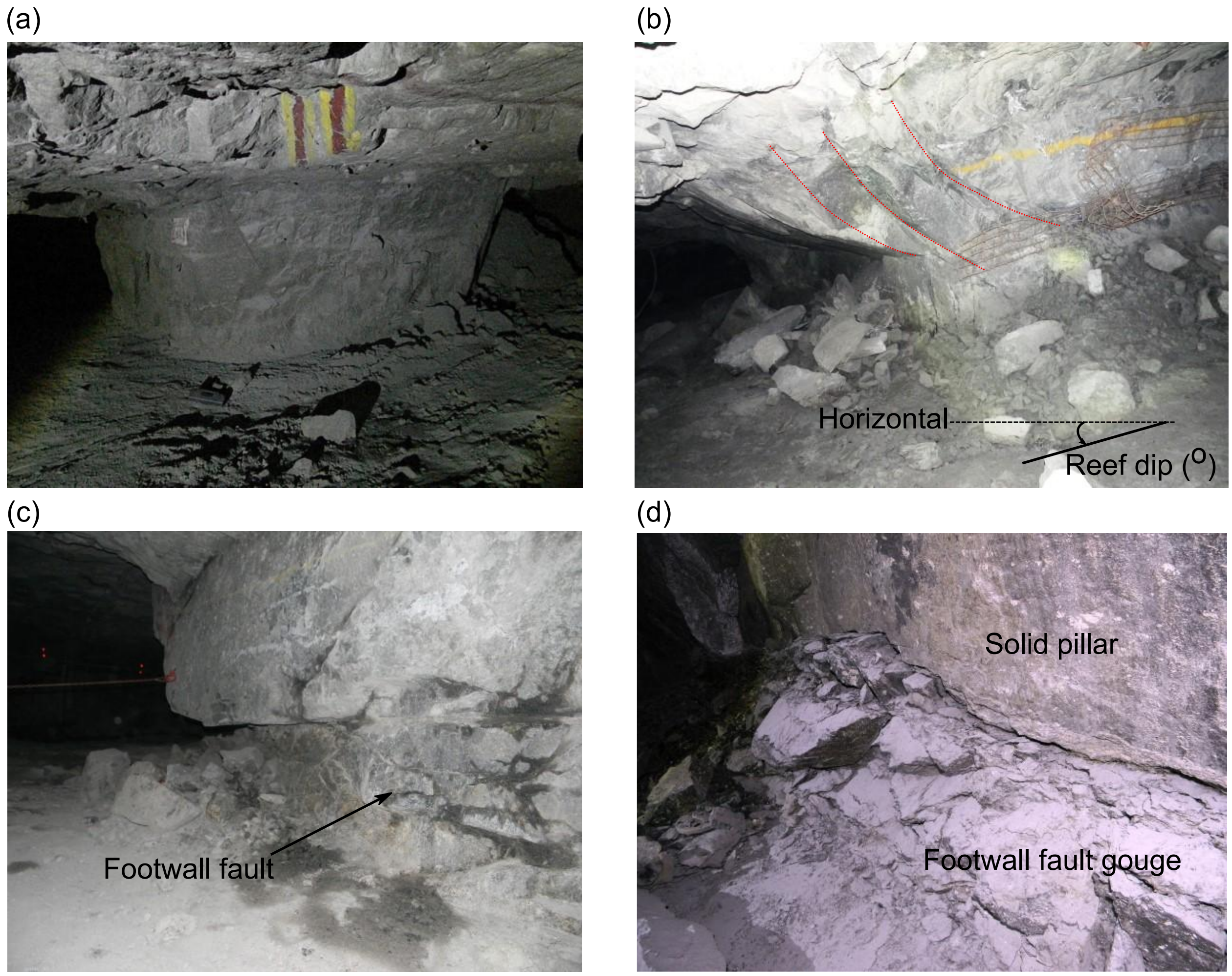

Fig. 2.4 Examples of pillar conditions at the case study mine. (a) Isometric view of an intact pillar, (b) pillar associated with a joint set J1 (marked in red) understood to cause pillar instabilities at the mine, (c) pillar with FwF material, and (d) pillar with weak FwF gouge squeezing out of the pillar bottom.

A shear zone, which is similar to the FwF in the case study mine, exists in one of the mining operations. This shear zone resulted in a significant collapse at the mine, as documented by Mushangwe (2018). Other notable structures are aplite dykes, shallow to moderately dipping joints, reef sub-parallel shear planes and dolerite dykes. Combinations of these geological features produce various rock mass conditions, leading to variable pillar behaviour. The pillar design techniques currently in use do not account for these structures as they were designed mostly for homogenous rock masses (Kaiser et al., 2011). Design techniques which include these structures are necessary to improve the stability and productivity of these mines.

Despite the challenging geological structures mentioned above, the rock mass in the Great Dyke is predominantly competent, and the pillars are stable. Intervention is primarily required when these structures are encountered. Additionally, TAT and the Hedley and Grant equation are conservative methods. While pillars are generally stable, a potential drawback of using these techniques is the tendency to cut overly large pillars, which can reduce the extraction ratio. It is recommended that the design of these pillars undergo continuous improvement.

2.3 Principles of pillar design

2.3.1 Pillar stress

In pillar design, FoS is a routine indicator for assessing pillar stability. FoS is the ratio between the pillar strength and the vertical stress acting on that pillar. The calculation of FoS implies that the average vertical pillar stress and strength must be known. Pillar stress is customarily determined using the TAT, PAT, or numerical modelling in room-and-pillar mines.

Critical evaluations of PAT and numerical modelling in pillar stress estimation have been dealt with in the previous Chapter. However, TAT will feature extensively in the succeeding sections of this research, and a brief introductory explanation of this concept is worth mentioning. TAT is a classical analytical method widely used to estimate the vertical stress on pillars. This technique is purely static and explicitly assumes that each pillar carries the entire weight of the superincumbent column of rock mass above the pillar's tributary area (A_T) (Brady & Brown, 2004; Salamon & Munro, 1967). As indicated in Fig. 2.5, the tributary area is the area between the pillar in consideration and the other eight adjacent pillars. The average vertical pillar stress is determined using Eq. (2.2):

$$TAT = \gamma H \left(\frac{A_{\mathrm{T}}}{A_{\mathrm{P}}} \right) \tag{2.2}$$

where *TAT* is the tributary area theory calculated pillar stress (MPa), γ is the unit weight of the overburden rock mass (MN/m^3), H is the depth below surface (m), A_T is the total tributary area, and A_P is the pillar area.

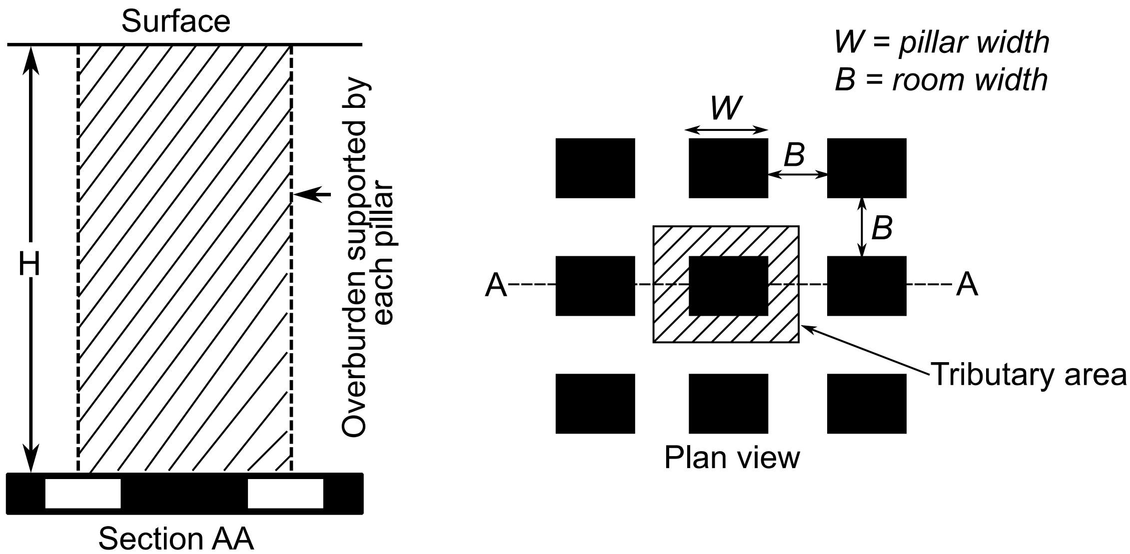

Fig. 2.5 An illustration of the tributary area theory concept for regular pillars.

Alternatively, and in essence, the vertical stress under the TAT concept is calculated as a function of the in-situ vertical stress ($\sigma_v = \gamma H$) and the extraction ratio (e) —the percentage of the extracted area under the tributary area to the total tributary area— as indicated in Eq. (2.3).

$$TAT = \frac{\gamma H}{(1-e)} \tag{2.3}$$

The TAT technique has been widely used to design numerous room-and-pillar mines due to its simplicity and tendency to produce conservative pillar designs. However, it relies on certain fundamental assumptions. Firstly, it ignores the influence of adjacent abutments and assumes that the pillars bear the total overburden load. Secondly, it assumes that each pillar carries the weight of the column of rock mass directly above it, without considering the relative differences of pillar stiffness. Due to these assumptions, TAT usually results in the maximum vertical pillar stress.

Additional research has been undertaken to address the conservative nature of TAT and the time-consuming drawback of numerical modelling. Hauquin et al. (2016) developed a quadratic function of the relative extraction ratio using numerically simulated data by a finite difference method (FDM). Compared to TAT and PAT, the quadratic function offered the best estimates of vertical pillar stress for irregular pillars. Dzimunya et al. (2023) successfully incorporated the influence of abutments into pillar stress estimation by establishing a multi-layer perceptron neural network (MLPNN) using numerically simulated data. Vlachogiannis and Benardos (2024) developed two analytical formulae to estimate vertical stress in square and rib pillar configurations. The analytical equations were derived using numerically simulated data using a 2D and 3D finite element method (FEM). Pillar stress for irregularly shaped pillars in room-and-pillar layouts of tabular orebodies has also been successfully modelled using DDM (Couto & Malan, 2023a; Ile & Malan, 2023; Le Roux & Malan, 2024; Napier & Malan, 2021, 2023).

2.3.2 Pillar strength formulae

Table 2.1 is a summary of the hard rock pillar design formulae that have been developed empirically from failed pillar cases around the world. The presentation is not exhaustive, but its purpose is to indicate that different rock mass conditions require unique empirical formulae. The equations were calibrated for the conditions in which they were inferred from. This means these techniques cannot be adopted into other rock mass environments from which they were not developed. Numerous authors have echoed this, and several equations are continuously being developed to suit different rock masses or mining conditions.

Table 2.1 A summary of hard rock pillar strength estimation formulae.

Authors	**Pillar strength formula**	**Eq.**
Hedley and Grant (1972)	$P_s = 133\left(w^{0.5}/h^{0.75}\right)$	(2.4)
Kimmelmann et al. (1984)	$P_s = 65\left(w^{0.46}/h^{0.66}\right)$	(2.5)
Krauland and Soder (1987)	$P_s = 0.354UCS\left[0.788 + 0.222\left(w/h\right)\right]$	(2.6)
Lunder and Pakalnis (1997)	$P_s = 0.44UCS\left[0.68 + 0.52\left(w/h\right)\right]$	(2.7)
Watson et al. (2008)	$P_s = 147\left[0.70 + 0.30\left(w/h\right)\right]$	(2.8)
Watson et al. (2008)	$P_s = 86\left(w^{0.76}/h^{0.36}\right)$	(2.9)
Roberts et al. (2007)	$P_s = 0.65UCS\left(w^{0.30}/h^{0.59}\right)$	(2.10)
Esterhuizen et al. (2011)	$P_s = 0.65 \times UCS \times LDF\left(w^{0.30}/h^{0.59}\right)$	(2.11)
Watson et al. (2021a)	$P_s = 67\left(w^{0.67}/h^{0.32}\right)$	(2.12)

Notes: *LDF* is the large discontinuity factor.

2.3.3 Numerical modelling and constitutive models

Numerical methods are advanced computational techniques used to solve complex engineering problems. This approach allows for the consideration of complex material behaviour and boundary conditions. Numerical methods are widely acknowledged for providing realistic estimates of pillar strength and stress. While empirical and analytical equations are typically used to estimate pillar strength and stress, respectively, numerical methods are also preferred among practising rock engineers in the mining industry for pillar strength and stress estimation. Recently, several researchers have established that numerical methods reliably evaluate the stress distribution of a pillar based on specific rock material properties (Elmo et al., 2021; Jessu & Spearing, 2019; Monsalve et al., 2020; Rafiei-Renani & Martin, 2018). Numerical modelling has not only enabled more realistic estimates of pillar strength but has also allowed researchers to model complex pillar behaviours and compare the modelling capabilities of different constitutive relationships (Mortazavi et al., 2009; Sinha & Walton, 2018; Walton et al., 2015).

Several programs have been developed specifically to support mine engineering operations. The FEM and FDM are the most popular approaches for solving rock engineering problems. These techniques enable the ease of modelling discontinuities, anisotropy, and changes in boundary conditions. Alternatively, the discrete element method (DEM), finite-discrete element method (FDEM), and the BEM — particularly the DDM — are also increasingly applied to solve various rock engineering problems. Generally, DEM and FDEM are more qualified to analyse the small-scale rock mass damage progressions (Ghazvinian et al., 2014; X. Li et al., 2019; Mayer & Stead, 2017) but the continuum approach is the principal tool for mine-scale models (Sinha & Walton, 2019b). The FDEM and DEM are suited for rock pillar modelling and analysis.

The outputs from modelling any excavation by numerical tools depend on the failure criterion. Various authors have undertaken to develop failure criteria with different levels of success. The cohesion-weakening-frictional-strengthening (CWFS) failure model was developed to address the challenge of modelling brittle damage around underground excavations. While this model has been successful in this application, its use in studying the behaviour of pillars has been questioned. Generally, pillars fail through tensile fracturing in the outer zone and shearing in the inner core. Sinha and Walton (2018) developed a progressive S-shaped yield criterion to mimic rock pillar behaviour. The progressive S-shaped yield criterion combines the shear yield and the CWFS strength criterion. However, other failure criteria have been used for modelling pillar behaviour namely strain-softening Mohr-Coulomb (Mortazavi et al., 2009), ultimate S-shaped criterion (Kaiser & Kim, 2015), brittle Hoek-Brown (Martin & Maybee, 2000) and the CWFS (Walton et al., 2015). A comparison of these continuum models was performed by Sinha and Walton (2019) using numerical modelling in FLAC3D. The comparison reviewed that, despite its complexity, the progressive S-shaped criterion is more applicable in capturing the extent of failure mechanisms in rock pillars. Also, the other criteria tended to overpredict the strength of the hard rock pillars except for the CWFS.

The usefulness of the CWFS model has also been echoed by Rafiei-Renani and Martin (2018). In their study, Rafiei-Renani and Martin (2018) proposed an enhanced CWFS model to simulate the progressive failure of hard rock pillars using two- and three-dimensional FDM analysis tools. The numerical models successfully split stable pillars from unstable/failed pillars and captured the progressive failure mechanisms of hard rock pillars. Pillar behaviour has also been successfully modelled using a combined three-dimensional continuum and two-dimensional bonded block modelling approach (Sinha & Walton, 2021). The idea was to overcome the problem of excessively long run times of complex mining problems by using a 2D bonded block model to study a 3D mining problem. On the other hand, DDM codes cannot effectively simulate the failure of pillars. However, the on-seam failure of pillars has been successfully modelled using a limit equilibrium constitutive model (Couto & Malan, 2023a; Napier & Malan, 2018, 2021).

Earlier presentations of rock mass conditions in hard rock room-and-pillar mines in Zimbabwe have indicated the potential presence of reef-parallel structures —FwF or shear zone— within the pillars. This, along with the influence of reef dip, could negatively impact the overall strength of the pillars. Considering these specific conditions, detailed numerical simulations are essential to quantify the extent of pillar strength reductions applicable for future simple and realistic estimates of the strength of pillars affected by such conditions. In this regard, design engineers in Zimbabwe can more accurately estimate pillar strengths by utilising previous discussions on constitutive relationships and numerical tools to enhance their pillar strength estimates for these and other applications.

The above discussion did not cover the time-dependent failure of underground pillars. However, most pillar failures are time-dependent. A grain-based time-to-failure (GBM-TtoF) model to simulate the strength degradation of brittle rocks was developed by Wang and Cai (2020). Wang and Cai (2021) investigated the time-dependent deformation of pillars using the GBM-TtoF model with UDEC. Their pillar model with an irregular boundary profile captured the time-dependent deformations observed in the field. The results concluded that the boundary profile of the pillars has a small effect on the short-term strength of the pillars. It was also noted that the long-term strengths of pillars are positively correlated to the *w:h* ratio. Sainoki and Mitri (2017) studied the time-dependent skin degradation of two pillar failure cases using a non-linear rheological model capable of simulating tertiary creep. Wessels and Malan (2023) investigated a time-dependent limit equilibrium model (Napier & Malan, 2018) to study the scaling of hard rock pillars over time. DDM was utilised to simulate pillar failures on a mine-wide scale in their research.

Time-dependent simulations are critical for long service pillars such as barrier pillars. The failure mode for these pillars is time-dependent, and a failure criterion that captures this phenomenon is suitable for simulating their behaviour. Barrier pillars are common at the case study mine in Zimbabwe and the previous discussion can enhance the construction of these pillars to improve their designs.

Numerical simulations are also applied to model large-scale mine layouts to estimate pillar stress. The DDM method is currently the most used technique in these applications. Table 2.2 summarises the numerical modelling applications in hard rock pillar design. The summary is of room-and-pillar mining and other applications that apply to this mining method.

Table 2.2 An overview of the numerical modelling application in hard rock pillar design.

Author(s)	Software	Application
Mortazavi et al. (2009)	$FLAC^{2D}$	Investigation of rock pillar failure mechanism
Napier & Malan (2011)	TEXAN	Computation of average pillar stress
Walton et al. (2015)	$FLAC^{3D}$	Influence of constitutive model on pillar stress and yield
Zhou et al. (2017)	PFC^{2D}	Mechanical response of multi-pillar supporting system under external loads
Sinha & Walton (2018)	$FLAC^{3D}$	Application of the progressive S-shaped yield criterion to study rock pillar behaviour
Rafiei-Renani & Martin (2018)	$FLAC^{3D}$	Simulating the progressive failure of hard rock pillars using finite difference analysis
Hauquin et al. (2018)	$FLAC^{2D}$	Predicting pillar burst using modelling of kinetic energy
Jessu & Spearing (2018)	$FLAC^{3D}$	Effect of dip on pillar strength
Jessu & Spearing (2019)	$FLAC^{3D}$	The effect of a large discontinuity on inclined pillars

Sinha & Walton (2019)	$FLAC^{3D}$	Analysis of pillar behaviour with variation in yield criterion, dilatancy, heterogeneity, and length-to-width ratio
Esterhuizen et al. (2019)	$FLAC^{3D}$	Simulation of a large section of a tabular mine to estimate pillar stress underneath variable topography
Sinha & Walton (2021)	$FLAC^{3D}$	Studying the damage process in a granite pillar
Elmo et al. (2021)	PLAXIS	Large mine simulation to study the behaviour of hard rock pillars
Napier & Malan (2021)	TEXAN	Large-scale tabular mine simulation to study pillar failure using the limit equilibrium model
Jessu et al. (2022)	$FLAC^{3D}$	Improved methodology to design pillars
Lavoie et al. (2022)	3DEC	Using a bonded block modelling approach to aid in support design for deep mining pillars
Soni et al. (2022)	3DEC	Estimating the strength of pillars with karst voids
Soni et al. (2023)	3DEC	Modified design of pillars based on estimated stress and strength
Napier & Malan (2023)	TEXAN	Assessing the performance of large-scale pillar layout while capable of modifying individual pillar behaviour
Esterhuyse & Malan (2023)	TEXAN	Simulating pillar reinforcement using the limit equilibrium model
Ile & Malan (2023)	TEXAN	Study of backfill confinement to reinforce pillars
Maritz & Malan (2023)	TEXAN	Effect of pillar shape on pillar strength
Couto & Malan (2023a)	TEXAN	Modelling large-scale pillar collapse where a shear zone is present
Couto & Malan (2023b)	TEXAN	Large-scale tabular mine simulation to estimate pillar stress and re-design barrier pillar arrangements
Dzimunya et al. (2023)	NUTEX	Large-scale tabular room-and-pillar mine simulations to estimate pillar stress

Notes: Tabular excavation analyser (TEXAN); fast Lagrangian analysis of continua (FLAC); particle flow code (PFC); plane strain and axial symmetry (PLAXIS); 3-Dimension distinct element code (3DEC).

2.3.4 Machine learning approaches

The stability analysis of geotechnical structures is inherently complex, due to uncertainties in rock mass characterisation and variability of rock parameters. The factors controlling the stability of underground pillars are numerous, and the values of these parameters can change abruptly from one geotechnical domain to another. Studying the effect of these parameters in isolation does not give a complete picture of pillar behaviour.

To respond to this, various authors have utilised machine learning to predict the stability and estimate stresses of hard rock pillars. Zhou et al. (2015) compared the prediction capabilities of six different supervised classifiers namely, linear discriminant analysis, multinomial logistic regression (MLR), MLPNN, support vector machine (SVM), random forest (RF), and gradient boosting machine. The dataset comprised 251 instances and six features: pillar width, pillar height, *w:h* ratio, UCS of the rock, pillar strength, and pillar stress. It was concluded that the SVM and the RF achieved comparable and favourable classification accuracies. Ghasemi et al. (2017) also performed a comparative assessment of J48 and support vector classification (SVC) classifiers using a dataset compiled from several hard rock mines worldwide. The J48 algorithm demonstrated classification superiority over the SVC and two stability graphs that can be easily used to predict the behaviour of hard rock pillars by design engineers were developed. Wattimena (2014) also developed pillar design charts using multinomial logistic regression. Idris et al. (2015) presented a stochastic assessment of pillar stability using MLPNN to incorporate uncertainties inherent to geotechnical input parameters in pillar design.

Other research contributions include estimating pillar stress using MLPNN (Dzimunya et al., 2023; Monjezi et al., 2011), prediction of pillar stability using the stochastic gradient boosting technique and comparing the same with RF, SVM, and MLPNN (Ding et al., 2018), and stability analysis of hard rock pillars through combining numerical simulation and a backpropagation neural network (Li et al., 2021). Li et al. (2023) performed a stability prediction of hard rock pillars using SVM optimised by three metaheuristic algorithms namely grey wolf optimiser, whale optimisation algorithm, and sparrow search algorithm.

Table 2.3 summarises the machine learning applications for hard rock pillar design. Although there are other studies available in the literature on coal pillar and crown pillar design, this compilation specifically focuses on studies related to hard rock pillars in room-and-pillar mines.

Machine learning is a lucrative alternative to pillar design and a dataset can be developed from the Zimbabwean hard rock platinum mines. This comprehensive dataset can be used to build charts and graphs for pillar design specific to the rock mass conditions in Zimbabwe by employing various machine learning algorithms. The general procedure to follow when using machine learning models is indicated in Fig. 2.6.

Table 2.3 Summary of the machine learning applications for hard rock pillar design.

Author(s)	ML method	Input variables	Dataset size	Performance
Wattimena (2014)	MLR	w:h, UCS, σ, σ/UCS	178	A_{Stable} = 86. 7% $A_{Unstable}$ = 62.0% A_{Failed} = 86. 7%
Zhou et al. (2015)	LDA, MLR, MLPNN, SVM, RF, GBM	w, h, w:h, UCS, P_S, σ	251	A_{LDA} = 67.8% A_{MLR} = 66.2% A_{MLPNN} = 81.1% A_{SVM} = 82.4% A_{RF} = 82.4% A_{GBM} = 79.7%
Idris et al. (2015)	MLPNN	E_m, σ_H, ε_{Axial}*	36	R = 0.99
Ghasemi et al. (2017)	J48, SVC	w:h, UCS, σ, σ/UCS	178	A_{J48} = 81.48% A_{SVC} = 74.04%
Ding et al. (2018)	SGB, RF, SVM, MLPNN	w, h, w:h, UCS, σ	205	A_{SGB} = 90.0 % A_{RF} = 85.0 % A_{SVM} = 82.5 % A_{MLPNN} = 80.0 %
Li et al. (2021)	BPNN	UCS, GSI, w:h, H	594	R = 0.91
Li et al. (2023)	GWO/WOA/SSA-SVM	h, w, w:h, UCS, σ	306	$A_{GWO-SVM}$ = 90.2 % $A_{WOA-SVM}$ = 86.9 % $A_{SSA-SVM}$ = 91.3 % A_{SVM} = 84.8 %
Dzimunya et al. (2023)	MLPNN	E_m, e, H, L, m, TAT, DfA	2355	R = 0.99

Notes: Machine learning (ML); multinomial logistic regression (MLR); linear discriminant analysis (LDA); multi-layer perceptron neural network (MLPNN); support vector machine (SVM); random forest (RF); gradient boosting machine (GBM); Java implementation of C4.5 algorithm (J48); support vector classification (SVC); stochastic gradient boosting (SGB); backpropagation neural network (BPNN); grey wolf optimiser (GWO); whale optimisation algorithm (WOA); sparrow search algorithm (SSA); pillar stress (σ); uniaxial compressive strength (UCS); pillar width (w); pillar height (h); width-to-height ratio (w:h); pillar strength (Ps); deformation modulus (E_m); horizontal in-situ stress (σ_H); axial strain (ε_{Axial}); geological strength index (GSI); depth of mining (H); extraction ratio (e); panel width (L); room-to-pillar width ratio (m), tributary theory area pillar stress (TAT), distance of pillar from abutment (DfA); accuracy (A); regression coefficient (R); *output variable.

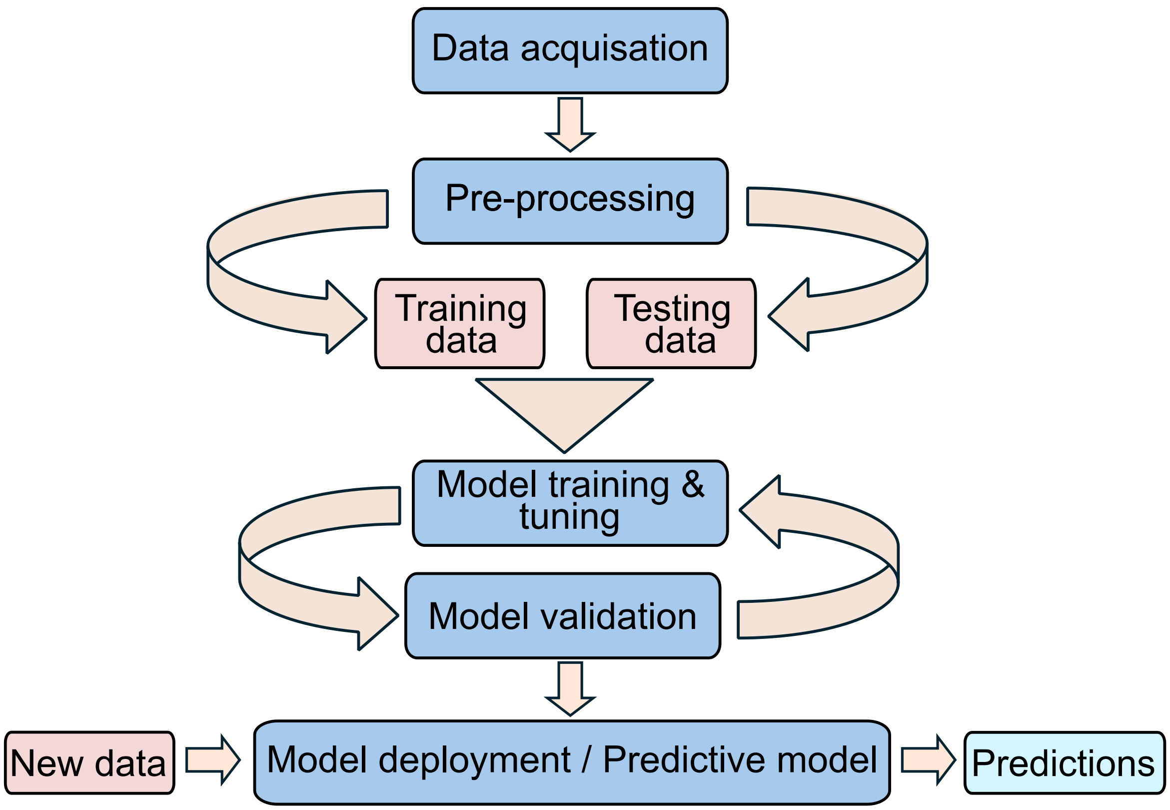

Fig. 2.6 General procedure to follow when implementing machine learning models.

2.3.5 Parametrical influences on pillar design

Pillar design formulae generally incorporate the pillar material's strength and the pillar's shape. In essence, several other factors contribute to the stability of pillars. Various researchers studied the effect of dip on pillar strength behaviour (Jessu & Spearing, 2018; Lorig & Cabrera, 2013). In room-and-pillar mining, the loading environment on pillars is quite complex, involving a combination of normal and shear stresses. Shear stresses can contribute to the instability of pillars, so when evaluating pillar stability, it's important to consider the effects of shear stresses carefully (Garza-Cruz et al., 2019; Maritz, 2015). Also, prominent geological structures within a pillar can weaken it. Even if a pillar has been well-designed, the presence of geological features like persistent joints or faults can lead to shear failure along these discontinuities. The impact of joints on pillar stability has been analysed (Esterhuizen et al., 2011; Y. Zhang et al., 2017), highlighting the need for design principles that consider all these factors when designing pillars. Responding to this research gap, Jessu et al. (2022) proposed a methodology that begins with using a suitable empirical formula to estimate the strength of the pillar and adjusting it by applying corrections for pillar inclination, blast damage, and the presence of an adverse discontinuity. Dzimunya and Fujii, (2024) proposed a universally applicable and user-friendly framework for estimating pillar strength, which can be customised to the specific characteristics of each mine and used for ongoing monitoring.

2.3.6 Barrier pillars

In shallow room-and-pillar mines, it is common to have pillar layouts that include small in-panel pillars and larger barrier pillars. Figure 2.7 illustrates the typical arrangement of in-panel and barrier pillar systems. When designing these barrier pillars, it is important to consider their strength and the distance between them. The barrier pillar must be indestructible and withstand any imposed stress redistributions in the event of localised or multiple in-panel pillar failures. According to Salamon (1974), a *w:h* ratio greater than 10 is sufficient, and the mining industry has widely adopted this recommendation. To ensure that the spacing of barrier pillars is appropriate, a conservative rule of thumb is to ensure that the *IBS* is less than one-quarter of the mining depth, *H* (Ryder & Ozbay, 1990). Additionally, to ensure adequate compartmentalisation, the *IBS* should not exceed 250 m (Ozbay et al., 1995).

Different barrier pillars serve distinct purposes in non-yield, crush, and deeper mines pillar systems. In crush pillar systems, barriers prevent excess closure and surface subsidence that may occur in panels only supported by crush pillars. In deeper mines, barriers can limit enhanced seismicity levels by controlling volumetric stope closures and subsequent seismic energy release possibilities (Ozbay et al., 1995). This present study is focused on shallow room-and-pillar non-yield pillar systems. Barrier pillars in this system are intended to accomplish the following objectives (Ozbay et al., 1995):

- Compartmentalise the mining region into separate zones. In case of a failure in one zone, the barriers will prevent the collapse from spreading into neighbouring compartments.
- Significantly enhance effective strata stiffness and reduce the possibility of large-scale pillar runs.
- Help control the hangingwall tensile zone, thus preventing the possibility of surface subsidence.

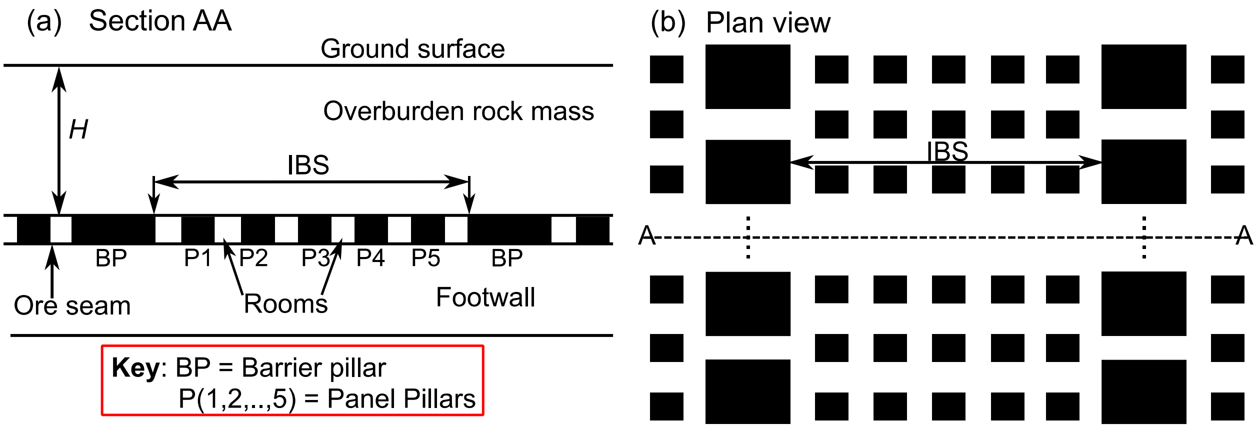

Fig. 2.7 Typical layout of in-panel and barrier pillars for shallow room-and-pillar mines.

Contrariwise, barrier pillars can negatively impact the extraction ratio and time required to open new mining blocks (Theron & Malan, 2024). In shallow hard rock room-and-pillar mines, in-panel pillars are typically designed to be non-yielding, providing substantial control of the hangingwall tensile zone by themselves. This means that the strength of these in-panel pillars is intended to exceed the average pillar stress by an appropriate FoS and to behave elastically throughout the mine's operational life. Theron and Malan (2024) emphasised, "*There is not a good technical motivation for these pillars if the FoS is high on the in-panel pillars.*" Considering this, barrier pillars may only be necessary to compartmentalise the mine in areas where alteration zones are present (Couto & Malan, 2023b), as well as in regions with the FwF or shear zone, such as those found in mines in Zimbabwe

2.4 Discussion

The design of support pillars in room-and-pillar hard rock mining operations is crucial for the safety of underground personnel and machinery, as well as for the profitability of the mining operation. Proper designs ensure a balance between safety and profitability. Pillars must be optimised in size to prevent large-scale collapses, which can lead to injuries or fatalities, damage expensive equipment, and result in the loss of valuable ore. However, overly conservative designs can lead to shorter mine lives and compromised productivity as valuable ore is left underground to support the overburden weight.

Current analysis of rock mass conditions in hard rock room-and-pillar mines in Zimbabwe suggests that using a formula developed for different rock mass conditions is inappropriate. Pillar failures have been attributed to unfavourably oriented geological structures, rather than high pillar loads, indicating that current pillar design techniques may be conservative, resulting in unmined ore underground. There is a need to continuously develop methods to support the pillars affected by these geological structures. Alejano et al. (2017) suggested strapping pillars with cables as an easy and effective way of enhancing the strength of deteriorating pillars.

Pillar strength equations are continually being developed to suit individual rock mass conditions, indicating that a universally applicable formula for pillar design does not exist. Most equations consider only the strength of the pillar material and the geometry of the pillar as input parameters. Only a few equations account for the detrimental effects of large discontinuities. Persistent and unfavourably oriented geological structures have the most significant influence on pillar failure based on a critical evaluation of pillar cases in Zimbabwe. Unfortunately, these factors are absent in most design equations, suggesting that current equations must be updated to incorporate the influence of geological structures. Additional support for the pillars can be implemented when adverse geological structures are encountered (Alejano et al., 2017; Malan & Napier, 2011).

Numerical modelling is useful for designing and analysing surface and underground excavations. However, the accuracy of the output relies heavily on the input parameters and choice of failure criterion implemented. A recent review suggests that the S-shaped failure criterion works best for pillar modelling, with the CWFS failure criterion offering similar performance. Both criteria closely mimic the progressive failure mechanisms seen in pillars. Shear stress loading can weaken rock pillars, so it's crucial to understand the loading mechanism and apply accurate boundary conditions in numerical models during pillar design (Sinha & Walton, 2021).

The review of parameters influencing pillar behaviour highlights the critical role of pillar dip in causing shear stress loading around pillar-roof contacts, leading to pillar destabilisation. Geological features like joints and faults impact pillar stability and can cause failure despite adequate sizing. Various geotechnical and geometric parameters introduce challenges to pillar design and analysis, but machine learning offers a faster and more cost-effective method to address these difficulties.

The complexity arising from various influencing parameters affecting pillar behaviour can be effectively addressed in design by applying machine learning principles. This is because machine learning can uncover hidden patterns within the data. As discussed in Section 2.3.4, the datasets used in the referenced studies did not include all the parameters responsible for pillar instability issues. For future studies using machine learning approaches, including critical parameters such as pillar dip and joint condition data in the datasets is important. This will enhance the comprehensiveness and reliability of pillar stability predictions in the future. In essence, estimating the stress and strength of pillars is the most crucial output for machine learning applications. Figure 2.8 outlines the suggested strategies for future machine learning applications in pillar design.

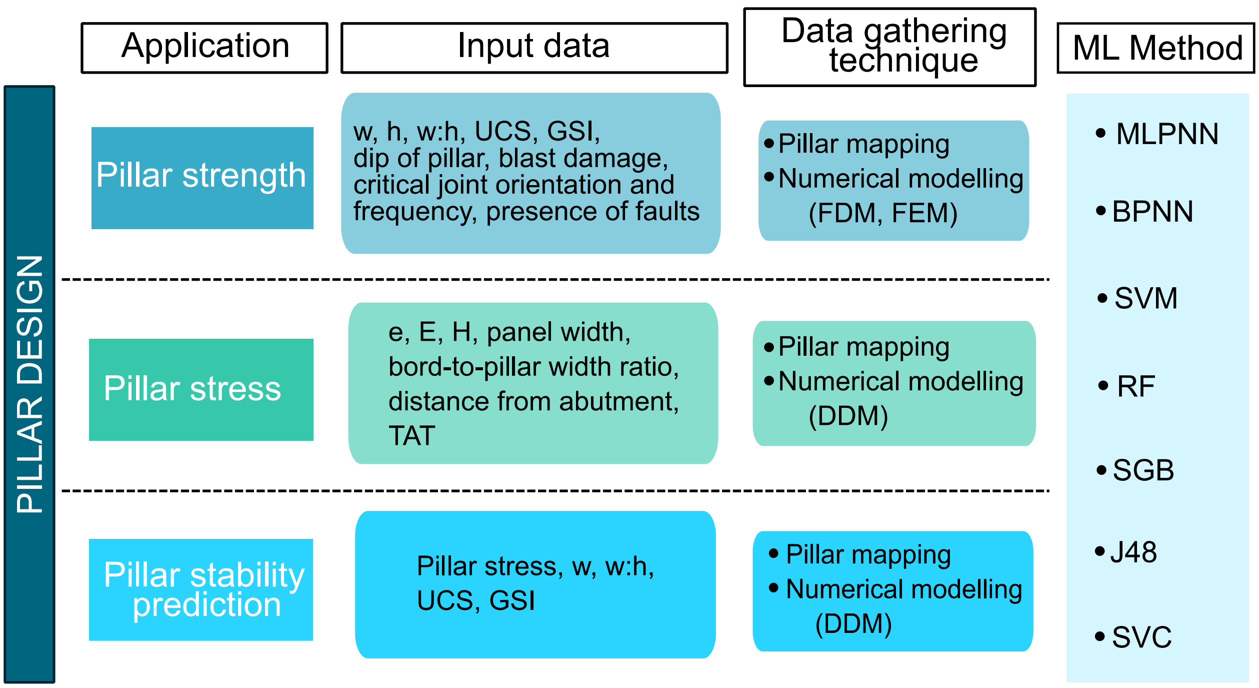

Fig. 2.8 Suggested strategies for future machine learning applications in hard rock pillar design.

The use and design procedures of barrier pillars are not consistent and require further research. Barriers are meant to prevent large collapses and minimise stress on panel pillars. Numerical simulations show that panel pillars closest to the barrier pillars experience the least stress due to the barrier pillars' larger size and increased stiffness (Fig. 2.9a). This suggests the potential for a staggered room-and-pillar mining method, using varying pillar sizes to improve ore recovery (Fig. 2.9b).

However, practical mining aspects should be considered when implementing the staggered room-and-pillar layout. It is stated in Theron and Malan (2024): "*A drawback of rock engineering designs is that it is often done in isolation without including the constraints imposed by practical mining* *considerations*." A key consideration in mining engineering when implementing this layout is maintaining uniform bord spans that optimally align with the specifications of the available mechanised mining equipment. This means that pillar widths can only be reduced along the strike direction (see Fig. 2.9b). If this guideline is not followed, it may lead to inconsistent bord spans in the layout. Implementing this inconsistency is impractical, as it can affect stable bord spans, support patterns, and the need for consistent bord widths for conveyor belts to smoothly run to the mining faces.

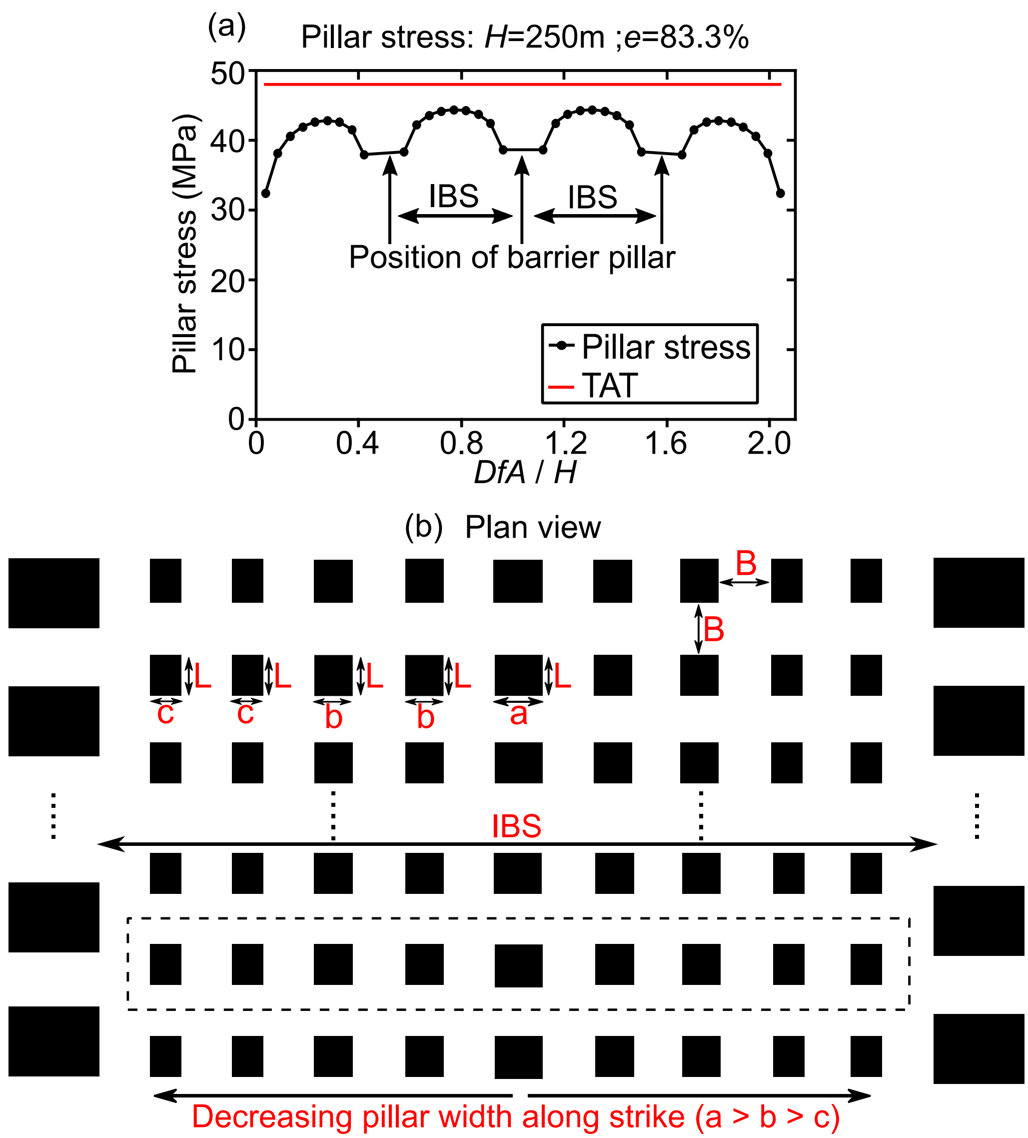

Fig. 2.9 Proposed improvements for the design of in-panel and barrier pillar mining layouts. (a) Pillar stress distributions in an example DDM simulation, and (b) proposed staggered room-and-

pillar mining method. **Notes:** *DfA* is the distance of the respective pillar from the left abutment of the DDM numerical models simulated in this research.

The staggered room-and-pillar layout offers three key benefits: Firstly, smaller pillars lead to less complex ventilation controls, which in turn shortens the time required to complete a full mining cycle (Theron & Malan, 2024). Secondly, smaller pillars enhance ore recovery and result in a higher extraction ratio (as shown in Table 2.4). This reduces the mining advance rate in the strike direction, which makes it take longer to reach the boundaries. Consequently, this alleviates pressure on the engineering department to advance the conveyors along the strike, yielding associated labour and cost advantages. Tramming cycles can also be minimised, reducing wear and tear on the mining equipment, since conveyors can be maintained closer to the mining faces. The comparison in Table 2.4 considers the enclosed area in Fig. 2.9b and is based on the bord and pillar dimensions indicated in the table. Thirdly, smaller pillars extend the life of mine and maximise resource extraction, providing significant benefits for both communities and society.

Table 2.4 Comparison of extraction ratios for the conventional and staggered layouts.

Layout –	**B** (m)	**L** (m)	**a** (m)	**b** (m)	**c** (m)	**A_P** (m^2)	**A_T** (m^2)	**e** (%)	**SMD** (m)
Conventional	8	6	6	6	6	324	1764	81.6	126
Staggered	8	6	6	5	4	252	1596	84.2	114

Notes: A_P is the total area of pillars; A_T is the total tributary/enclosed area; e is the extraction ratio; SMD is the strike mining distances.

CHAPTER 3 AN ARTIFICIAL NEURAL NETWORK MODEL FOR ESTIMATING PILLAR STRESS

3.1 Introduction

The analytical methods mentioned in Chapter 1 provide valuable estimations of pillar stresses, but no existing method effectively considers the influence of abutments in hard rocks. This Chapter proposes a solution to estimate vertical loads on regular pillars based on numerical modelling and machine learning. This solution factors in the influence of abutments and assumes linearly elastic rock behaviour. The analysis proceeds as follows: Factors that govern pillar stresses are analysed; A dataset is numerically developed using the DDM; A MLPNN is then trained on the dataset; A mine layout is simulated in FLAC3D and the results are compared with MLPNN predictions for validation purposes; The MLPNN model is adapted for use in a mine layout that consists of evenly spaced barrier pillars; Finally, the adapted model is applied to an actual mine case study. The machine learning model development flowchart is summarised in Fig. 3.1.

3.2 Dataset development using 3D DDM

A dataset is an integral part of machine learning. Datasets house several data that can be used to train machine learning algorithms. This study used DDM to simulate numerous mine layouts to develop a dataset for subsequent pillar stress predictions using machine learning. DDM-based software NUTEX (Fujii, 2004; Fujii et al., 1997) was used, and the code was developed to simulate stresses and displacements in tabular deposits numerically. The software was developed on Microsoft Fortran Power Station and is compatible with Microsoft Windows. Successful implementations of NUTEX can be found in Fujii et al. (2001) and Sinkala et al. (2019, 2022), and other separate applications of the DDM (Napier & Malan, 2011; Tuncay et al., 2021).

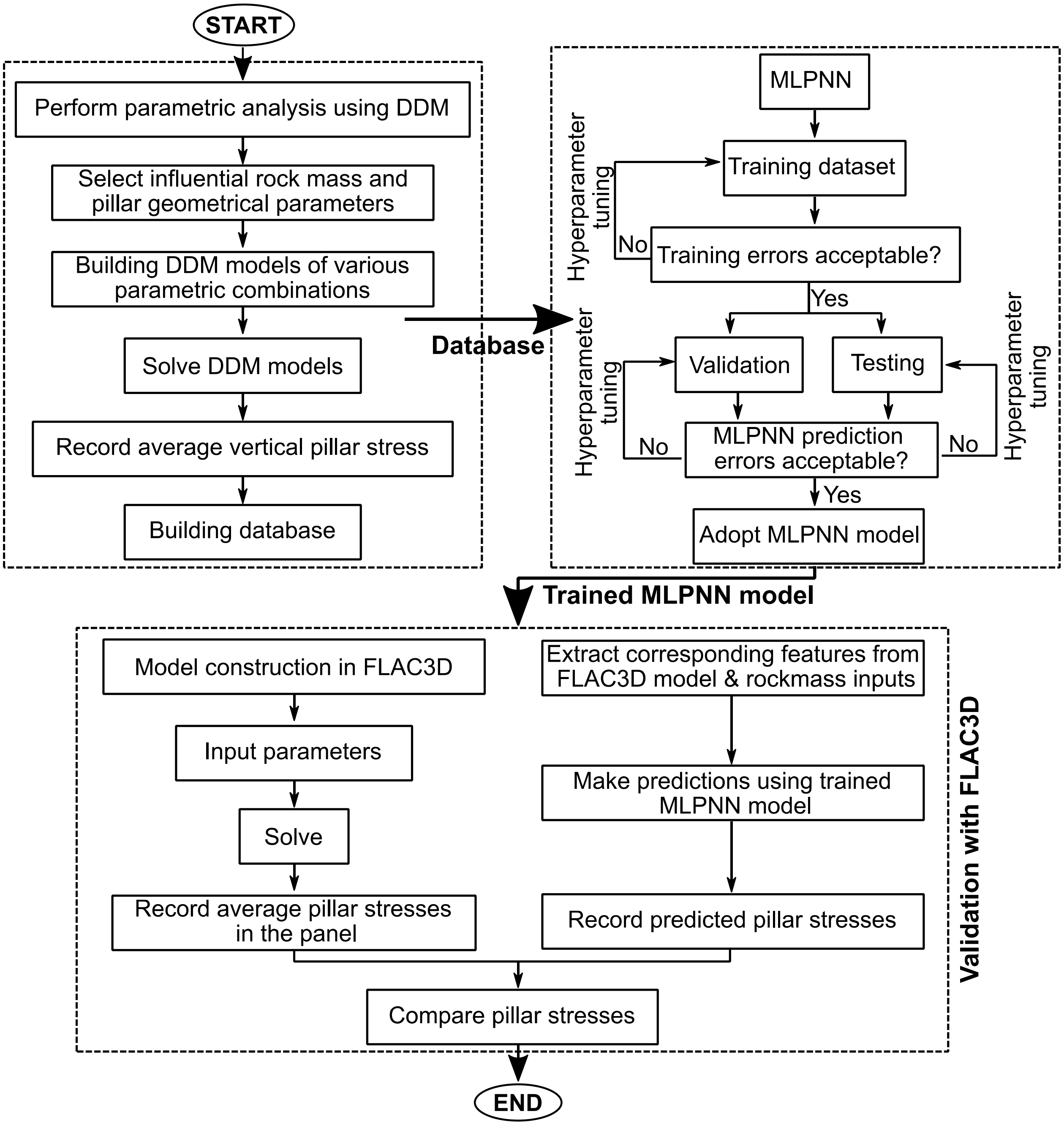

Fig. 3.1 Flowchart of machine learning model development.

3.2.1 DDM brief theory and model construction

DDM is a variant of the BEM and uses displacement and stress due to displacement discontinuity (difference in displacement between fracture surfaces) in an infinite medium as fundamental solutions. The ore is regularly divided by square elements and the boundary conditions are assigned.

Boundary conditions are described as follows: *x*- and *y*-axes are in the dip and strike directions, respectively, and the *z*-axis is normal to the ore seam. *b* is the displacement discontinuity. b_x and b_y represent slip along *x*- and *y*-axes. Negative or positive b_z represents closure or opening of the roof and floor. For the mined ore seam elements and the ground surface,

$$\tau_{zx} = \tau_{yz} = \sigma_z = 0 \ , \tag{3.1}$$

where τ and σ are shear and normal stresses, respectively. If b_z surpasses the adjusted working height of the ore seam elements,

$$b'_z = -\alpha t \ , \tag{3.2}$$

where α and t are a coefficient and the mining height, respectively. And

$$b'_x = b_x \frac{b'_z}{b_z} \ , \ b'_y = b_y \frac{b'_z}{b_z} \ . \tag{3.3}$$

Conversely,

$$\text{If } \tau_{max} = \sqrt{\tau_{zx}^2 + \tau_{yz}^2} \geq -\sigma_z \tan\phi,$$

$$\tau'_{zx} = \tau_{zx} \frac{-\sigma_z \tan\phi}{\sqrt{\tau_{zx}^2 + \tau_{yz}^2}} \ , \ \tau'_{xy} = \tau_{yz} \frac{-\sigma_z \tan\phi}{\sqrt{\tau_{zx}^2 + \tau_{yz}^2}} \ , \tag{3.4}$$

where ϕ is the angle of internal friction. For the unmined elements,

$$\tau_{xz} = \frac{b_x}{t} G + \tau_{xz}^0 \ , \ \tau_{yz} = \frac{b_y}{t} G + \tau_{yz}^0 \ , \ \sigma_z = \frac{b_z}{t} E + \sigma_z^0 \ , \tag{3.5}$$

$$G = \frac{E}{2(1+v)} \ , \tag{3.6}$$

where τ_{xz}^0, τ_{yz}^0, σ_z^0, *E*, *G*, and *v* are the initial stresses, Young's modulus, shear modulus and Poisson's ratio, respectively.

Displacement discontinuity values can be obtained by solving boundary integral equations for all the elements. Displacements and stresses at arbitrary points can be obtained from these displacement discontinuity values (Crouch, 1976; Crouch & Fairhurst, 1973). BEM efficiently solves large-scale problems characterised by complicated geometries such as room-and-pillar mines. In such cases, using FEMs, which depend on discretising the entire volume rather than boundaries, as in the case of BEM, would take very long run times, which are prohibitive, especially at mine sites where solutions may be required quickly. Even though DDM can take relatively shorter solution times, some of the mine layouts of vast lateral extensions, as simulated in this analysis, required more than one day to converge.

Model construction in NUTEX is relatively simple. Three steps must be followed to obtain the average vertical stress of the pillars: (1) create data files related to the layout of the mine (assigning 1's to unmined elements and 0's to mined elements) with initial stress and mechanical parameters, (2) analyse with NUTEX, and (3) record the average pillar stresses.

3.2.2 Parameter analysis for dataset feature identification

The essential undertaking in building machine learning datasets is identifying the attributes/features that constitute the dataset. In this study, feature identification was accomplished via parameter analysis from past studies and through selecting well-known factors that influence pillar stresses. It is well known that pillar stresses depend on mining depth (*H*), extraction ratio (*e*, %), and overburden unit weight (γ). However, for reasons of simplicity, γ was maintained as 2.7 tonnes/m^3 for all the DDM simulations. In cases of a prediction involving different overburden γ, simple proportions would be considered valid.

Sensitivity analysis of the effect of Poisson's ratio v on pillar stress was done in NUTEX. The analysis indicated that v has little influence, and thus it was not considered an important parameter. A constant v of 0.2 was used for all the DDM simulations. Young's modulus *E* influences pillar stresses (Zhou et al., 2017). Modulus ratio (MR), ratio of the overburden *E* to that of the seam, has been reported to influence pillar stresses. However, this ratio is more pronounced in coal mines where the coal seams are usually softer than the surrounding rocks. The focus of this investigation was on hard rock room-and-pillar mines, and in such cases, it has generally been reported that MR is usually very close to unity (similar stiffness of ore seam and host rock) and thus *E* for host rock and pillars was assumed to be equal in the DDM models.

The panel width influence on pillar stresses was also investigated. Three different panel widths of 100, 300, and 700 m were simulated for a layout with 6 m square pillars, 6 m room width, *E* of 20

GPa, and 200 m mining depth. Figure 3.2 shows the average vertical pillar stress distribution for the three cases. It is clear from the plot that panel width has a considerable influence on pillar stresses. The pillar stresses increase as the distance from the abutment increases. Maximum average pillar stress in the panel approaches the TAT stress asymptote as the size of the panel increases. Pillars adjacent to the abutments have significantly lower stresses because the abutments carry some of the load. This Chapter focuses on a machine learning model that can reproduce the trends in Fig. 3.2.

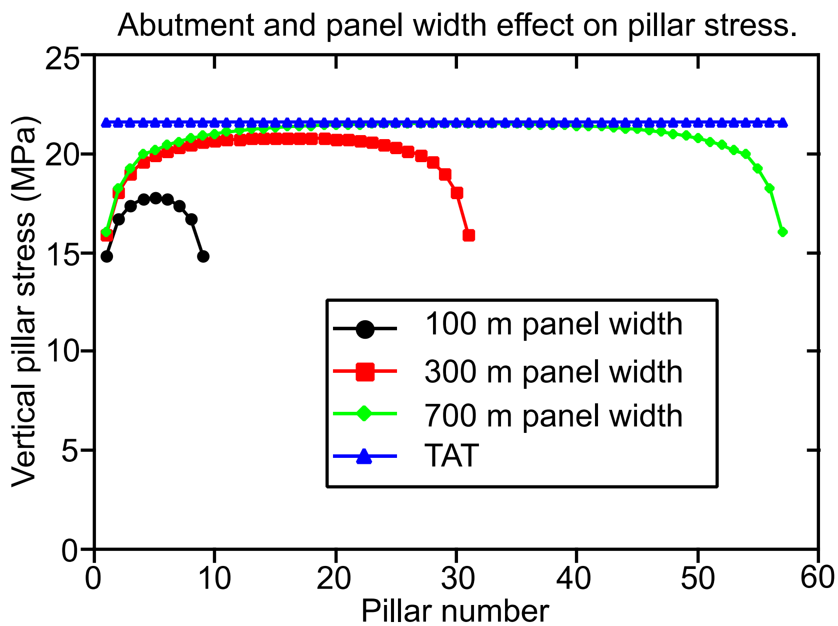

Fig. 3.2 Effect of panel width on pillar stress distribution.

In addition, it is well understood that the horizontal-to-vertical stress ratio (*k*) has an extensive range of values, typically at shallow depths (Hoek et al., 1995), where the room-and-pillar mining method is often applicable. This fact suggests that the influence of *k* must be considered when studying pillar stress distributions. In a study (Hauquin et al., 2016), numerical simulations of several regular pillars revealed that the magnitude of the in-situ horizontal stress has a minimal influence on the vertical pillar stresses. The maximum difference observed in a scenario where *k* was 0.5 and 2 amounted to a 2% difference. This difference was deemed negligible, and *k* was maintained as 1 for all simulations in DDM. Contrariwise, *k* influences the stability of the rooms and must be carefully incorporated in such designs. A tensile zone exists in the roof of any tabular mining excavation due to the deflection of the hanging wall. As a result, the roof of the excavation is exposed to vertical 'deadweight' tensile stresses. The extent of this tensile zone increases with the increase of *k* ratio (Ozbay et al., 1995).

It is important to note that all numerical simulations in this analysis were performed assuming linear elastic rock behaviour. The target pillars in this study are non-yield pillars. The main consideration in designing such pillars is to warrant that pillar strength always exceeds, by an appropriate FoS, the maximum pillar stress imposed by the overburden load of the superincumbent rock mass. This implies that non-yield pillars are intended to remain essentially intact and elastic throughout the mine life. At stress levels in a pillar below the corresponding pillar strength, the pillar remains intact and reacts elastically to the increased state of stress (Brady & Brown, 2004). Consequently, the linear elasticity assumption in this analysis can be reasonable as an initial design approach.

3.2.3 Dataset development

Since numerical modelling is the superior method for rock mechanics problems, it is acceptably logical to simulate numerous combinations of realistic rock mass and pillar configurations and make future predictions of actual cases based on the simulated data. Other studies founded on numerically simulated datasets include (Hauquin et al., 2016; Li et al., 2021). The parameters chosen as variable features are *H*, *E*, *e*, and panel width. Numerical simulations in DDM were then conducted based on a parametric study of these model variables. Random values were assigned to these four variable parameters, and extensive numerical simulation was undertaken with all possible combinations of these parameters, as illustrated in Table 3.1.

Table 3.1 Summary of the variable values and the total number of DDM simulations.

Variable	Values	Count	Total simulations
e (%)	55.5, 75, 80, 84, 88	5	
E (GPa)	20, 50, 75	3	$5 \times 3 \times 4 \times 3 =$ **180**
H (m)	100, 200, 500, 800	4	
Panel width (m)	100, 300, 700	3	

Pillar sizes and room widths typically used in hard rock mines were chosen, and configurations that satisfy the extraction ratios in Table 3.1 were simulated. In total, 180 numerical models were simulated. Pillars in each simulation were sampled, as indicated in Fig. 3.3. Each pillar's distance from the abutment (DfA) was recorded, and DfA was added as a feature to the dataset. Pillar stress was computed as the average stress within each element constituting the pillar. This is the most convenient approach because in NUTEX pillars are formed by very few elements: a modelling constraint imposed by the need to model large areas of pillar outlines.

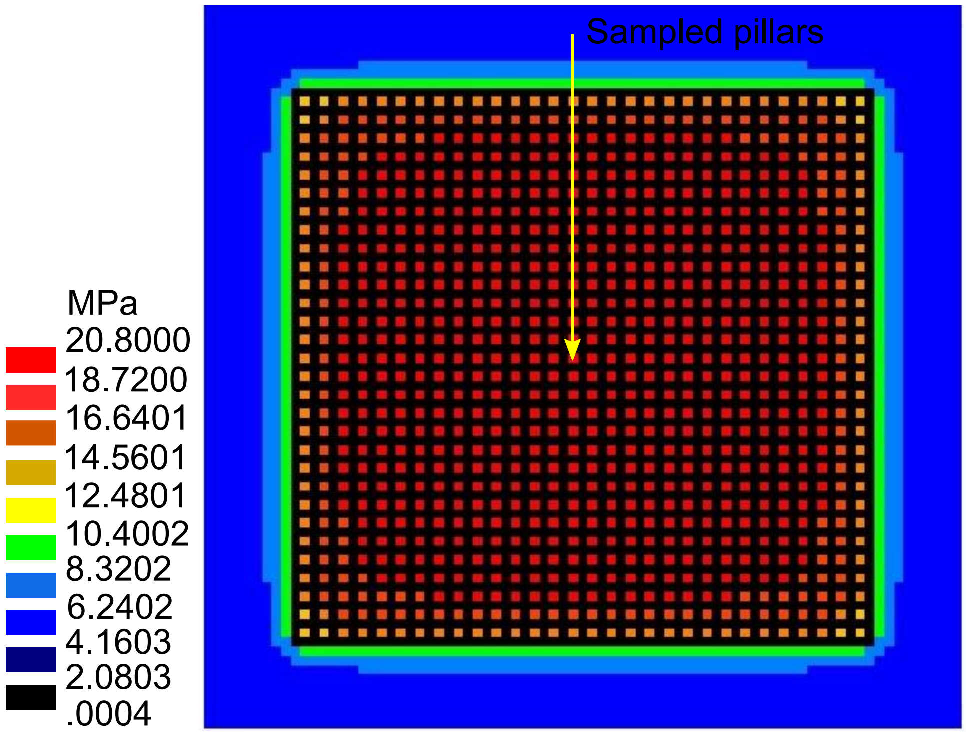

Fig. 3.3 Normal stress distribution on an example of sampled pillars in one of the DDM simulations.

Depending on the model size and the number of sampled pillars, the dataset eventually consisted of 2355 data points. TAT stress and *m* (ratio between room width and pillar width) were also added to the dataset. When different room widths exist along the dip and strike, an average value is considered to represent room width. Finally, an original numerically developed dataset for geometric and pillar stress prediction was achieved, and Table 3.2 displays the top five and bottom five instances of this dataset.

Table 3.2 Top and bottom five rows of the dataset.

e	***E***	***H***	**Panel width**	***m***	**TAT**	**DfA**	**Pillar stress**
–	(GPa)	(m)	(m)	–	(MPa)	(m)	(MPa)
0.84	20	100	712	1.50	16.88	316.0	16.76
0.84	75	500	712	1.50	84.38	116.0	73.35
0.75	20	800	300	1.00	86.40	21.0	71.35
0.80	20	200	300	1.25	27.00	92.0	24.61
0.80	50	500	700	1.25	67.50	124.0	62.26
…	…	…	…	…	…	…	…
…	…	…	…	…	…	…	…
0.75	20	800	114	1.00	86.40	33.0	69.58
0.75	20	200	300	1.00	21.60	33.0	19.01
0.75	50	200	300	1.00	21.60	141.0	20.37
0.84	75	800	712	1.50	135.00	76.0	111.30
0.88	20	100	115	2.00	24.55	12.5	12.66

3.3 Machine learning model and its verification by FLAC3D

Estimation of vertical pillar stress in room-and-pillar mines is always a challenging task. The main reason is that several parameters influence pillar behaviour. This complexity requires techniques to make reliable pillar stress estimations while accommodating all the influencing parameters. Machine learning has proved useful in handling challenges encompassing numerous variables. In recent decades, researchers have progressively applied machine learning to pillar stability problems with great success (Ding et al., 2018; Ghasemi et al., 2017; Li et al., 2021; Monjezi et al., 2011; Wattimena, 2014; Wattimena et al., 2013; Zhou et al., 2015).

Several machine learning algorithms, such as RF, ANN, SVMs, gradient boosting, logistic regression, and many others, have been extensively applied in geotechnical studies. The scope of this study was not to thoroughly examine each of the available algorithms but to easily select any algorithm capable of effectively predicting pillar stresses based on the previously developed dataset.

Based on the authors' experience and available literature, RF and MLPNN were handpicked for subsequent quick comparison.

3.3.1 Selection of suitable regressor for pillar stress estimation

Three statistical measures were used for the RF and MLPNN comparison, namely: regression coefficient (R), mean absolute error (MAE), and root mean squared error (RMSE). R is a widespread statistical measure used to obtain the level or significance of linear relationships between two or more variables in statistical experiments. In machine learning, R values greater than 0.90 show a high and perfect correlation between actual and predicted values (Idris et al., 2015). On the other hand, MAE and RMSE are calculated according to Eqs. 3.7 and 3.8, respectively:

$$\mathrm{MAE} = \frac{\sum_{i=1}^{N} \left| Y_{\mathrm{pred}} - Y_{\mathrm{act}} \right|}{N} \tag{3.7}$$

$$\mathrm{RMSE} = \sqrt{\frac{\sum_{i=1}^{N} (Y_{\mathrm{pred}} - Y_{\mathrm{act}})^2}{N}} \tag{3.8}$$

where N is the sample size, Y_{pred} is the predicted values, and Y_{act} is the actual values. Error margins must be minimised; thus, the smaller the MAE and RMSE, the better the model performance.

The two algorithms were trained and tested on the dataset, and Table 3.3 compares the models on the test set. Details of how the dataset was split into testing and training sets are described in the following Subsection 3.3.3.

Table 3.3 RF and MLPNN comparison on testing data.

Regressor	***R* score**	**MAE**	**RMSE**
RF	0.99	0.24	0.61
MLPNN	0.99	0.78	1.14

The performances of the two models are comparatively similar. However, MLPNN was selected for the subsequent development of the pillar stress estimation model because it is self-adapting and has good generalisation capabilities. Also, MLPNN can capture non-linear relationships, characteristic of the dataset variables involved in this analysis, between input variables. On the contrary, RF was avoided because decision trees are often prone to overfitting.

3.3.2 MLPNN algorithm

MLPNN is the most used ANN for a wide variety of problems. MLPNNs are established on a supervised learning procedure and contain three fully connected types of layers: input, hidden, and output. The processing elements in ANN are called perceptrons or neurons (Walczak & Cerpa, 2003). Each connection between neurons is associated with a weight (w_{ij}), and every neuron is associated with a bias (b_k). The basis of MLPNN training involves two steps: forward propagation and backpropagation. Training means continuously adjusting the weights and biases until the error between the predicted output and the actual is minimal. In the forward propagation, the input data is fed into the network and gets transmitted into each neuron through a linear operation (Eq. 3.9) and outputted from the neuron by a non-linear operation via the activation function (e.g., rectified linear unit (ReLu), sigmoid, and hyperbolic tangent (Tanh)).

$$Y_{\text{inp}} = b_k + \sum w_{ij} x_i \tag{3.9}$$

where Y_{inp} is the input to the neuron, b_k is the kth bias associated with that neuron, x_{i} is the ith input from the previous layer, and w_{ij} is the weights associated with connections to that neuron.

When an initial forward pass of the first training example is wholly transmitted through the network, an initial prediction is achieved. This initially predicted output is then compared with its corresponding actual value. At this point, a method is implemented that can update weights (w_{ij}) and biases (b_k), so that the error between prediction and actual is reduced. This procedure is the backpropagation step. Backpropagation is typically achieved by performing gradient descent. Gradient descent is a mathematical first-order iterative optimisation algorithm to find a local minimum of a differentiable function. In the case of MLPNN, the differentiable function is the error/cost function (Eq. 3.10).

$$\text{cost} = (Y_{\text{pred}} - Y_{\text{act}})^2 \tag{3.10}$$

Gradient descent is made by calculating the partial derivatives of the cost function for the parameters (w_{ij} and b_k) (Eq. 3.11) and moving in the negative direction of these derivatives (slopes).

$$\frac{\partial \text{cost}}{\partial w_{ij}} \quad , \frac{\partial \text{cost}}{\partial b_k} \tag{3.11}$$

The chain rule is used to trace back each parameter and consequently solve its partial derivative. The gradient descent along the cost function is made possible by taking small steps, η, also called the learning rate in ANN. The updating of w_{ij} and b_k is thus completed by using Eq. 3.12.

$$w_{ij}^{+} = w_{ij} - \eta \frac{\partial \text{cost}}{\partial w_{ij}} \quad , \quad b_k^{+} = b_k - \eta \frac{\partial \text{cost}}{\partial b_k} \tag{3.12}$$

where w_{ij}^{+} and b_k^{+} are the updated weight and bias, respectively. Weights and biases are updated using one training example at a time. That cycle is called an epoch when the entire training data has been used in forward and backpropagation. Thus, to fully train the MLPNN, multiple epochs must be achieved. Training is stopped when the errors of the cost function hardly change. The architecture of the MLPNN used in this analysis is indicated in Fig. 3.4, signifying the fully connected input, hidden and output layers.

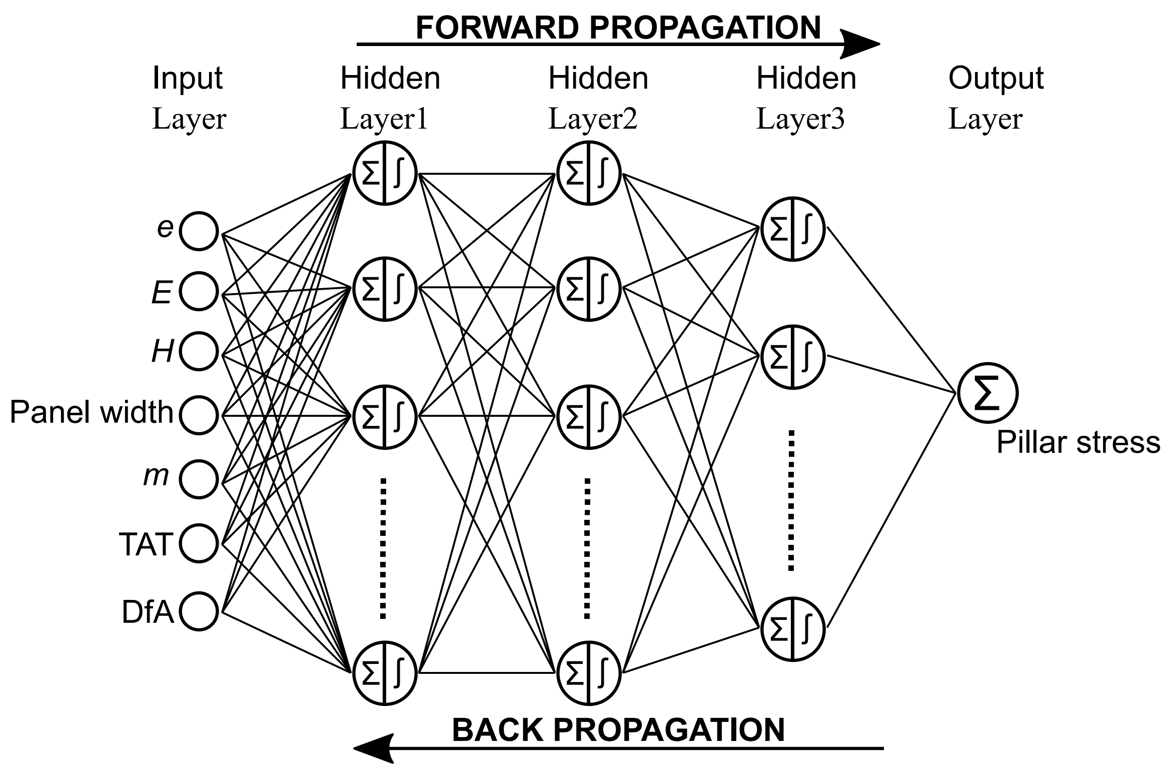

Fig. 3.4 Proposed MLPNN architecture for pillar stress prediction.

The MLPNN was built in the Scikit-learn open-source machine learning library. *GridSearchCV* was used to obtain the best model hyperparameters. The optimum model hyperparameters were selected and are summarised in Table 3.4.

Table 3.4 MLPNN model hyperparameters and architecture.

Max_iterations	**Activation**	**Architecture**	**Solver**	**Learning rate**	**Alpha**
2000	ReLu	7-150-150-50-1	Adam	Adaptive	0.05

3.3.3 MLPNN training, testing, and validation

A perfect MLPNN model denotes that the predicted pillar stresses are infinitely close to the actual values. In other words, the MLPNN model must learn as much as possible from the dataset to minimise errors in future prediction applications. In supervised machine learning, the performance of an algorithm must be assessed on a given dataset before using it to make predictions on new data. This criterion is satisfied by splitting the original dataset into three subsets: training, testing, and validation datasets. The training set is utilised to construct the model and set model hyperparameters. The testing and validation sets are used as independent checks to assess the model performance on new unseen data. The 2355 data points were divided into 70% training, 20% testing, and 10% validation. Figure 3.5 indicates the regression plots of the MLPNN model for the testing and validation sets. The R-value is limited to two decimal places, and in Fig. 3.5, R-values of 0.99 (testing) and 0.99 (validation) are realised for predicting average pillar stresses. These high R-values indicate the high performance of the MLPNN model in predicting average vertical pillar stresses.

The error margins of the MLPNN model are also indicated in Table 3.5. The error margins are reasonably small; thus, the MLPNN model has been sufficiently trained and can make good generalisations when presented with new data.

Table 3.5 Error margins on the testing and validation sets.

Statistical measure	**Testing**	**Validation**
MAE	0.78	0.85
RMSE	1.14	1.29

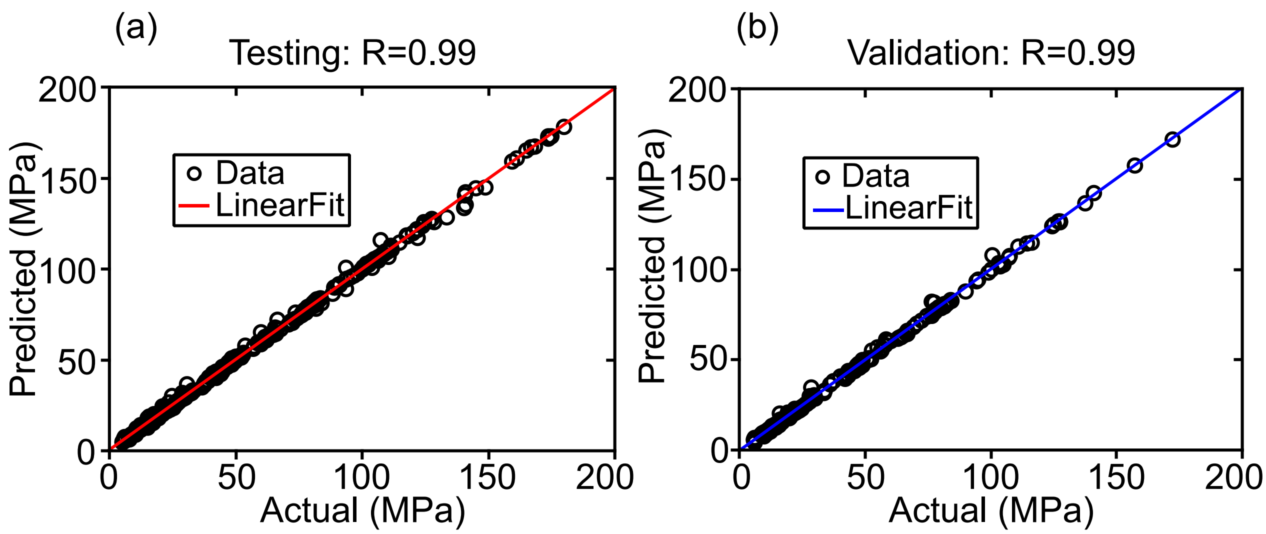

Fig. 3.5 Actual and predicted output values. (a) Testing set, and (b) validation set.

3.3.4 Model construction in FLAC3D

To further verify the reliability of the MLPNN model, pillar stresses of a unique mine layout were predicted by the MLPNN model. These predictions were compared to numerical simulations of the same design using another widely accepted numerical tool. FLAC3D was chosen for such a comparison, and version 5.0 (Itasca, 2012) was used in this study.

FLAC3D is a commercially available code developed by Itasca Ltd. The software is a widely used numerical tool that exploits FDM. The response of the simulated continuous medium derives from a specific mathematical model on the one hand, and a specific numerical implementation on the other (Itasca, 2016). The mechanics of the medium are derived from general principles (definition of strain and laws of motion) and the use of constitutive equations that define the rock mass behaviour. The mathematical system involves a group of partial differential equations, connecting mechanical (stress) and kinematic (strain rate and velocity) variables. These equations must be resolved for properties and geometries, given specific initial and boundary conditions.

The method of solution in FLAC3D depends on the nature of the problem and is characterised by three approaches: finite volume, discrete model and dynamic solution approach. Exploiting these approaches, the laws of motion for the medium studied are transformed into discrete forms of Newton’s law at the nodes of the elements making up the medium. The resultant structure of ordinary differential equations is then numerically solved, employing an explicit finite difference approach in time (Itasca, 2016). To date, numerous studies have been completed using FLAC and examples related to pillar design include (Chen & Mitri, 2021; Kostecki & Spearing, 2015; Rafiei-Renani & Martin, 2018; Sainoki & Mitri, 2017; Sinha & Walton, 2019a).

A simple linear elastic constitutive model was utilised. The simulated mine layout was a large rectangular model with its bottom and lateral boundaries positioned 200 m from the mine edges to avoid model mechanical boundary effects. Roller boundaries were placed on the lateral and bottom limits of the model. The model grid is comprised of quadrilateral elements of varying sizes. Smaller square elements of 1 m sides constituted the pillar regions, and these elements gradually increased into rectangular elements of increasing sizes towards the model boundaries. The pillar layout and model configuration are illustrated in Fig. 3.6.

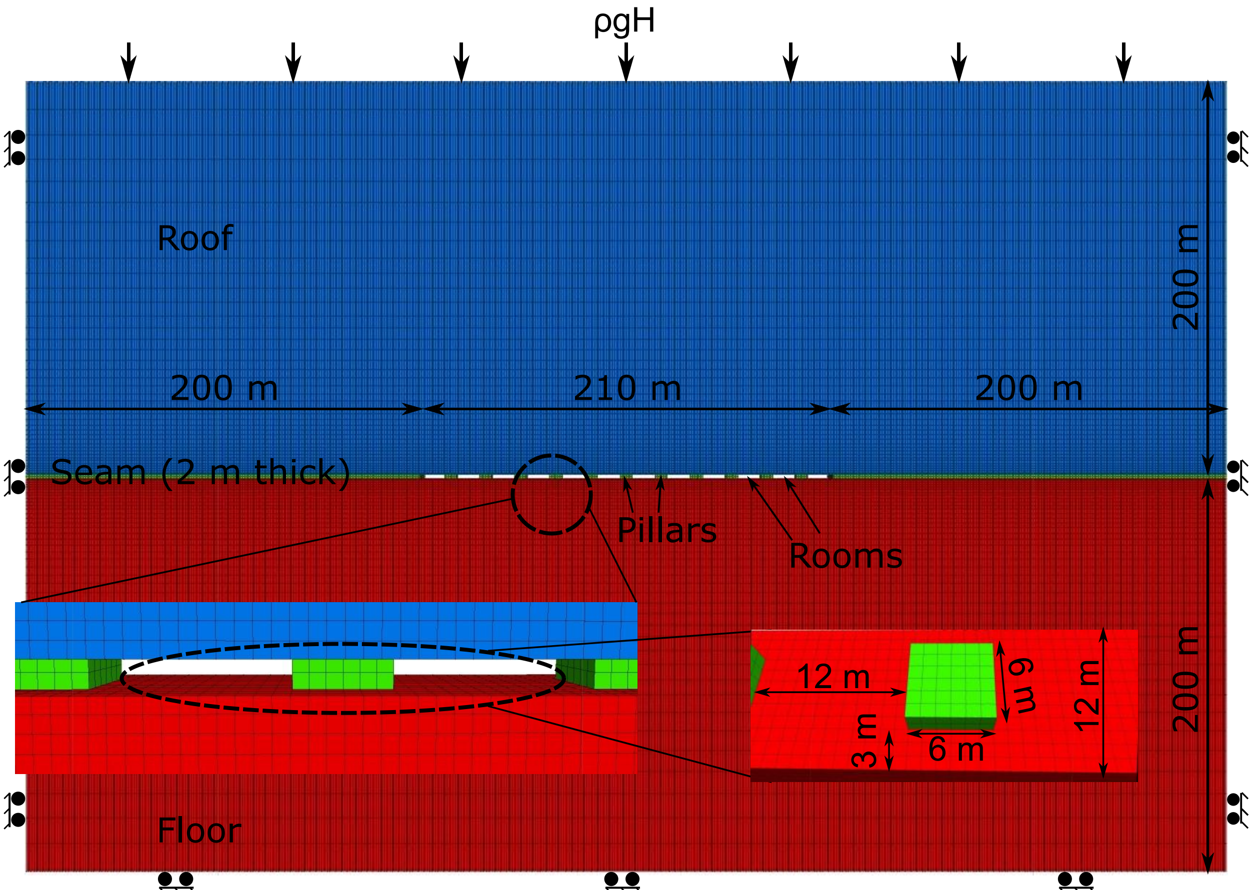

Fig. 3.6 FLAC3D model of the simulated layout.

The pre-mining stress was of gravity type. The physical and elastic properties of the rock mass are summarised in Table 3.6.

Table 3.6 FLAC3D model input parameters.

Parameter	**Value**
Young's modulus, *E*	45
Poisson's ratio, *ν*	0.25
Density, *ρ*	2700 kg/m^3
Constitutive behavior	Linear elastic model

3.3.5 MLPNN and FLAC3D comparison

After the simulation in FLAC3D, the average pillar stresses were recorded together with the corresponding pillar distances from the abutments. The pillar stress in FLAC3D was recorded as the average along the central section of each pillar. This was done to suppress the mesh-dependent effects at the corners of the pillars and to avoid stress relaxations around the periphery of the pillar. Figure 3.7 is a stress contour plot of the numerical simulation. Figure 3.7(a) shows the vertical stress contours for the entire model, and Fig. 3.7(b) and (c) show the closest pillar to the abutment and the centre pillar, respectively. The pillar load increased away from the abutment, as indicated by increasing compressive stresses above the pillars with increasing distance from the abutment (Fig. 3.7(a)). This stress variation is also illustrated in Fig. 3.7(b) and (c). The vertical stresses within the pillar are more concentrated in the furthest pillar from the abutment, Fig. 3.7(c), compared to the closest pillar to the abutment, Fig. 3.7(b).

The pillar stresses in the FLAC3D simulated mine layout were then predicted using the MLPNN model. Figure 3.8 is a comparison of FLAC3D, and the MLPNN predicted result. Figure 3.8(a) represents the calculated pillar stresses plotted against the pillar location concerning the abutments. In this case, pillars 1 and 11 are the closest to the abutments, while pillar 6 is the furthest from the abutment. The MLPNN model predictions closely agree with the simulated pillar stresses in FLAC3D. This close agreement implies that the MLPNN model has been sufficiently trained to allow stress predictions to consider the influence of nearby abutments.

Figure 3.8(b) shows a regression plot of the MLPNN predictions and the FLAC3D simulated results. The MLPNN model can make reasonably accurate predictions with a correlation coefficient equal to 0.99. Conversely, MLPNN model stresses are consistently smaller than FLAC3D stresses. The negligible difference may result from the inherent differences in problem formulation between FLAC3D (domain and differential method) and DDM (boundary and integral method), and the slight difference in pillar stress computing procedures used for DDM and FLAC3D in this analysis.

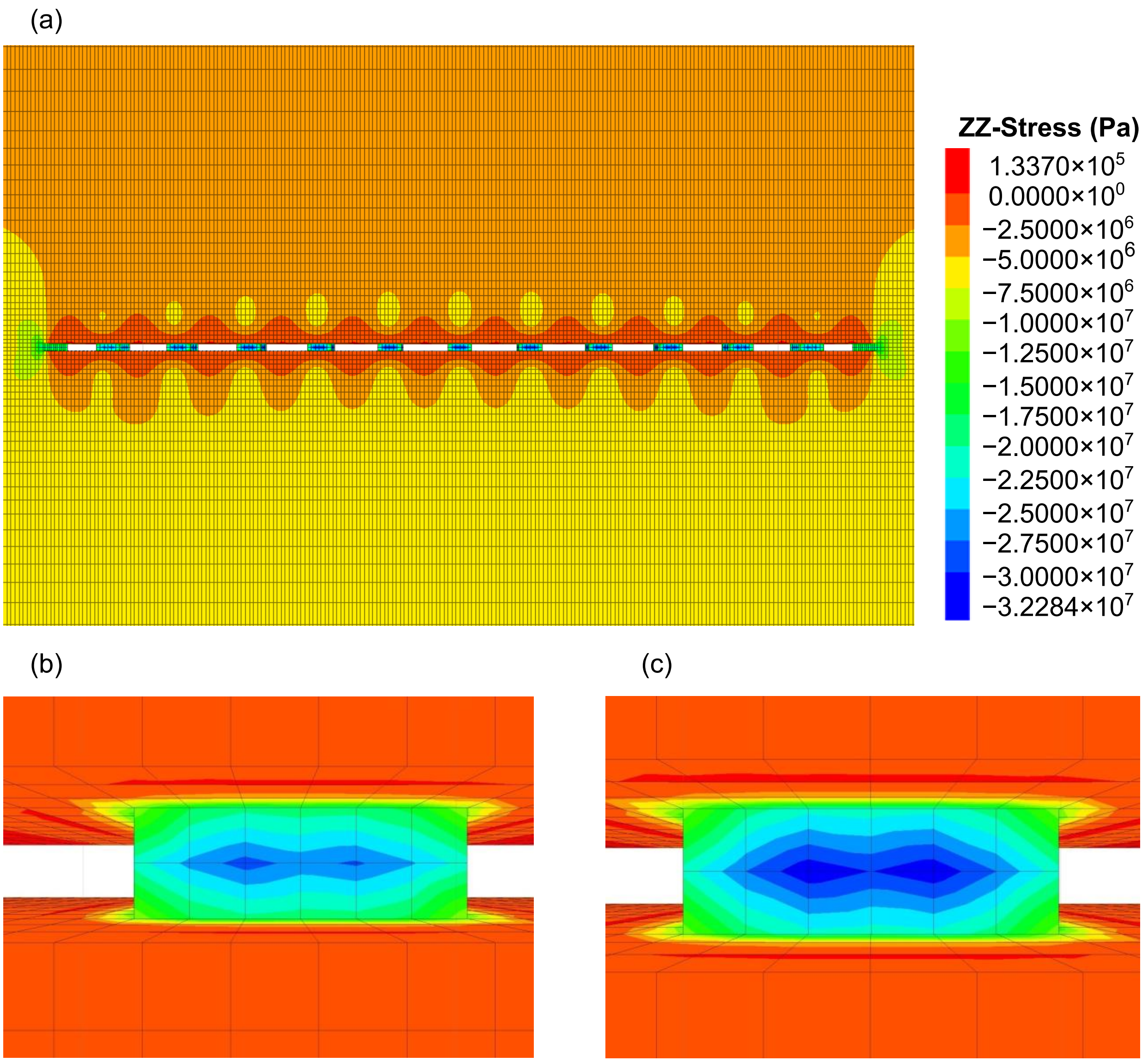

Fig. 3.7 Vertical stress contours in FLAC3D. (a) Entire model, (b) closest pillar to the abutment, and (c) most centre pillar.

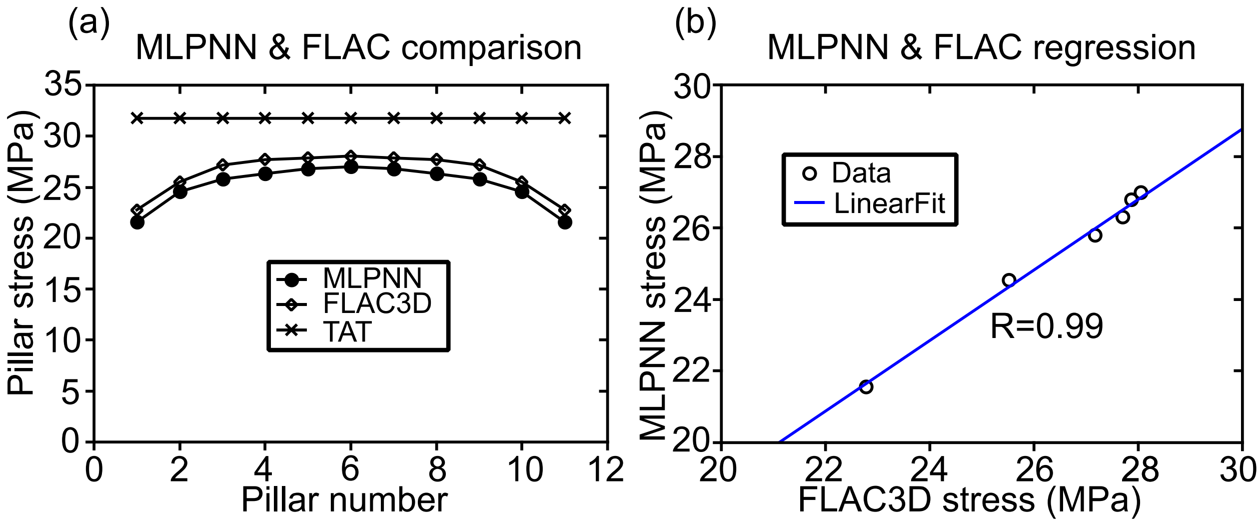

Fig. 3.8 Verification of MLPNN by FLAC3D. (a) Stress comparisons, and (b) regression analysis.

3.4 MLPNN model extension to panels with evenly spaced barrier pillars

Room-and-pillar mine layouts that encompass regular pillars arranged between evenly spaced barrier pillars are common. This arrangement is helpful as it shields against large-scale collapses. Pillars in such arrangements have part of their load borne by these barriers, and their stresses cannot reach the TAT stress asymptote. In such a scenario, a clever way to estimate the maximum and minimum pillar stresses within the panel can be helpful. Pillar design can be improved when engineers at such mine sites are presented with that method. The MLPNN model was adapted to these layouts, as illustrated in the following sub-sections.

3.4.1 Adapting MLPNN model

Figure 3.9 is a simulation of a mine layout by DDM. The layout is at a depth of 400 m, and the *IBS* is 100 m. The extraction ratio within the panel is 83.3%. The region of interest is the central part of the pillar stress plot, as this is where the main abutments no longer influence the pillar stresses, a realistic scenario within extensive panels. The troughs in Fig. 3.9 indicate the positions of the barrier pillars. $\sigma_{\max}$ and $\sigma_{\min}$ are the maximum and minimum pillar stresses in the panel, respectively.

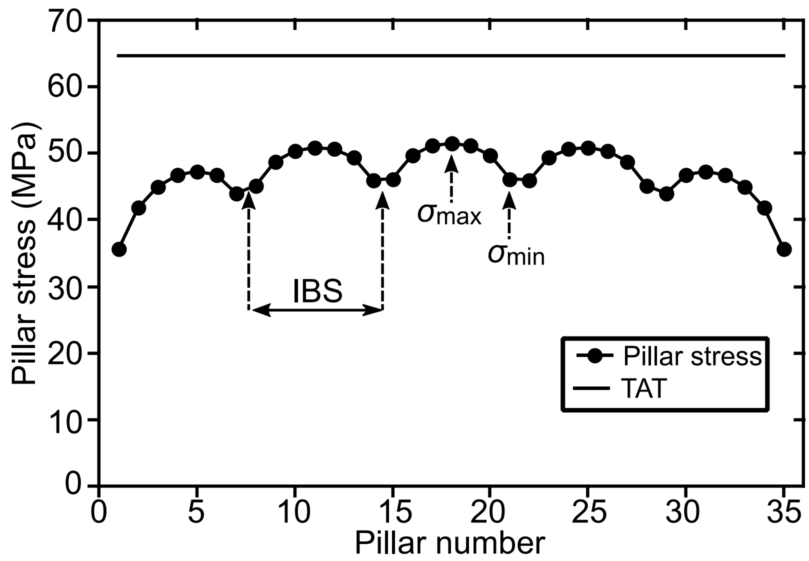

Fig. 3.9 DDM simulated pillar stresses of a large panel with barrier pillars.

It is visible from Fig. 3.9 that σ_{max} can never approach the TAT stress because the barrier pillars, with their higher stiffness, are carrying the extra load that was supposed to be exerted on the panel pillars. From previous simulations and predictions, it became evident that pillar loads increase with the increasing size of the panel. Thus, it is understandably logical to assume that σ_{max} and σ_{min} are bound between the maximum pillar stress in a large panel (≥700 m panel width according to the database) and the maximum stress (IBS_{max}) in a panel with a width equivalent to *IBS*. This logical assumption is made more evident by visualising Fig. 3.10.

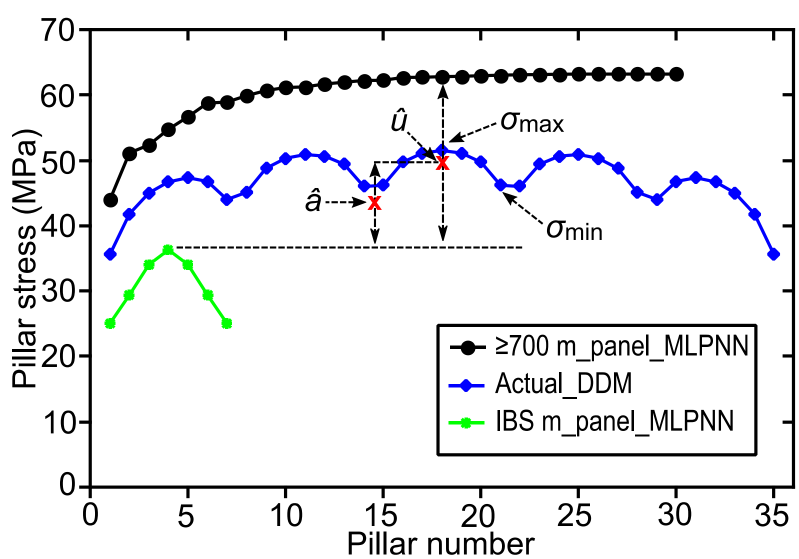

Fig. 3.10 Relationship between pillar stresses by MLPNN and actual DDM simulations.

The average ($\hat{u}$) of the MLPNN predictions of the maximum stresses in a large panel and IBS_{max} is reasonably close to σ_{max}. Similarly, the average of $\hat{u}$ and IBS_{max} is approximately equivalent to σ_{min}. This average of $\hat{u}$ and IBS_{max} is termed $\hat{a}$. The above trend was the same when comparing DDM simulations and MLPNN predictions for other pillar layouts. Multivariate regression analysis of these comparisons was then performed to develop models that can estimate σ_{max} and σ_{min}. The hydraulic radius of the barrier pillars was initially considered as an independent variable. However, its observed significance level (*P*-value) from the statistical analysis was found to be greater than 0.05. As a result, it was excluded from the subsequent models used to estimate σ_{max} and σ_{min}. Equations 3.13 and 3.14 are the adapted MLPNN model equations to estimate σ_{max} and σ_{min}, respectively, in any large panel layout with equally spaced barrier pillars.

$$\sigma_{max} = 0.36 + 1.02\hat{u} \tag{3.13}$$

$$\sigma_{min} = 1.12\hat{a} - 1.57 \tag{3.14}$$

where σ_{max} , σ_{min}, $\hat{u}$ and $\hat{a}$ are all in MPa.

3.4.2 Case study application

Equations 3.13 and 3.14 were applied to an actual room-and-pillar mine — presented in Subsection 2.2.2 — used for a case study in Zimbabwe. The mine is a large-scale hard rock operation with typical mining depths averaging 180 to 350 m. Pillars at the mine are usually 6 m × 6 m and the rooms are with 6 m vent holings and 12 m boards. The average UCS of the pyroxenite rocks at the mine is 205 MPa (according to mine reports and tests —Appendix A— by the author performed at the Rock Mechanics Laboratory, Hokkaido University). The density of the rock is approximately 3200 kg/m^3. *E* varies between 90 – 130 GPa. However, the deformation modulus of the rock mass (*E*' = 75 GPa) was estimated, according to Zhang and Einstein (2004), using a rock quality designation (RQD) value of 90 (according to the mine reports). The mine employs a robust pillar layout system to ensure regional stability; thus, panel pillars are accompanied by evenly spaced barrier pillars, as indicated in Fig. 3.11.

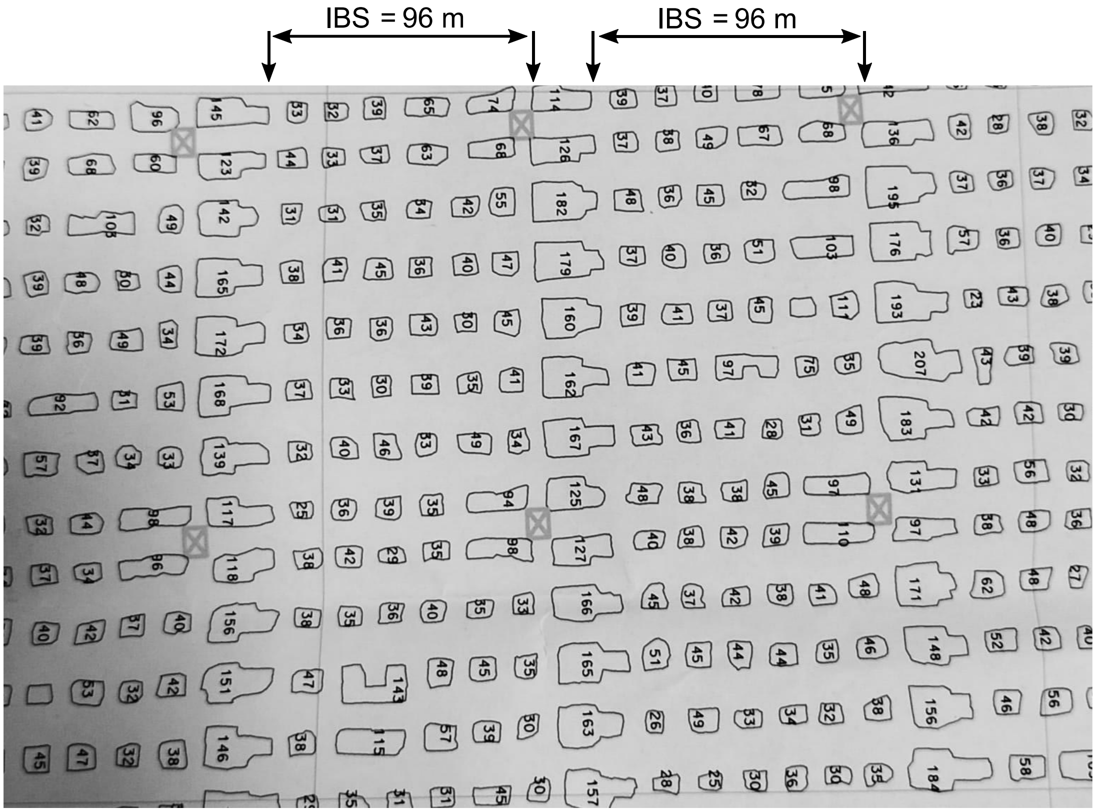

Fig. 3.11 Snap of pillar layout at the case study mine.

The steps to determine $\sigma_{\max}$ and $\sigma_{\min}$ for this mine are as follows:

1) Identifying the features of the mine layout and rock mass properties to input into the MLPNN model. For this case study (e = 83.3%, E = 75 GPa, H = [180, 200, 250, 300, and 350 m], panel width = [700 m and IBS], m = 1.5, TAT = [28.59, 31.76, 39.71, 47.65, and 55.59 MPa], DfA = [350 m and 48 m for 700 m and IBS panel widths respectively]). Notice, H is taken to represent the range of mining depths at the mine, and the corresponding TAT stress is calculated using a density of 2700 kg/m^3, according to the database. However, the predicted stresses by MLPNN must be corrected to reflect a density of 3200 kg/m^3 at the mine using simple proportions.

2) Prediction of maximum pillar stress for a large panel at a depth of 180 m. The MLPNN prediction was obtained as 28.73 MPa and corrected to 34.05 MPa by proportion.

3) Prediction of IBS_{max} at a depth of 180 m. This was predicted as 15.46 MPa and corrected to 18.32 MPa by proportion.

4) Calculation of averages, $\hat{u}$ (26.19 MPa) and $\hat{a}$ (22.25 MPa).

5) Substitution of $\hat{u}$ and $\hat{a}$ into Eqs. 3.13 and 3.14 to obtain $\sigma_{\max}$ and $\sigma_{\min}$. Finally, $\sigma_{\max}$ and $\sigma_{\min}$ were obtained as 27.07 MPa and 23.35 MPa, respectively.

Steps 2 to 5 were repeated for the other mining depths of 200, 250, 300, and 350 m, and the results are summarised in Table 3.7. FoS is used at the mine to judge the stability of pillars. Pillar strength at the mine is calculated using the Hedley and Grant formula (Eq. 2.1). *K* at the mine is taken as 0.33UCS, and the typical mining height is 1.8 m.

Table 3.7 Summary of pillar stress estimations for the case study mine.

		MLPNN				**TAT**	
Depth, *H*	**P_s**	**σ_{max}**	**FoS**	**σ_{min}**	**FoS**	**Stress**	**FoS**
(m)	**(MPa)**	**(MPa)**	**-**	**(MPa)**	**-**	**(MPa)**	**-**
180	106.63	27.07	3.9	23.35	4.6	28.59	3.7
200	106.63	30.29	3.5	26.39	4.0	31.76	3.4
250	106.63	37.73	2.8	33.63	3.2	39.71	2.7
300	106.63	44.36	2.4	40.68	2.6	47.65	2.2
350	106.63	51.46	2.1	47.99	2.2	55.59	1.9

Pillar designs are acceptable if the FoS is greater than 1.6. The FoS calculated in Table 3.7 reasonably agrees with those obtained from a mine-wide FLAC3D numerical simulation (Fig. 3.12) performed at the mine. The findings of the simulations revealed that most of the panel pillars have FoS ranging from 3 to 5, and other proportionately fewer panel pillars between 2 and 3. FoS greater than five was only observed on the barrier pillars (grey stripes in Fig. 3.12). Although this comparison was not aimed at specific pillar stress measurements, the FoS values are reasonably within similar magnitudes, thus proving that the MLPNN-adapted pillar stress estimation procedure can approximate pillar stresses in similar applications. Table 3.7 also indicates the calculations for the TAT approach. The TAT method tends to be conservative because the panel pillars near the lines of barrier pillars or any permanent abutments carry smaller stresses than predicted by the TAT method, regardless of the IBS.

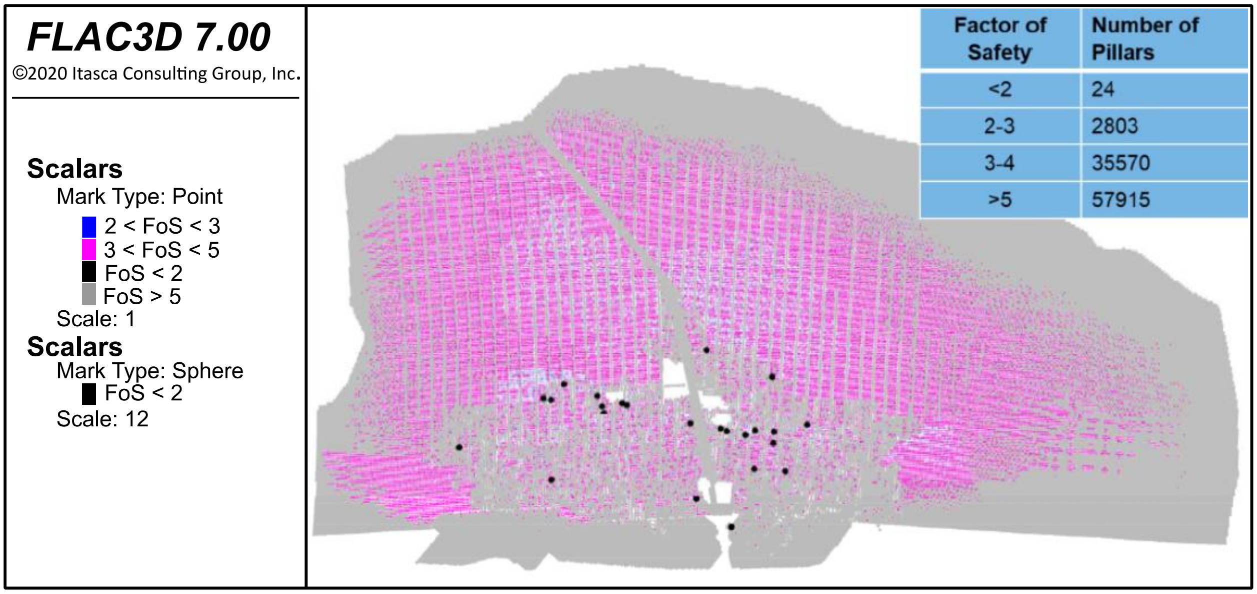

Fig. 3.12 Mine-wide FLAC3D simulation at the case study mine (mine reports).

3.5 Discussion

The main objective of this Chapter was to train a machine learning model capable of estimating average vertical pillar stresses while considering the influence of abutments. As presented in the analysis, an MLPNN model was successfully trained on a numerically developed database.

3.5.1 Overall analysis of model

The success of building any machine learning model is hinged on the features selected for the database. Several features/factors are understood to influence vertical stresses in room-and-pillar mines. The parametric analysis in this study underlined that several factors (e, E, H, panel width, and DfA) affect pillar stresses. The density of the overlying strata, as well as the parameters H and e, are commonly included in most empirical equations for estimating pillar stresses. However, the panel width and relative position of a pillar from the abutments significantly influence how pillar stresses are distributed. The complexity introduced by these additional parameters has been handled with a reasonable degree of success by the MLPNN model.

From the numerical simulations performed in this analysis, it was observed that the panel width significantly influences pillar stresses. Also, the DfA of the pillar is critical in estimating pillar stresses. In some parametric analysis that prompted the idea in Chapter 5, when the DfA was roughly more than 90 m, the influence of the abutments (unmined host rock) disappeared. This distance varied between 90 – 120 m, depending on the panel width-to-depth ratio. This distance agrees with the results of Hauquin et al. (2016), in which the authors concluded that their quadratic and linear equations for pillar stress estimation had high variances within approximately 72 m of the abutments. The high variances may imply that panel widths of less than 250 m (two times the DfA of 120 m since 120 m will be the centre of the panel) can have significantly low maximum pillar stresses compared to their corresponding TAT stresses. MLPNN predictions of the centre pillar stress (maximum stress) in such small panels were significantly smaller than the TAT stress as H increased, an observation also reported (Roberts et al., 2002). The variation in pillar stress introduced by different panel widths and respective pillar DfAs has been effectively addressed by the MLPNN model.

It is well understood that a more significant portion of the overburden weight is transferred to the abutments in narrow panels. Similarly, when the panel widths increase, assuming H remains constant, the deflection of the overburden also increases, and thus more load is transferred to the pillars. The numerical models in DDM also clearly indicated a decrease in pillar loads for the pillars closer to the abutments. Logically, this is because the flexural displacement of the overburden decreases close to the abutments. The proximity of the stiff abutment causes this decrease, and the load of these peripheral pillars decreases. Thus, including panel width and DfA in the database enabled the MLPNN model to capture this phenomenon (which is absent in other techniques such as TAT, quadratic, and linear equations) and predict more accurate pillar stresses.

The analysis of the parameters also indicated that the distribution of pillar stress is mainly influenced by geometrical parameters at the mine. Therefore, in similar studies, much emphasis must be placed on these parameters rather than the rock deformation parameters. Although not directly compared with other pillar stress estimation techniques, such as the quadratic and linear equations, the MLPNN model has sufficiently addressed the drawbacks of these available techniques in capturing the effect of abutments on pillar stresses.

3.5.2 Applicability of the proposed MLPNN model

The MLPNN model was trained using seven variables that can quickly be evaluated for underground room-and-pillar mines. The model is typically applicable in regular pillar outlines. In the case of large panel widths (more than 700 m), the TAT technique can be used to determine stresses in the centre of the panel. For mine layouts that use narrow panel widths (typically less than 300 m) enclosed between regional pillars, the MLPNN model gives the best vertical pillar estimates. When the stability of individual pillars close to the abutments is considered, the MLPNN model is useful. In such cases, the model helps avoid constructing complex numerical models that may require several days to converge.

The model is superior in mine layouts comprising extensive panels separated by equally spaced barrier pillars. TAT and the quadratic equation can significantly overestimate the pillar stresses in such scenarios, while this model can give more approximate pillar stresses following the procedures outlined in Subsection 3.4. In such cases, pillar stresses are restricted from approaching the TAT stress asymptote because of the higher stiffness of the barriers, which carry more load than the panel pillars under consideration.

It is critical to emphasise that the MLPNN model was developed assuming flat ore seams and can thus give accurate predictions for such situations. However, the model can still be applied to slightly inclined ore seams similarly as the classic TAT, which has been customarily used.

Finally, the steps in developing the MLPNN model insinuate the possibilities of optimising the IBS. The 90 – 120 m distance beyond which abutments have been seen to cease influencing pillar stresses can be a starting point to optimise IBS distances in mines interested in controlling large-scale pillar collapses. This will be addressed in Chapter 5 of this dissertation. Also, the model can increase room-and-pillar operations profitability by increasing the extraction ratios in narrow panels and areas close to the abutments. The maximum distance from the abutment where this increased extraction can occur is subject to further studies.

3.5.3 Limitations

The MLPNN model has some limitations based on how the database was developed. The model cannot accurately estimate stresses for pillars with irregular shapes because the model does not include irregular pillar outlines. Also, the MLPNN model can only be used for single exploited ore seams and cannot be used for multiple mined ore seams. The MR was considered a unity in developing the database; thus, this MLPNN model cannot be accurately applicable in cases of different modulus ratios. However, to establish the model's reasonable range of applicability, the effect of MR was simulated in DDM. The simulations comprised models situated at a mining depth of 200 m, and all other parameters were unchanged except MR (MR = 0.5, 0.75, 1, 1.25, 1.5, and 2). Taking MR = 1 as the actual result, absolute percent error was used to illustrate the effect of MR. If the acceptable error margin is within 5% the model can be judiciously used within a MR range of 0.5 to 2 as indicated in Fig. 3.13.

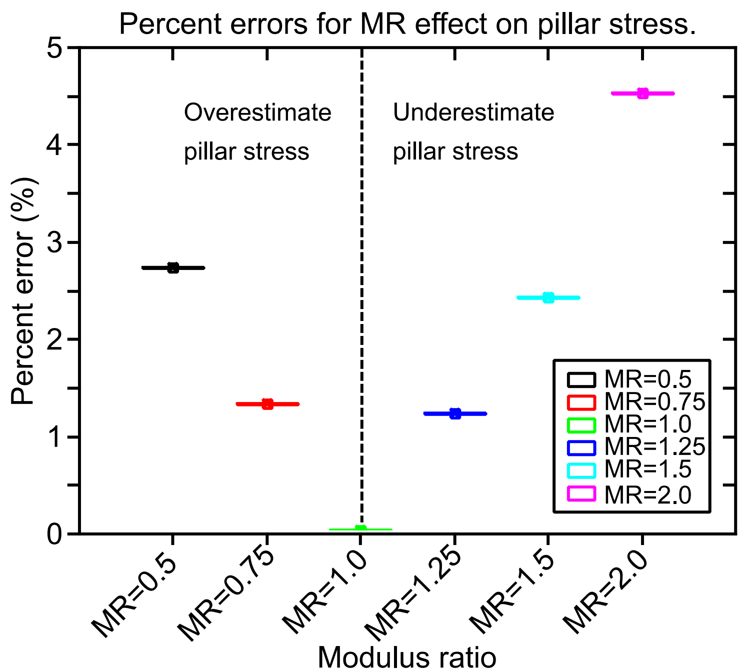

Fig. 3.13 Effect of MR on vertical pillar stresses.

It should be noted that the elastic and homogenous rock mass conditions assumed in this analysis are simplifications of actual rock mass conditions and may have a considerable impact on the predictions that this model can produce. Rock masses are generally discontinuous (bedding planes and discontinuities may separate pillars and host rock) and often have anisotropic and heterogeneous properties. The elastic and homogenous assumption adopted in developing the MLPNN model may not accurately represent the stress field. The model is particularly recommended as a first approach to design. During mining, when the pillars have been fully excavated, the importance of physical inspections, and deformational and stress measurements can never be over emphasised. Further research is required to compare MLPNN predictions with in-situ stress measurements from selected underground pillars to enhance understanding of the model's limitations.

This model is also limited to the design of non-yield pillars where all the analysed pillars are intended to remain intact. However, in some cases the pillars can attain their strength level and fail; thus, deviating from linear elastic behaviour. Additionally, if the failure of other pillars in the system occurs, the model cannot handle the redistributed stresses, and other separate studies may be needed in such scenarios.

CHAPTER 4 PILLAR STRENGTH ESTIMATION FRAMEWORK

4.1 Introduction

The concept of this Chapter is derived from the description of various pillar conditions in a case study mine presented in Subsection 2.2.2. This description was considered to emphasise that pillars may behave differently in reality, even if they have the same design specifications. To address this issue, this Chapter introduces a framework that involves ongoing detailed pillar mapping, risk management decision making, numerical modelling, and an analytical hierarchy process (AHP) to estimate pillar strength.

4.2 Proposed framework

The previous brief discussion of actual pillar conditions at a case study mine (Subsection 2.2.2) indicated that, at every mine, pillars with identical design specifications can behave differently in reality. Some of these pillars can be unstable and it would be convenient for the mining industry to have an inexpensive methodology available that can easily be used to identify such pillars to stabilise them. Figure 4.1 presents the proposed framework of the methodology to estimate pillar strength considering underground pillar mapping, risk management decision making, AHP implementation, and numerical modeling. This framework is divided into six stages: detailed pillar mapping, numerical modelling, AHP implementation, estimation of pillar strength variance (Δ_s), pillar strength estimation, and validation. These stages are described in the following sub-sections.

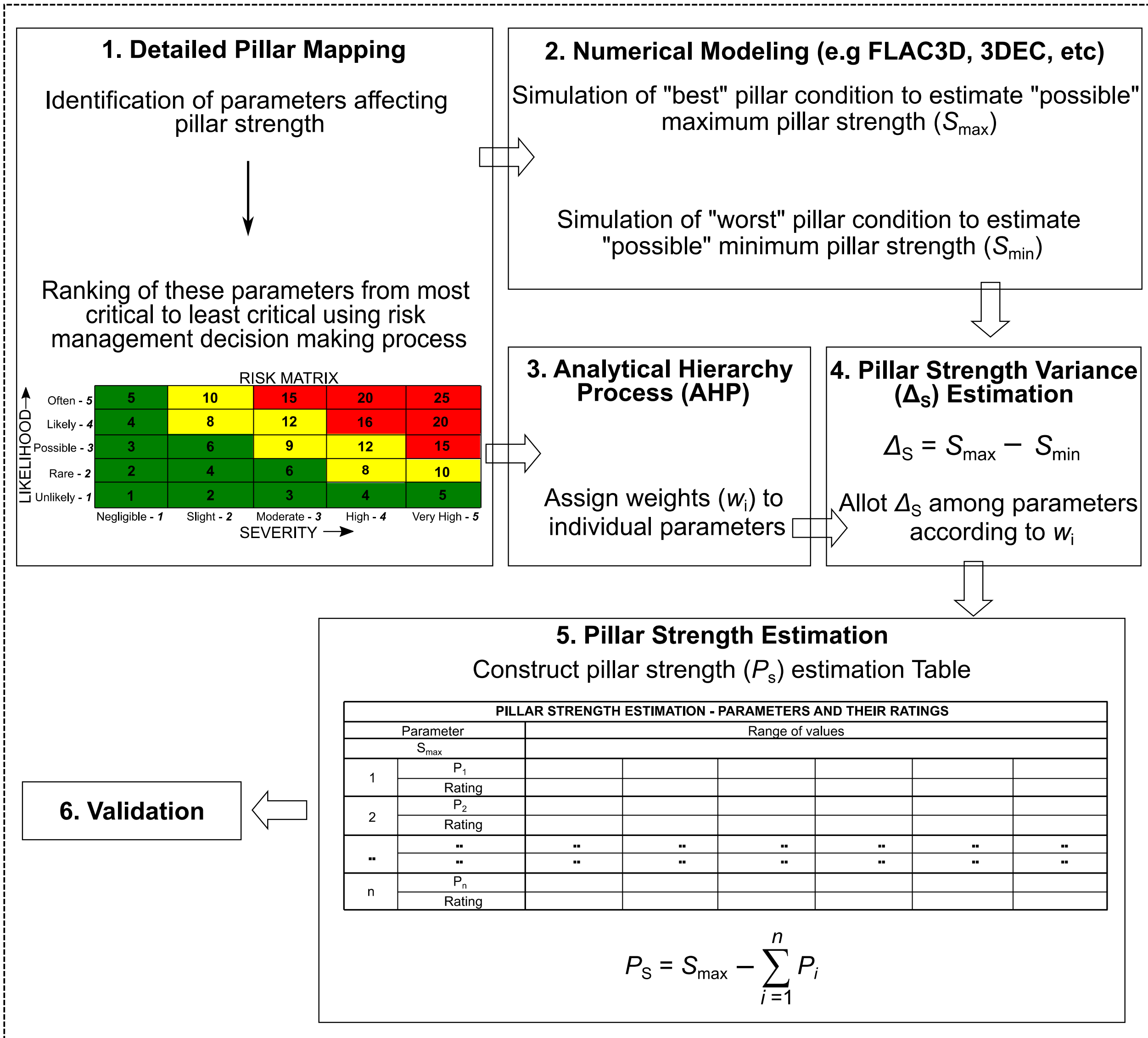

Fig. 4.1 Proposed framework for estimating pillar strength.

4.2.1 Detailed pillar mapping

Observational methods and ongoing underground pillar monitoring are critical activities in every room-and-pillar mine. These activities enable site engineers and mine operators to have better knowledge of mining domains with the most stable, deteriorating or even failed pillars. A thorough analysis of deteriorating and failed pillars is necessary to understand the parameters negatively affecting the stability of the pillars. Consequently, areas of interest that can yield a reasonably adequate database of pillar conditions are then analysed. Once the areas of interest are identified, a detailed pillar mapping should be done to accomplish two things. Firstly, the critical geometrical, geotechnical, and rock mass parameters affecting pillar strengths are identified. Secondly, these parameters must be ranked from most critical to least critical using a simple risk management decision making process.

Ranking of parameters must be accomplished by resident rock mechanics and mining engineers to gain solid input and feedback from diverse expertise. The risk matrix in combination with linear or non-linear risk ranking scales can be used to achieve a systematic ranking of the parameters. The likelihood that a parameter in question is present in each pillar and its corresponding severity to pillar stability is considered, and a “risk level” is assigned to each parameter. The magnitudes of the “risk levels” are then used to rank the parameters. This ranking allows treatment of the parameters more systematically than by some random ranking order based on engineering judgement only. The information from this detailed pillar mapping activity is used as inputs to the following numerical modelling and AHP stages.

As an example, the parameters critical to pillar stability at the case study mine are namely: J1 discontinuity, FwF where it exists, dip of the reef, blast damage (BD), *w:h* ratio, and rock mass quality. Table 4.1 summarises a preliminary ranking of the parameters at the mine using the risk matrix. It is important to note that the "risk levels" mentioned in Table 4.1 are not the actual representation of risk. Rather, they are used to systematically rank the parameters that affect the strength of pillars at the mine.

Table 4.1 Preliminary ranking of parameters at the mine using the risk matrix.

Parameter	Likelihood	Severity	“Risk Level”
J1	Likely	Very high	20
FwF	Likely	High	16
Reef dip	Often	Moderate	15
BD	Likely	Moderate	12
w:h ratio	Rare	Very high	10
Rock mass	Likely	Slight	8

4.2.2 Numerical modelling

Numerical methods are advanced computational techniques used to solve complex engineering problems. This approach allows for the consideration of complex material behaviour and boundary conditions. Numerical methods are widely acknowledged for providing realistic estimates of pillar strengths. The development of the pillar strength estimation framework depends on simulating the "best" and "worst" pillar conditions at the mine based on the findings from detailed pillar mapping activities. The numerical simulation of the "best" and "worst" pillar conditions will yield possible maximum ($S_{\max}$), and minimum ($S_{\min}$) theoretical pillar strengths evaluated in MPa, respectively. In actual practice, it is not feasible to capture these two conditions accurately and explicitly. The purpose is to reasonably facilitate the evaluation of the discrepancy introduced by the various parameters that affect pillar strength. Table 4.2 summarises a preliminary assessment of possible "best" and "worst" pillar conditions at the case study mine. It is assumed that the rock mass conditions for the "worst" case are those of the FwF.

Table 4.2 "Best" and "worst" pillar conditions for numerical simulations.

Parameter	**Description**	**"Best"**	**"Worst"**
w:h ratio	–	3	2
Reef dip	(°)	0	15
J1	Dip (°)	–	39
	Spacing (m)	–	1.1 – 15
	Cohesion (*c*) (MPa)	–	0.5*
	Friction angle (ϕ) (°)	–	29
	Dilation angle (°)	–	10 – 12
FwF	Thickness (m)	–	0.5
	Cohesion (MPa)	–	1.5*
	Friction angle (°)	–	15 – 25
Rock mass	GSI#	60 – 75	20 – 30
	Cohesion (MPa)	15*	1.5
	Friction angle (°)	47	25
BD	Disturbance factor	0.8*	0.9*

#GSI: Geological strength index *Estimated

If a mine has experienced localised pillar failures, $S_{\min}$ is assumed to be the maximum pillar stress that the failed pillar was exposed to. TAT or an advanced DDM can be used to obtain a crude estimate of pillar stresses. These estimates may not be very accurate, but the inaccuracies are of little consequence given that the intended use of $S_{\max}$ and $S_{\min}$ is not to dogmatically match the pillar strengths at the mine, but to evaluate the reduction in strength that can reasonably be related to more general observations and behaviour of pillars.

Pillar strength can be estimated using numerical software such as FLAC3D or 3DEC. Pillar geometries, rock mass, and discontinuity properties are considered in the simulations. Discontinuity properties assumed within the two pillar cases are used to generate discrete fracture networks in the selected numerical software. Displacement at a constant rate is applied at the boundaries of a simulated pillar, and a stress versus time step plot is generated as the numerical simulation progresses. The pillar strength for each case is evaluated as the point at which the pillar starts to exhibit strain-softening behaviour.

4.2.3 Analytical Hierarchy Process

The AHP (Saaty, 1977, 1980) is a decision making technique used to establish priorities in multivariate environments. This technique is primarily used for establishing priority weights for alternatives (elements of the decision making process). In the pillar strength estimation framework problem, the elements of the decision making process are the parameters identified and ranked in Subsection 4.2.1. Initially, a pair-wise comparison matrix $A = \left[a_{ij} \right]$ is constructed with the engineer's assessments a_{ij}, evaluated on a subjective ratio scale (Saaty, 1977) of the relative dominance of parameter *i* over parameter *j*. Matrix *A* is positive and satisfies the reciprocal characteristic $a_{ji} = 1/a_{ij}$.

From matrix *A*, a procedure called prioritisation is used to determine the priority weights w_i, $i = 1, 2, ..., n$, where *n* is the number of parameters considered in the framework, $w_i > 0$, and $\sum_{i=1}^{n} w_i = 1$.

There are several methods of prioritisation, but the additive normalisation method (Saaty, 1980) can be considered here because of its simplicity and frequent use. The vector w of the priority weights is determined by dividing each element in each column of matrix *A* by the corresponding sum of the elements in this column. The row summations of the normalised elements are taken and finally, each resulting sum is divided by the rank of matrix *A*. A preliminary determination of priority weights for the parameters at the case study mine is summarised in Table 4.3.

Table 4.3 Priority weights for parameters at case study mine.

Parameter	**Weight (** w_i **)**
J1	0.355
FwF	0.246
Reef dip	0.165
BD	0.106
w:h ratio	0.079
Rock mass	0.049

The final step is to check the consistency of the engineers in constructing matrix *A*. The consistency ratio (CR) (Saaty, 1977) is calculated, in two steps, to judge the consistency. Firstly, the consistency index (CI) is evaluated using Eq. 4.1:

$$\mathrm{CI} = \frac{\lambda_{\max} - n}{n - 1} \tag{4.1}$$

where n is the number of parameters or simply the rank of matrix *A*, and $\lambda_{\max}$ is the maximum eigenvalue of matrix *A*. Secondly, CR is calculated using Eq. 4.2. The random index (RI) in Eq. 4.2 depends on the rank of matrix *A* and can be easily obtained from a simple table developed by Saaty (1980).

$$\mathrm{CR} = \frac{\mathrm{CI}}{\mathrm{RI}} \tag{4.2}$$

CR must be lower than 0.10 otherwise the decision makers were inconsistent, and matrix *A* must be re-evaluated. CR corresponding to the weights in Table 4.3 is 0.048. The implementation of the AHP to derive weights to capture the relative importance of the parameters in the pillar strength estimation framework is shown in Fig. 4.2.

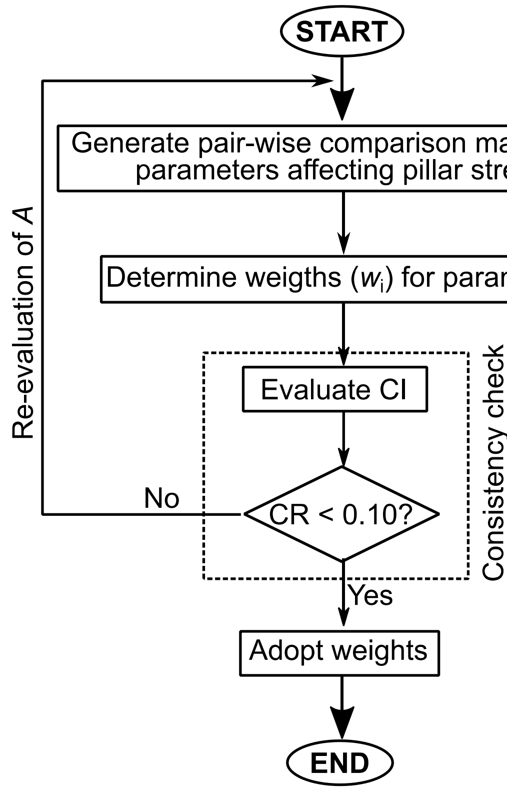

Fig. 4.2 Flow of the AHP to determine priority weights.

4.2.4 Estimation of pillar strength variance

The pillar strength variance (Δ_S), MPa, is then determined from the pillar strengths S_{max} and S_{min} resulting from the numerical simulation. Δ_S is necessary to capture the total magnitude of pillar strength reduction introduced by the parameters from the pillar mapping procedure. Equation 4.3 is used to calculate Δ_S.

$$\Delta_S = S_{\max} - S_{\min} \tag{4.3}$$

Considering the priority weights w_i, Δ_S is allotted among each parameter using the relationship described in Eq. 4.4:

$$S_i = w_i \times \Delta_S \tag{4.4}$$

where S_i (MPa) corresponds to the magnitude of the portion of pillar strength that parameter *i* is reducing from S_{max}. Automatically, parameters observed to dominate the behaviour of deteriorating or failed pillars during the detailed pillar mapping procedure will assume the highest S_i and vice versa. For example, most deteriorating pillars at the case study mine are associated with the J1 joint set. If the parameter ranking and AHP procedures are carefully implemented, the J1 joint set should assume a relatively high priority weight and consequently high S_i. In addition, the attributes of J1 such as c, ϕ, roughness, and degree of weathering should be evaluated and considered as these can strongly influence the assigning of ratings to these attributes in the final pillar strength estimation procedure following.

4.2.5 Pillar strength estimation

Resulting pillar strength influencing parameters, their corresponding S_i values, and the attributes for each parameter are used to develop a table for ultimately estimating pillar strength (P_s). This P_s is the target variable for the pillar strength estimation framework and should not be confused with the other pillar strengths previously discussed. The range of values for the attributes of each parameter identified from the detailed pillar mapping procedure is decided upon. To avoid arbitrary allocation of S_i among the range of values for attributes, AHP is used again to assign weights to different categories of attributes. The format of the table (Table 4.4) for estimating P_s is very similar to rock mass classification tables used in the rating of rock masses.

Table 4.4 Pillar strength (P_s) estimation table.

PILLAR STRENGTH ESTIMATION – PARAMETERS AND THEIR RATINGS					
Parameter		**Range of values**			
S_{max}					
1	P_1				
	Rating				
2	P_2				
	Rating				
..	…	…	….	…	…
	…	…	….	…	…
n	P_n				
	Rating				

To ensure consistency and logic, the maximum rating for an attribute of a particular parameter must be equal to the S_i of that parameter. Equation 4.5 is used to finally arrive at the pillar strength (P_s):

$$P_s = S_{\max} - \sum_{i=1}^{n} P_i \tag{4.5}$$

where P_s is in MPa, n is the number of pillar strength reduction parameters in Table 4.4, and P_i is the magnitude of strength (MPa) that an attribute of parameter i is subtracting from $S_{\max}$.

4.2.6 Validation

Validation is a crucial step in the framework. If any of the pillars have failed at the mine, the P_s determined through the framework should be compared to either the estimated strength of the pillars evaluated using a numerical model, or the estimated stress of the failed pillars. On the other hand, if there are no failed pillars, such as in the case study mine, deteriorating or unstable pillars can be identified to validate the framework. In this case, numerical models can be used to estimate the strength of the pillars based on typical pillar conditions, which can then be compared to the P_s estimated from the framework.

4.3 Discussion

Estimation of the strength of pillars is critical for their design. However, it is also equally important to estimate, with reasonable accuracy, the strength of these pillars once they are formed. The true conditions of each pillar only become visible to the engineer once the pillar is formed. As previously discussed, the objective of this Chapter was to introduce a new approach for estimating the strength of pillars by combining various useful techniques in a single framework. The techniques involved in the framework include observational methods, risk management decision making, numerical modelling, and AHP.

The accurate evaluation of pillar strength for each pillar at a mine requires a much more complicated formula or tremendous effort and impracticable timeframes to model each pillar numerically. However, the motivation behind this framework is to achieve a suitable trade-off between accuracy and simplicity. The framework has the potential to offer a better way to overcome the weakness of empirical methods, which are only applicable within the confines of the databases used to develop them. The methodology presented in this Chapter can be customised to any room-and-pillar mine. It can be applied to underground pillar monitoring practices to identify potentially unstable pillars that need remedial support. Additionally, it presents a relatively quick method to estimate the strength of pillars during the design stage and also to facilitate easy mapping of pillar factors of safety on mine plans. The procedures of developing the framework also advance the understanding and detailed analysis of parameters critical to pillar stability in that mine.

It is important to consider the limitations of the framework when applying it. Firstly, the pillar strength obtained from the framework is not an absolute measure, but rather an estimate. This is because certain assumptions are made to derive the "possible" maximum and minimum pillar strengths at the mine. However, if detailed underground pillar mapping, sound engineering judgment and numerical modelling are implemented, the errors introduced by these assumptions cannot be too large. Secondly, the framework requires the availability of numerous pillars to geotechnically map. Therefore, it cannot be reliably used in the early stages of mining when few pillars are present or geotechnical information is inferred from development openings. As mining progresses and additional parameters are encountered, the development and operation of the proposed pillar strength estimation framework must be treated as a continuous process that requires regular review and revision.

The significance of the pillar strength estimation framework lies in its customisation to capture the pillar conditions at any mine. Future studies should focus on applying the framework to different case study mines to confirm its validity and identify possible improvements.

CHAPTER 5 REGIONAL SUPPORT SPACING LINEAR MODEL

5.1 Introduction

The Chapter presents a new method for estimating *IBS* simply and efficiently. Estimating *IBS* easily and correctly is essential in room-and-pillar design. This explains the present interest in developing a formula that is simple enough for practical mine applications and yet provides realistic *IBS* values. The Chapter features the principles of TAT and rules of thumb for estimating *IBS* previously described in Section 2.3. DDM was used to conduct large-scale numerical simulations of various room-and-pillar mine layouts, and the resulting data on model input and the corresponding extent of the effects of abutments were compiled into a dataset. Multivariate regression analysis was applied to this dataset to develop a linear model for estimating *IBS*. The linear model was evaluated in the context of the case study mine and an arbitrary hypothetical mine and compared to the rules of thumb. Finally, this Chapter concludes with a discussion on the physical meaning, applicability, limitations, and future research prospects that the proposed linear model opens regarding the design of regional support in room-and-pillar mines.

5.2 Methodology

The following methodology was used to develop and evaluate the linear model for estimating *IBS* in room-and-pillar hard rock mines.

5.2.1 Elastic numerical simulation

A frequently used technique for estimating stresses in mine pillars is numerical simulation. In large-scale tabular layouts, DDM is a well-suited numerical technique to analyse pillar systems, where the plan projection of the mine layout may span several square kilometres. DDM was used in this study to simulate various room-and-pillar mine layouts with different characteristics. NUTEX software (Fujii et al., 1997) was used and this DDM-based numerical code was developed to estimate stresses and displacements in tabular deposits. Several studies have been carried out using NUTEX, including (Fujii et al., 2001; Sinkala et al., 2022).

An elastic numerical approach was used to develop the *IBS* estimating model. This is valid because pillars in shallow room-and-pillar mines should not yield and are designed to remain intact and elastic throughout the mine life.

5.2.2 Linear model development procedure

Several studies have found that the geometry of the mine largely influences the distribution of pillar stresses in room-and-pillar mines (Hauquin et al., 2016; Wagner et al., 2016). Thus, rock mass deformational parameters remained constant for all numerical simulations in this analysis while only geometrical parameters were varied. The manipulated geometrical variables were mining depth (H) and extraction ratio (e, %). Table 5.1 summarises model input parameters and the total number of simulations. The horizontal stress, Young's modulus E or Poisson's ratio v does not affect the calculated stress under the elastic assumption as long as the mined-out areas do not show complete closure.

The simulated numerical models were represented by square plan regions with a side length of 700 m. The numerical model simulation aimed to determine the distance —zone of influence (ZI)— at which abutments no longer affect pillar stresses. Figure 5.1 illustrates how the ZI was determined using the pillar stresses from each simulation. The density does not affect ZI values since they are not determined based on stress magnitude but on the shape of the stress distribution.

Table 5.2 summarises ZI and the variables representing the geometry of each simulation. Multivariate regression analysis of the contents in Table 5.2 was used to develop the IBS model.

Table 5.1 Model input parameter values and the total number of DDM simulations.

Variable	Values	Count	Total simulations
e (%)	55.5, 75, 80, 84, 88	5	
H (m)	100, 200, 500, 800	4	
Young's modulus, E (GPa)	50	1	5 × 4 = **20**
Poisson's ratio, v	0.2	1	
Density, ρ (kg/m^3)	2700	1	

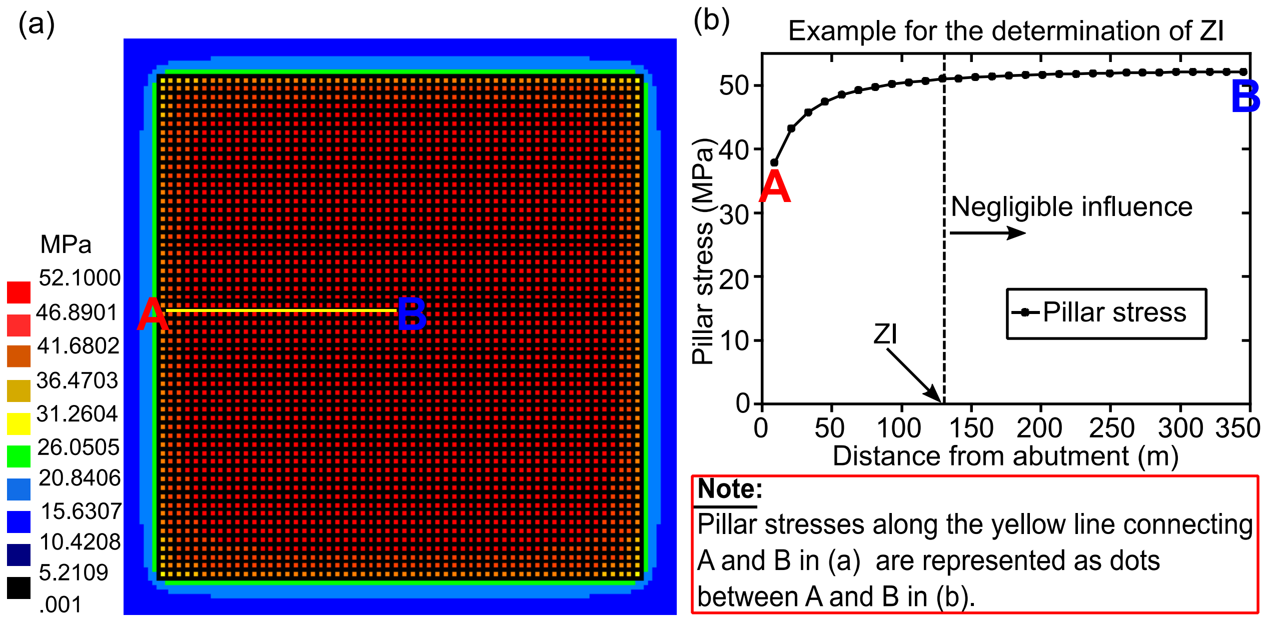

Fig. 5.1 Illustration of procedure to determine ZI. (a) Example NUTEX model indicating the normal stress distribution on the sampled pillars (MPa), and (b) plot of the sampled pillar stresses and the determination of ZI.

Table 5.2 Summary of numerical models' geometry variables and ZI.

Simulation	***H***	***e***	**ZI**	**Simulation**	***H***	***e***	**ZI**
–	**(m)**	**–**	**(m)**	**–**	**(m)**	**–**	**(m)**
1	100	0.56	85	11	500	0.80	140
2	200	0.56	93	12	800	0.80	140
3	500	0.56	100	13	100	0.84	96
4	800	0.56	100	14	200	0.84	116
5	100	0.75	87	15	500	0.84	176
6	200	0.75	100	16	800	0.84	176
7	500	0.75	126	17	100	0.88	103
8	800	0.75	126	18	200	0.88	118
9	100	0.80	92	19	500	0.88	178
10	200	0.80	108	20	800	0.88	178

5.2.3 Evaluation of the linear model

A reliable model for estimating *IBS* should be capable of accurately estimating the spacing of barrier pillars for different mining layouts. Moreover, it should increase the stiffness of the effective pillar system by preventing the maximum pillar stress (σ_{max}) from reaching the *TAT* stress asymptote by a reasonable threshold.

The proposed model was tested on the case study mine and an arbitrary hypothetical mine. The estimation of *IBS* was carried out by considering *H* and *e* for each case. The *TAT* stress was computed using Eqs. 2.2 or 2.3. DDM was employed to develop numerical models of room-and-pillar mine layouts, with in-panel pillars and barrier pillar lines spaced by the corresponding *IBS*. The average vertical pillar stresses obtained with TAT and the stresses of all the pillars along the centre, —analogous to line AB in Fig. 5.1 but considering all pillars from the left to the right abutment— were plotted against the normalised distance of each pillar from the left abutment. The corresponding *H* was utilised to normalise the distance from the abutment.

The proposed model was compared with the rules of thumb for mining depths of 100, 250, and 500 m, considering various extraction ratios. The comparison was conducted using the same procedure described in the previous paragraph. Additionally, I proposed a relatively simple parameter, called delta pillar stress (Δ_{PS}) (Eq. 5.1), to facilitate the comparison.

$$\Delta_{PS} = \frac{TAT - \sigma_{max}}{TAT}, \% \tag{5.1}$$

Δ_{PS} measures how far σ_{max} is from the *TAT* pillar stress. In shallow hard rock room-and-pillar mining, non-yield in-panel pillars are used, which must be able to control the tensile zone of the hangingwall above. Barrier pillars are an additional shield and should only compartmentalise the mining panels and keep the stresses of the pillars below the *TAT* asymptote. Therefore, I suggest that an ideal *IBS* estimating model should have a Δ_{PS} of between 5–10%. If Δ_{PS} is less than 5%, *IBS* is overestimated, and if Δ_{PS} is greater than 10%, *IBS* is underestimated.

5.3 Results

5.3.1 The IBS model

The IBS model was developed using the results of the numerical stress analysis discussed in Subsection 5.2.2. In the regression analysis, ZI was used as the dependent variable. This parameter was used directly to estimate the spacing of barrier pillars due to two fundamental reasons: Firstly, doubling ZI, since the models are symmetrical and ZI is only half, would result in an excessively large *IBS*, which would render the stress management in the pillar system ineffective. Secondly, the effect of barrier pillars on pillar stresses is much smaller compared to the effect of the solid abutments used in the models.

From the above, the outcome of the regression analysis is given by Eq. 5.2. It is this equation that will hereafter be referred to as the IBS Model.

$$IBS = \frac{76}{1000}H + 153.3e - 25.8 \qquad (5.2)$$

where *IBS* is the inter-barrier pillar spacing (m), *H* is the mining depth from surface (m), and *e* is the extraction ratio expressed as a decimal. The model should be able to reasonably estimate the spacing of barrier pillars for various mining layouts and ensure pillar stress management by prohibiting $\sigma_{\max}$, in the system, from reaching the *TAT* stress asymptote by a reasonable threshold.

5.3.2 Application of the IBS model to the case study mine

The validity of the IBS model was first tested in the case study presented in Subsection 2.2.2. For recapping purposes, the mine is a PGM operation, which exploits shallow-seated tabular deposits. This mine is located on the Great Dyke of Zimbabwe, which is a lopolith made up of mafic and ultramafic rocks. The mine is a large-scale shallow hard rock operation with mining depths of less than 425 m. Different extraction ratios are used at this mine depending on the rock mass quality, and mining depth. Additionally, the orebody is bounded by major normal faults, vertical faults, hangingwall faults and the FwF. This FwF is of specific concern to pillar stability and runs parallel and is in the footwall of the reef. These structures produce discontinuities in their vicinity rendering the geology unpredictable and complex.

Examples of pillar cases at the mine are presented in Fig. 2.4. The hybrid pillar conditions depicted in Fig. 2.4 and encountered at the mine pose instability risks. Thus, a robust pillar layout system involving in-panel pillars and evenly spaced barrier pillars is used at the mine to ensure adequate local and regional stability (Fig. 3.11).

DDM and rules of thumb for barrier pillar spacing have been used at the mine to determine IBS. However, due to the tedious process of constantly adjusting the spacing between barriers in the numerical models, the mine employs a constant spacing of 96 m irrespective of the extraction ratio and mining depth. This spacing may have been influenced by the need to position the ore tipping points, which are determined by the specified tramming distances of the mining equipment. Although rock engineering designs must align with practical mining considerations, these two processes should be treated separately. When tipping points are located far from the barrier pillars, the surrounding pillars should be sized appropriately, without relying on the tipping point locations to determine IBS. Table 5.3 summarises the different specifications of pillar layouts at the mine. The IBS model was applied to two scenarios of the case study mine. DDM was used to numerically simulate the pillar systems and estimate pillar stress. Figure 5.2 shows one of the two scenarios.

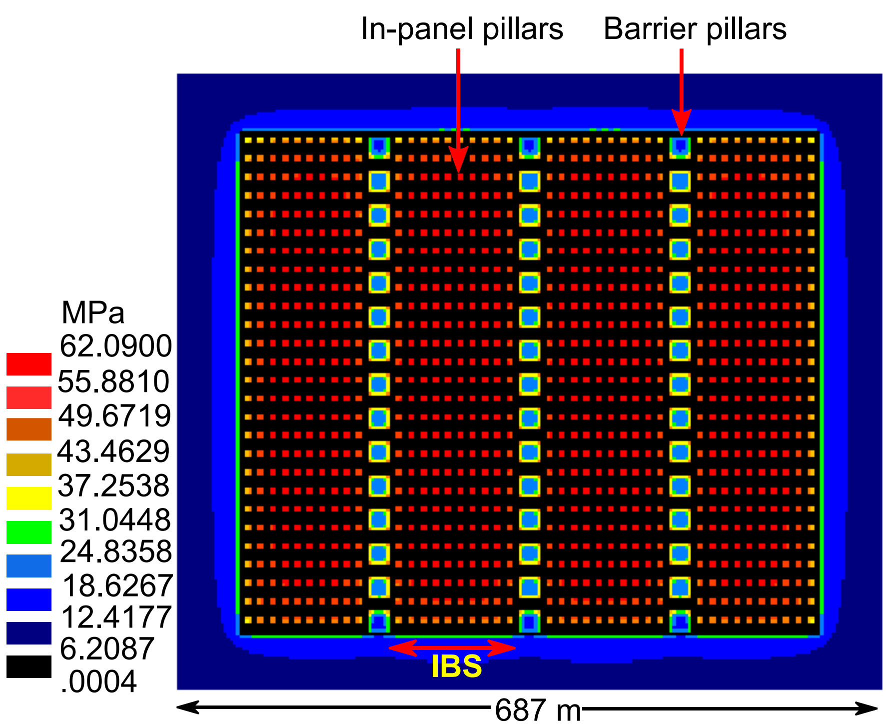

Fig. 5.2 DDM simulation result indicating the normal stress distribution for the case study mine scenario of 350 m mining depth and 83.3% extraction ratio.

The IBS model pillar stresses were compared to the *TAT* pillar stress as indicated in Fig. 5.3. For the case study mine, it is evident that the IBS model can manage pillar stresses by adequately separating the barriers and ensuring reasonable pillar stress management. σ_{max} in each case is prohibited from reaching the *TAT* stress asymptote because the barriers are adequately spaced, and they carry a portion of the overburden load intended for the smaller in-panel pillars. In all the conditions Δ_{PS} is 7.5 and 7.4% for the cases under Fig. 5.3a and 5.3b, respectively.

Table 5.3 Barrier pillar spacing at the case study mine.

***H* (m)**	100–250	250–275	275–300	300–325	325–350	350–375	375–400
***IBS* (m)**	96	96	96	96	96	96	96
***e* (%)**	85.3	83.5	83.5	82.5	81.0	80.0	78.5

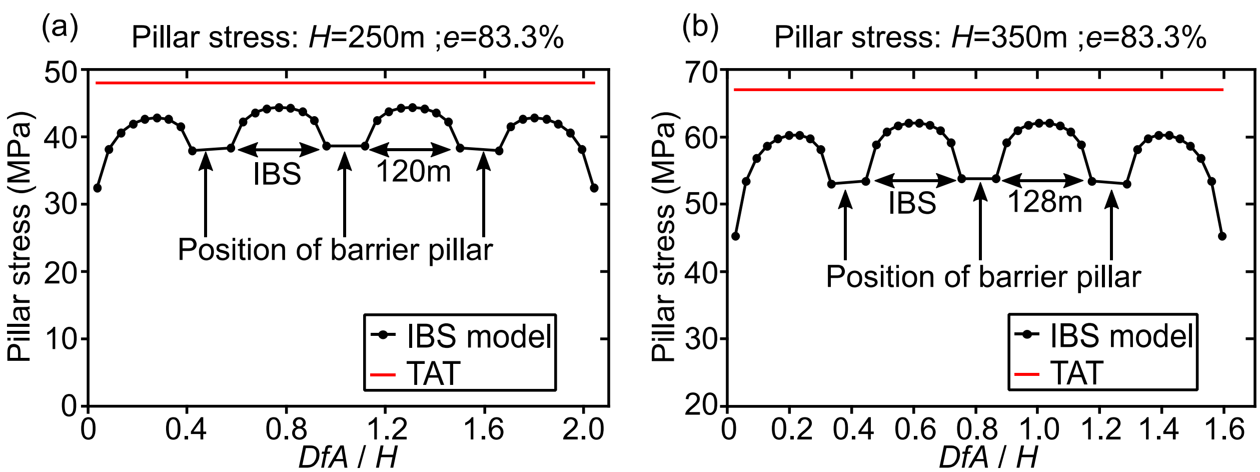

Fig. 5.3 Comparison of *TAT* and the IBS model pillar stresses for the case study mine. (a) Case of 250 m mining depth and 83.3 % extraction ratio, and (b) case of 350 m mining depth and 83.3 % extraction ratio.

5.3.3 Application of the IBS model to an arbitrary case

The IBS model was further applied to an arbitrary scenario — but different from the mine case study. This was to ensure that the model fully applies within the range under which it was developed. A mining depth of 750 m and an extraction ratio of 78% was used for this application. The presentation in this case is for illustrative purposes only because such an extraction ratio, and use of non-yield pillars, are typically unlikely for a mining depth of 750 m. The choice was inspired by the motivation to produce a large *IBS* and then show that pillar stress management, in such a layout, is still possible using the IBS model. Figure 5.4 shows the result of this application, and the same procedure described in Section 5.2.3 was used to develop this plot. In this application, Δ_{PS} is 6.4% and the IBS model ensured acceptable pillar stress management by adequately estimating *IBS* and prohibiting $\sigma_{\max}$ from reaching *TAT* stress.

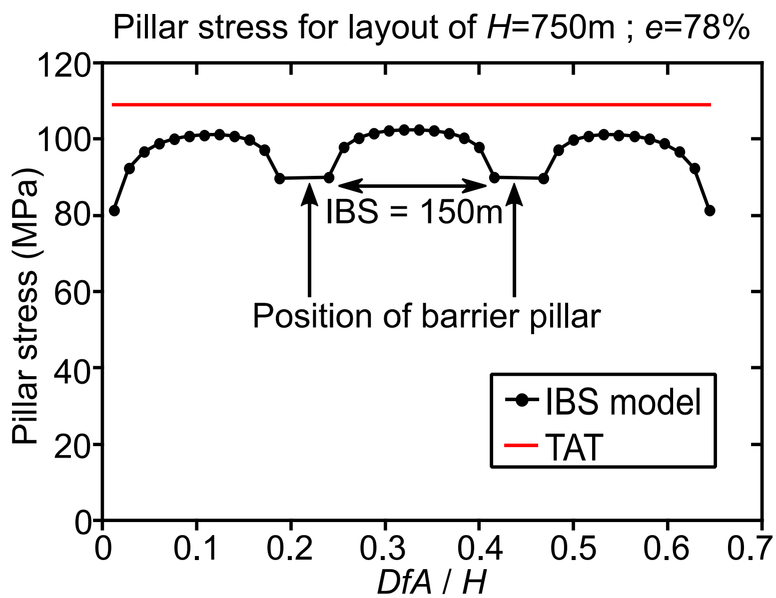

Fig. 5.4 Comparison of TAT and the IBS model pillar stresses for the arbitrary case.

5.3.4 Comparison of the IBS model and rules of thumb

The IBS model was further evaluated by comparing it to the rules of thumb. Various models of pillar layouts were simulated using DDM. Vertical pillar stresses obtained from the DDM models were compared using the plots of pillar stress versus the normalised distance of each pillar from the abutment as described in Section 5.2.3. The rules of thumb for estimating *IBS* are H/2 and H/4. These rules were compared to the IBS model under the following conditions:

- H = 100 m; e = 83.3% and 55.5%
- H = 250 m; e = 77.8% and 55.5%
- H = 500 m; e = 75% and 55.5%.

NUTEX software uses half-element widths to represent the actual lengths of the modelled domains. Due to this modelling constraint, it was not possible to model the actual *IBS* calculated by the IBS model and rules of thumb in some cases. Therefore, the closest allowable *IBS* was used instead of the actual *IBS* as summarised in Table 5.4.

Table 5.4 Summary of the calculated and modelled *IBS*.

		IBS Model		Rules of thumb			
				H/2		H/4	
H **(m)**	***e*** **(%)**	**Calculated**	**Modelled**	**Calculated**	**Modelled**	**Calculated**	**Modelled**
100	83.3	110	111	50	51	25	27
100	55.5	67	65	50	50	-*	-*
250	77.8	113	114	125	126	63	66
250	55.5	78	80	125	125	63	65
500	75	127	126	250	246	125	126
500	55.5	97	95	250	245	125	125

* *IBS* was too small to be practically modelled under these conditions.

Figure 5.5 illustrates the comparison between the IBS model and rules of thumb. The findings indicate that the estimates produced by the IBS model consistently outperform those derived from the rules of thumb in most cases. This indicates that the IBS model offers the best estimation of *IBS*, which is visible in Fig. 5.5a, 5.5c, and 5.5e. In Fig. 5.5a, the rules of thumb tend to underestimate *IBS*, particularly H/4. Fig. 5.5c shows that both the IBS model and H/2 achieved better results, but H/4 still underestimates *IBS*. In Fig. 5.5e, the IBS model and H/4 overlapped and produced a better estimate of *IBS*. However, in this case, H/2 overestimated *IBS*, and it was revealed in Fig. 5.6 that stress management is no longer adequate when Δ_{PS} is used to conclude the comparisons.

An interesting finding in Fig. 5.5b, 5.5d, and 5.5f is that for low extraction ratios, barrier pillars may only be necessary to separate the panels and not to achieve any pillar stress management. This may be because low extraction implies closely spaced in-panel pillars, which allows these pillars to have high stiffness. Therefore, the stiffness of the bigger barrier pillars relative to the individual in-panel pillar stiffness is counterbalanced by the pack of these closely spaced in-panel pillars that surround it.

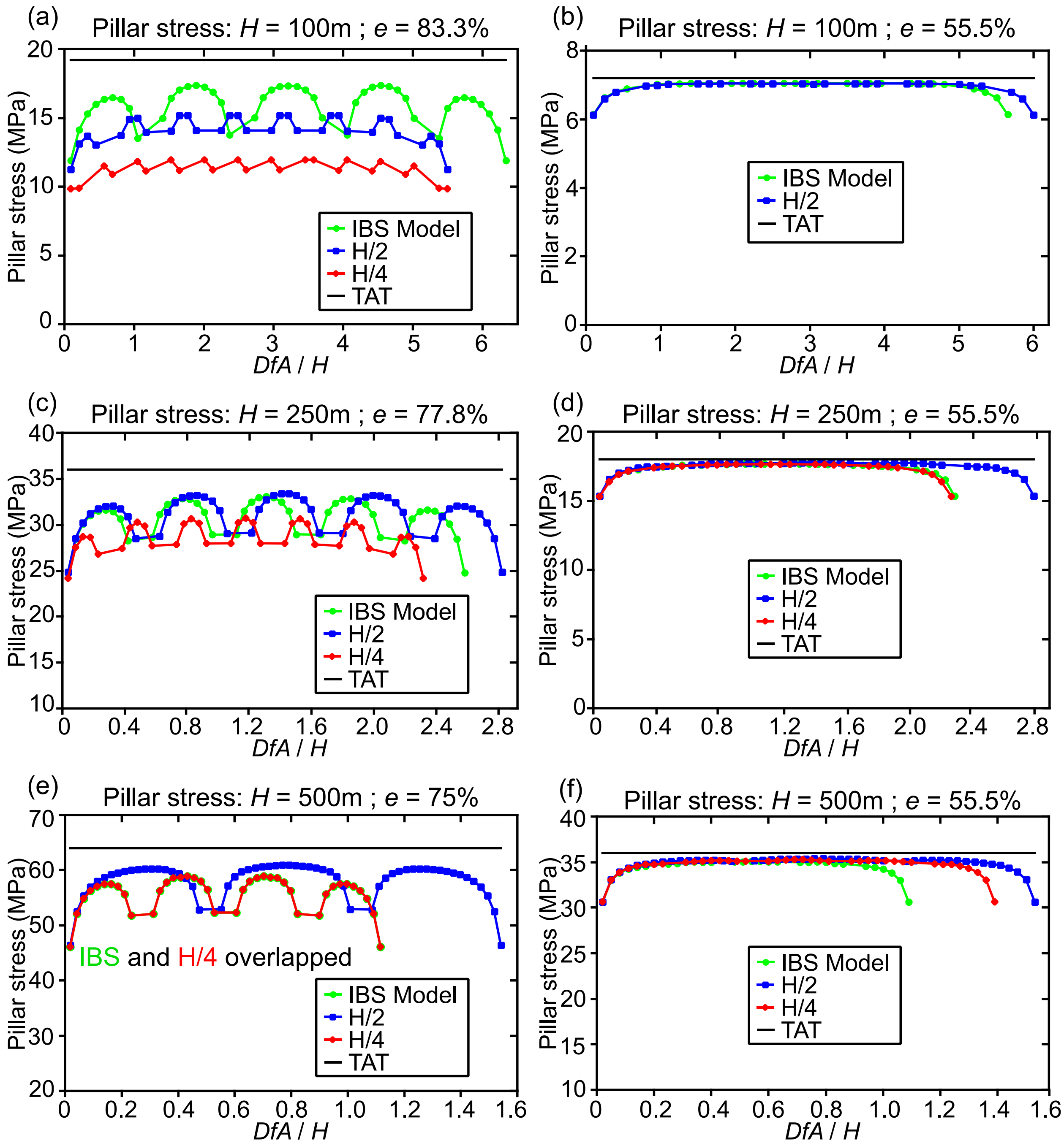

Fig. 5.5 Comparison of the IBS model and the rules of thumb. (a) Case of 100 m mining depth and 83.3% extraction ratio, (b) 100 m mining depth and 55.5% extraction ratio, (c) 250 m mining depth and 77.8% extraction ratio, (d) 250 m mining depth and 55.5% extraction ratio, (e) 500 m mining depth and 75% extraction ratio, and (f) 500 m mining depth and 55.5% extraction ratio.

The rules of thumb significantly underestimate *IBS* at shallow depths of mining (Fig. 5.6). As a crude estimate, when $H < 300$ m and $H < 200$ m, H/4 and H/2 should not be used to estimate *IBS*, respectively. H/2 is practically applicable in the range $200 < H \leq 450$ m while H/4 can only be applicable at the tail end of shallow room-and-pillar hard rock mining conditions. Contrariwise, the IBS model appears to offer a more consistent result across all the mining depths under which the room-and-pillar mining method is usually applied. Δ_{PS} for the IBS model is consistently within the desired range — as previously suggested by the author — of 5 to 10%.

Pillar stress distribution has largely been attributed to the mine geometry. The reason behind the inconsistency and ambiguity of the rules of thumb in estimating *IBS* can be ascribed to the absence of *e* in the derivation of *IBS*.

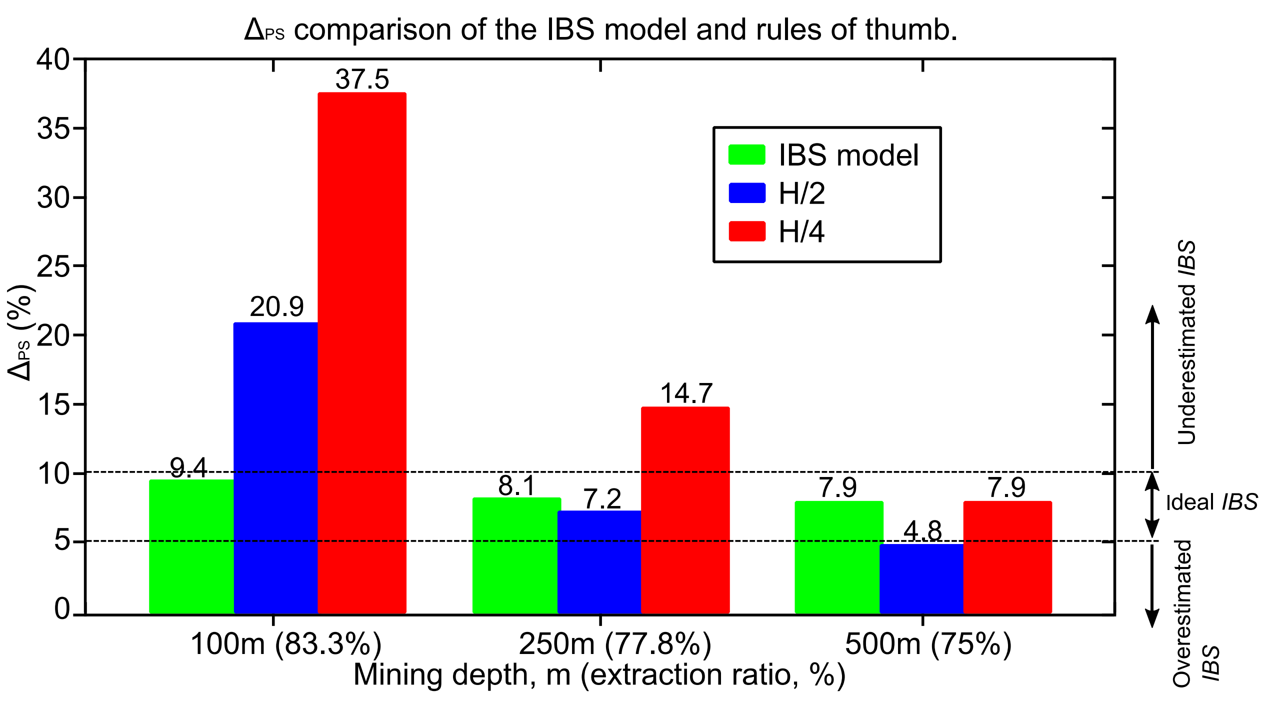

Fig. 5.6 Comparison of the IBS model and the rules of thumb using Δ_{PS}.

5.4 Discussion

Barrier pillars are known to provide robust shielding against major mining disasters in shallow room-and-pillar mines like large-scale pillar runs and regional backbreaks. The main objective of this Chapter was to develop a formula to design the inter-row spacing of barrier pillar lines. As presented in the previous discussions, the IBS model was successfully developed as an initial approach to reasonably space barrier pillar lines.

5.4.1 Interpretation of the IBS model

The IBS model considers two independent parameters, mining depth (*H*) and extraction ratio (*e*), which affect the dependent variable, *IBS*. The *IBS* is represented by a linear function of these parameters. The procedure to develop the IBS model which culminated in concluding the linearity between *IBS* and *H* agrees well with the result of previous studies, (Abel, 1988; Poulsen, 2010), which indicated that load transfer distance increases with mining depth. The possibility of operating large *IBS* as *H* increases can be scientifically explained as follows: The overburden of any tabular mining excavation is exposed to vertical "deadweight" tensile stresses. As concluded by Ozbay et al. (1995) and according to elastic theory, the depth of this tensile zone increases with an increasing ratio of *IBS*/*H* and decreases as the horizontal-to-vertical stress ratio decreases. The former implies that an increasing *H* results in comparatively smaller tensile zones, which sequentially allows larger *IBS*. Conversely, at shallow depths, the hangingwall is usually characterised as a weak heavily jointed rockmass subjected to increased deadweight tension. However, as *H* increases, the rockmass quality improves, and horizontal "clamping" stresses make the hangingwall a virtually self-supporting beam (Ozbay et al., 1995). This negative effect of the weak hangingwall rockmass, at shallow depth, is somehow compensated for by the positive effect of the *k* ratio. At shallow depths, where *k* is often large, the model predicts a smaller *IBS* and vice versa for larger *H*, under which *k* is usually small.

The relationship between *IBS* and *e* seems illogical at first glance. However, a closer examination of the sequence of designing the in-panel and barrier pillars clears this irrationality. Initially, the design procedure begins with designing the in-panel pillars. This means that a higher extraction ratio implies favourable or good rock mass conditions. Thus, higher extractions permit the operation of larger *IBS* because of the relatively strong rockmass.

Additional elasto-plastic numerical simulations, in which the ore seam was assumed to be a Mohr-Coulomb material with a friction angle of 30° and zero residual cohesion under a hydro-static stress state, were performed to clarify the importance of the parameters constituting the IBS model. Several simulations were run to establish a model separating the stable and unstable regions to visualise the effect of different parameters (Fig. 5.7). The horizontal axis is the *IBS* of each simulation represented by *H*/2 for simplicity in generating models. Figures 5.7a and 5.7b demonstrate the effect of *H* and *e*, while Figs. 5.7c and 5.7d analyse the impact of *H* and the size of the barrier pillar (*w*:*h*). Figure 5.8 summarises the stable and unstable regions from Fig. 5.7, with each model indicating the region below it as the zone of failure and above it as the stable zone. The findings highlighted that the most significant parameters affecting the behaviour of the pillar system are *e* and *H* (Fig. 5.8a). The size of the barrier pillar has an insignificant influence on the *IBS* (Fig. 5.8b), which means that estimating *IBS* using only *e* and *H* is reasonable.

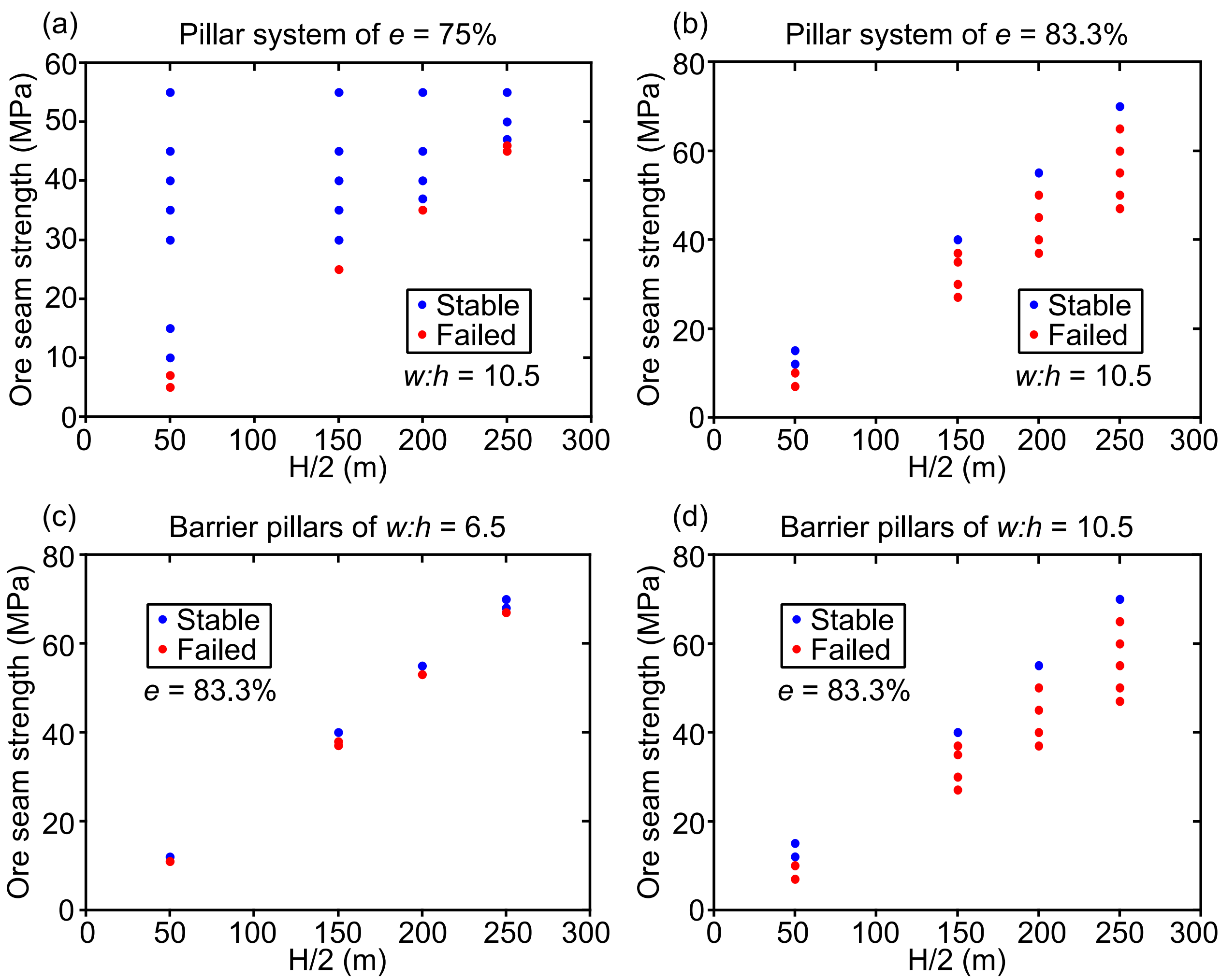

Fig. 5.7 Individual elasto-plastic simulation results to study the effect of different model geometrical parameters. (a) Pillar system of 75% extraction ratio, (b) pillar system of 83.3% extraction ratio, (c) pillar system with barrier pillars of *w*:*h* = 6.5, and (d) pillar system with barrier pillars of *w*:*h* = 6.5.

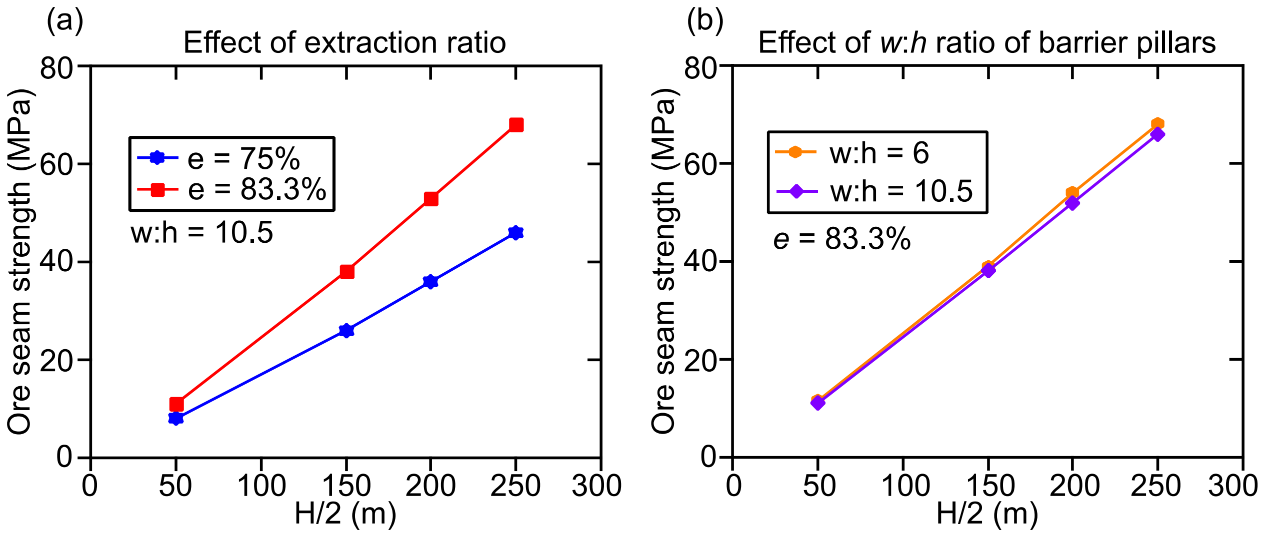

Fig. 5.8 Summarised elasto-plastic simulations to improve understanding of the influence of different parameters. (a) Effect of extraction ratio, and (b) effect of *w:h* ratio of barrier pillar.

5.4.2 Application of the IBS model

The IBS model was developed from parameters that can easily be evaluated for any room-and-pillar mine. The model offers a better way to design regional support systems in room-and-pillar hard rock mines affected by weak alteration layers that substantially reduce the pillar strengths. Such conditions are highlighted in the case study mine and by Couto and Malan (2023b).

The IBS model was developed using numerical simulations assuming a maximum *H* of 800 m. However, it is strongly recommended to use this model for *H* up to 600 m only. The reason is that this model is specifically designed for shallow room-and-pillar mines where non-yield pillar systems are applicable. Although effective in estimating *IBS*, it should not be considered a superior alternative to detailed numerical modelling for designing barrier pillar spacings. However, when such considerations arise, the IBS model can provide a more convenient starting point for numerical simulations that involve continuous iterations of *IBS*.

It is important to note that the IBS model was formulated with the assumption of perfectly horizontal ore seams. As a result, it can provide accurate *IBS* predictions, especially for such conditions. However, the IBS model can still be useful for slightly inclined ore seams that are typical for the room-and-pillar mining method. In addition, the model was evaluated based on a *w:h* ratio of 10.5 for the barrier pillars. While the generally acceptable *w:h* ratio for barrier pillars is at least 10, the results of Fig. 5.8b and other elastic simulations (not presented in this study) may require further research to improve the design of barrier pillar sizes for different mining conditions.

Furthermore, this Chapter's findings improve our understanding of how different extraction ratios can affect the suitability of barrier pillars. The fact that pillar stresses in low extraction ratios (55.5% in this analysis) are not affected by barrier pillars opens new opportunities for future research aimed at determining the minimum extraction ratio for applying barrier pillars to improve the overall stiffness of the pillar system. According to this study, this critical extraction ratio threshold will be between 55.5% and 75% (Fig. 5.5). This range appears to be consistent with the findings documented by Roberts et al. (2002) and Hauquin et al. (2016), where the authors stated that when the extraction ratio exceeds 65%, a significant portion of the weight of the overburden is transferred to the abutments and, of course, to the larger barrier pillars due to an arch effect.

5.4.3 Limitations

It is important to consider the limitations of the model when applying it. Firstly, the *IBS* obtained from the model is not an absolute measure, but rather an estimate. This is because certain simplifying assumptions are made to develop the DDM and subsequently derive the dataset used to develop the IBS model. Nonetheless, it is possible to obtain a tolerable approximation of the *IBS* acceptable for mining engineering necessities, based on these simplified considerations. Secondly, the model only incorporates mine geometrical parameters in estimating the *IBS*. Though previously mentioned to be of lesser influence than the geometrical parameters, the deformational parameters may have to be considered in future if the continuous updating of this model is necessary.

CHAPTER 6 CONCLUSIONS

This dissertation focused on the design of pillars in shallow hard rock room-and-pillar mines. The design of these pillars encompasses various aspects that were studied in this research. The current study addressed research gaps related to pillar stress estimation, pillar strength determination, and regional support design. The outcomes of this dissertation aim to enhance the understanding of designing stable and more economical pillar layouts in room-and-pillar mines. The methods outlined in this dissertation are recommended for the initial pillar design and should not be considered absolute measures. Once the pillars have been fully cut during mining, detailed monitoring, stress, and deformation measurements become critically important. The contents and findings of this dissertation are summarised as follows:

1) Chapter 2 provides a critical presentation of rock mass conditions and pillar design methodologies in Zimbabwe, general principles of pillar design, and a discussion to offer better insights into the limitations of current methods and propose directions for future research.

2) Chapter 3 presented the development of an MLPNN model to estimate average vertical pillar stresses while considering the influence of abutments. The dataset used to train the model was numerically developed using DDM. The features constituting the dataset were extraction ratio (*e*), Young's modulus (*E*), mining depth (*H*), panel width, the ratio of room to pillar width (*m*), tributary area theory pillar stress (*TAT*), and distance of pillar from abutment (*DfA*). The MLPNN model was successfully trained, and its performance on the testing and validation datasets was acceptable, yielding *R* score values of 0.99 each. Further validation of the MLPNN model was done through a comparison with FLAC3D results. Predictions of the MLPNN model and the FLAC3D pillar stresses reasonably agreed with a regression coefficient of 0.99. The MLPNN model was also adapted to mine layouts of large panel widths with evenly spaced barrier pillars. The adapted model was then applied to an actual mine case study in Zimbabwe, and the estimated pillar stresses by the model satisfactorily agreed with simulations done at the mine.

3) Chapter 4 described a new methodology to determine the strength of mine pillars in room-and-pillar mines. The proposed framework follows a step-by-step procedure using four techniques namely: observational methods, risk management decision making, numerical modelling, and analytical hierarchy process. This framework has two main advantages. Firstly, it allows consideration of all the factors that can affect pillar stability, such as orebody geometry, pillar geometry, rock mass quality, and adverse geological structures. Secondly, it can easily be customized to any room-and-pillar mining operation. Implementing this framework has the potential to improve both overall pillar design and mine safety by actively and systematically identifying unstable pillars that require remedial support. Finally, this proposed framework should nevertheless be tested in different room-and-pillar mine cases to ensure its effectiveness.

4) Chapter 5 presents a new method for estimating the spacing of barrier pillars by using numerical simulations and multivariate regression analysis. The method is called the IBS model and consists of two parameters: mining depth (H) and extraction ratio (e). The linear model was confirmed using a case study of a hard rock room-and-pillar mine in Zimbabwe and an arbitrary hypothetical mine case of H = 750 m and e = 78%. Additionally, the model was compared to the rules of thumb for different mining depths and extraction ratios. Its application proved to provide adequate regional mine support and optimised stiffness of the entire pillar system. This formula is recommended for use in shallow hard rock mines, where H is less than 600 m, as it is more reliable than the conventional rules of thumb. The latter may result in ore reserve sterilisation and unreliable designs in specific circumstances. Finally, the study findings have improved our understanding of how various extraction ratios can affect the effectiveness of barrier pillars. In low extraction ratio room-and-pillar mines, there may not be a need for barrier pillars, or they may only be required to compartmentalise the mine. However, it is recommended that future studies establish the threshold extraction ratio.

The author would be greatly appreciative if the results of this dissertation help enhance the rational design of pillar layouts in hard rock room-and-pillar mining operations, to improve overall pillar design and the economic efficiency of room-and-pillar mines. In a typical mining setup where routine pillar stress and strength estimations are inevitable, numerical modelling does not provide simple procedures for determining these parameters. Models are naturally difficult to construct, and usually, onerous computer run times are unavoidable. Such a scenario is burdensome at mine sites where quick solutions are demanded. The MLPNN model, pillar strength estimation framework, and the IBS model thus afford alternatives that feature easily accessible mine geometrical and rock mass parameters that can quickly be applied in underground mines. Though not serving as absolute measures, these models can sufficiently be used as initial pillar design approaches as substantiated by the series of successful training, testing, validation, and actual case study applications of the models in this study.

In conclusion, additional research is necessary to develop pillar design guidelines and extraction ratios suitable for the staggered room-and-pillar mining method applicable to layouts of in-panel and barrier pillars.

REFERENCES

Abel, J. F. (1988). Soft rock pillars. *International Journal of Mining and Geological Engineering*, *6*(3), 215–248. https://doi.org/10.1007/BF00880975

Alejano, L. R., Arzua, J., Castro-Filgueira, U., & Malan, F. (2017). Strapping of pillars with cables to enhance pillar stability. *Journal of the Southern African Institute of Mining and Metallurgy*, *117*(6), 527–540. https://doi.org/10.17159/2411-9717/2017/v117n6a3

Brady, B. H., & Brown, E. T. (2004). *Rock Mechanics for underground mining* (3rd ed.). Kluwer Academic Publishers.

Chaumba, J. B. (2022). A review of the emplacement and formation of magmatic platinum-group elements-enriched deposits in large layered mafic/ultramafic intrusions, with special reference to the “big three” (Stillwater Complex, Great Dyke, and Bushveld Complex). *Journal of African Earth Sciences*, *194*, 104603. https://doi.org/10.1016/j.jafrearsci.2022.104603

Chen, T., & Mitri, H. S. (2021). Strategies for surface crown pillar design using numerical modelling – A case study. *International Journal of Rock Mechanics and Mining Sciences*, *138*, 104599. https://doi.org/10.1016/j.ijrmms.2020.104599

Couto, P. M., & Malan, D. F. (2023a). A limit equilibrium model to simulate the large-scale pillar collapse at the Everest Platinum Mine. *Rock Mechanics and Rock Engineering*, *56*(1), 183–197. https://doi.org/10.1007/s00603-022-03088-z

Couto, P. M., & Malan, D. F. (2023b). Bord-and-pillar design for the UG2 Reef containing weak alteration layers. *Journal of the Southern African Institute of Mining and Metallurgy*, *123*(5), 245–251. https://doi.org/10.17159/2411-9717/2482/2023

Crouch, S. (1976). *Analysis of stress and displacements around underground excavations: An application of the displacement discontinuity method.* University of Minnesota.

Crouch, S. L., & Fairhurst, C. (1973). *The mechanics of coal mine bumps and the interaction between coal pillars, mine roof and foor*.

Cui, X., Gao, Y., & Yuan, D. (2014). Sudden surface collapse disasters caused by shallow partial mining in Datong coalfield, China. *Natural Hazards*, *74*(2), 911–929. https://doi.org/10.1007/s11069-014-1221-5

Ding, H., Li, G., Dong, X., & Lin, Y. (2018). Prediction of pillar stability for underground mines using the stochastic gradient boosting technique. *IEEE Access*, *6*, 69253–69264. https://doi.org/10.1109/ACCESS.2018.2880466

Dzimunya, N., Fujii, Y., & Kawamura, Y. (2023). Integrating the effect of abutments in estimating the average vertical stress of elastic hard rock pillars by combining numerical modelling and artificial neural networks. *Underground Space*, *13*, 121–135. https://doi.org/10.1016/j.undsp.2023.03.008

Dzimunya, N. Z., & Fujii, Y. (2024). A proposed framework to estimate pillar strength in room-and-pillar hard rock mines. *58th U.S. Rock Mechanics/Geomechanics Symposium*. https://doi.org/10.56952/ARMA-2024-0116

Elmo, D., Cammarata, G., & Brasile, S. (2021). The role of numerical analysis in the study of the behaviour of hard-rock pillars. *IOP Conference Series: Earth and Environmental Science*, *833*(1), 012132. https://doi.org/10.1088/1755-1315/833/1/012132

Esterhuizen, G. S., Dolinar, D. R., & Ellenberger, J. L. (2011). Pillar strength in underground stone mines in the United States. *International Journal of Rock Mechanics and Mining Sciences*, *48*(1), 42–50. https://doi.org/10.1016/j.ijrmms.2010.06.003

Esterhuizen, G. S., Iannacchione, A. T., Ellenberger, J. L., & Dolinar, D. R. (2006). Pillar stability issues based on a survey of pillar performance in underground limestone mines. *25th International Conference on Ground Control in Mining*, 355–361.

Esterhuizen, G. S., Tyrna, P. L., & Murphy, M. M. (2019). A case study of the collapse of slender pillars affected by through-going discontinuities at a limestone mine in Pennsylvania. *Rock Mechanics and Rock Engineering*, *52*(12), 4941–4952. https://doi.org/10.1007/s00603-019-01959-6

Esterhuyse, J. C., & Malan, D. F. (2023). Simulating pillar reinforcement using a displacement discontinuity boundary element code. *Journal of the Southern African Institute of Mining and Metallurgy*, *123*(5), 211–221. https://doi.org/10.17159/2411-9717/2450/2023

Fujii, Y. (2004). *Numerical simulation system for rockbursts and microseismicity due to tabular excavation*.

Fujii, Y., Balusu, R., Deguchi, G., & Ishijima, Y. (2001). Numerical simulation on microseismicity due to mining at one of the Collieries in Australia. *20th International Conference on Ground Control in Mining*, 287–296.

Fujii, Y., Ishijima, Y., & Deguchi, G. (1997). Prediction of coal face rockbursts and microseismicity in deep longwall coal mining. *International Journal of Rock Mechanics and Mining Sciences*, *34*(1), 85–96. https://doi.org/10.1016/S1365-1609(97)80035-4

Garza-Cruz, T., Pierce, M., & Board, M. (2019). Effect of shear stresses on pillar stability: a back analysis of the Troy Mine experience to predict pillar performance at Montanore Mine. *Rock Mechanics and Rock Engineering*, *52*(12), 4979–4996. https://doi.org/10.1007/s00603-019-02011-3

Ghasemi, E., Kalhori, H., & Bagherpour, R. (2017). Stability assessment of hard rock pillars using two intelligent classification techniques: A comparative study. *Tunnelling and Underground Space Technology*, *68*, 32–37. https://doi.org/10.1016/j.tust.2017.05.012

Ghazvinian, E., Diederichs, M. S., & Quey, R. (2014). 3D random Voronoi grain-based models for simulation of brittle rock damage and fabric-guided micro-fracturing. *Journal of Rock Mechanics and Geotechnical Engineering*, *6*(6), 506–521. https://doi.org/10.1016/j.jrmge.2014.09.001

González-Nicieza, C., Álvarez-Fernández, M. I., Menéndez-Díaz, A., & Álvarez-Vigil, A. E. (2006). A comparative analysis of pillar design methods and its application to marble mines. *Rock Mechanics and Rock Engineering*, *39*(5), 421–444. https://doi.org/10.1007/s00603-005-0078-z

Griffiths, D. V., Fenton, G. A., & Lemons, C. B. (2002). Probabilistic analysis of underground pillar stability. *International Journal for Numerical and Analytical Methods in Geomechanics*, *26*(8), 775–791. https://doi.org/10.1002/nag.222

Hauquin, T., Deck, O., & Gunzburger, Y. (2016). Average vertical stress on irregular elastic pillars estimated by a function of the relative extraction ratio. *International Journal of Rock Mechanics and Mining Sciences*, *83*, 122–134. https://doi.org/10.1016/j.ijrmms.2015.12.004

Hauquin, T., Gunzburger, Y., & Deck, O. (2018). Predicting pillar burst by an explicit modelling of kinetic energy. *International Journal of Rock Mechanics and Mining Sciences*, *107*, 159–171. https://doi.org/10.1016/j.ijrmms.2018.05.004

Hedley, D. G. F., & Grant, F. (1972). Stope-and-pillar design for Elliot Lake Uranium Mines. *Bulletin of the Canadian Institute of Mining and Metallurgy*, *65*, 37–44.

Hoek, E., Kaiser, P. K., & Bawden, W. F. (1995). In situ and induced stresses. In *Support of underground excavations in hard rock* (1st ed., pp. 71–89). CRC Press.

Idris, M. A., Saiang, D., & Nordlund, E. (2015). Stochastic assessment of pillar stability at Laisvall mine using Artificial Neural Network. *Tunnelling and Underground Space Technology*, *49*, 307–319. https://doi.org/10.1016/j.tust.2015.05.003

Ile, D., & Malan, D. F. (2023). A study of backfill confinement to reinforce pillars in bord-and-pillar layouts. *Journal of the Southern African Institute of Mining and Metallurgy*, *123*(5), 223–233. https://doi.org/10.17159/2411-9717/2452/2023

IMPLATS. (2019). *Implats Mineral resource and mineral reserve statement as at 30 June 2019 - Regional geological settings*.

Itasca. (2012). *FLAC3D – Fast Langrangian analysis of continua in three-dimension, Version 5.0.*

Itasca. (2016). *FLAC 3D Version 5.0: Theory and background*.

Jessu, K. V., & Spearing, A. J. S. (2018). Effect of dip on pillar strength. *Journal of the Southern African Institute of Mining and Metallurgy*, *118*(7). https://doi.org/10.17159/2411-9717/2018/v118n7a10

Jessu, K. V., & Spearing, A. J. S. (2019). Performance of inclined pillars with a major discontinuity. *International Journal of Mining Science and Technology*, *29*(3), 437–443. https://doi.org/10.1016/j.ijmst.2018.09.006

Jessu, K. V., Spearing, A. J. S., & Sharifzadeh, M. (2022). An improved pillar design methodology. *Journal of the Southern African Institute of Mining and Metallurgy*, *122*(10), 587–596. https://doi.org/10.17159/2411-9717/1983/2022

Kaiser, P. K., Kim, B., Bewick, R. P., & Valley, B. (2011). Rock mass strength at depth and implications for pillar design. *Mining Technology*, *120*(3), 170–179. https://doi.org/10.1179/037178411X12942393517336

Kaiser, P. K., & Kim, B.-H. (2015). Characterization of strength of intact brittle rock considering confinement-dependent failure processes. *Rock Mechanics and Rock Engineering*, *48*(1), 107–119. https://doi.org/10.1007/s00603-014-0545-5

Kersten, R. W. O. (2019). An alternative pillar design methodology. *Journal of the Southern African Institute of Mining and Metallurgy*, *119*(5). https://doi.org/10.17159/2411-9717/16/388/2019

Kimmelmann, M., Hyde, B., & Madgwick, R. (1984). The use of computer applications at BCL Limited in planning pillar extraction and design of mining layouts. *Design and Performance of Underground Excavations: ISRM Symposium — Cambridge*, 53–63.

Kostecki, T., & Spearing, A. J. S. (2015). Influence of backfill on coal pillar strength and floor bearing capacity in weak floor conditions in the Illinois Basin. *International Journal of Rock Mechanics and Mining Sciences*, *76*, 55–67. https://doi.org/10.1016/j.ijrmms.2014.11.011

Krauland, N., & Soder, P. E. (1987). Determining pillar strength from pillar failure observations. *Engineering and Mining Journal*, *188*(8), 34–40.

Lavoie, T., Eberhardt, E., & Pierce, M. E. (2022). Numerical modelling of rock mass bulking and geometric dilation using a bonded block modelling approach to assist in support design for deep mining pillars. *International Journal of Rock Mechanics and Mining Sciences*, *156*, 105145. https://doi.org/10.1016/j.ijrmms.2022.105145

Le Roux, P. J., & Malan, D. F. (2024). Back analysis of LG6/LG6A chromitite pillar strength using displacement discontinuity modelling. *Journal of the Southern African Institute of Mining and Metallurgy*, *124*(11), 605–616.

Li, C., Zhou, J., Armaghani, D., & Li, X. (2021). Stability analysis of underground mine hard rock pillars via combination of finite difference methods, neural networks, and Monte Carlo simulation techniques. *Underground Space*, *6*(4), 379–395. https://doi.org/10.1016/j.undsp.2020.05.005

Li, C., Zhou, J., Du, K., & Dias, D. (2023). Stability prediction of hard rock pillar using support vector machine optimized by three metaheuristic algorithms. *International Journal of Mining Science and Technology*, *33*(8), 1019–1036. https://doi.org/10.1016/j.ijmst.2023.06.001

Li, X., Kim, E., & Walton, G. (2019). A study of rock pillar behaviors in laboratory and in-situ scales using combined finite-discrete element method models. *International Journal of Rock Mechanics and Mining Sciences*, *118*, 21–32. https://doi.org/10.1016/j.ijrmms.2019.03.030

Lorig, L. J., & Cabrera, A. (2013). Pillar strength estimates for foliated and inclined pillars in schistose material. In H. Zhu, C. Detournay, R. Hart, & M. Nelson (Eds.), *Proceedings of the 3rd International FLAC/DEM Symposium*. ITASCA.

Lunder, P. J., & Pakalnis, R. (1997). Determination of the strength of hard-rock mine pillars. *Bulletin of the Canadian Institute of Mining and Metallurgy*, *68*, 55–67.

Malan, D. F., & Napier, J. A. L. (2011). The design of stable pillars in the Bushveld Complex mines: a problem solved? *Journal of the Southern African Institute of Mining and Metallurgy*, *111*(12), 821–836.

Malan, Daniel. F. (2012). Pillar design in the hard rock mines of South Africa. *International Journal of Mining and Geo-Engineering*, *46*(2), 163–191.

Mandingaisa, O. (2018). *Quantification of the impacts of rock mass quality on stope width control and pillar stability in a hard rock narrow reef mine* [MSc]. University of the Witwatersrand.

Maritz, J. A. (2015). *The effects of shear stresses on pillar strength* [Masters]. University of Pretoria.

Maritz, J. A., & Malan, D. F. (2023). A study of the effect of pillar shape on pillar strength. *Journal of the Southern African Institute of Mining and Metallurgy*, *123*(5), 235–244. https://doi.org/10.17159/2411-9717/2473/2023

Martin, C. D., & Maybee, W. G. (2000). The strength of hard-rock pillars. *International Journal of Rock Mechanics and Mining Sciences*, *37*(8), 1239–1246. https://doi.org/10.1016/S1365-1609(00)00032-0

Mayer, J. M., & Stead, D. (2017). Exploration into the causes of uncertainty in UDEC Grain Boundary Models. *Computers and Geotechnics*, *82*, 110–123. https://doi.org/10.1016/j.compgeo.2016.10.003

Monjezi, M., Hesami, S. M., & Khandelwal, M. (2011). Superiority of neural networks for pillar stress prediction in bord and pillar method. *Arabian Journal of Geosciences*, *4*(5–6), 845–853. https://doi.org/10.1007/s12517-009-0101-x

Monsalve, J. J., Soni, A., Ripepi, N., & Rodriguez-Marek, A. (2020). A preliminary investigation on stochastic discrete element modeling for pillar strength determination in underground limestone mines from a probabilistic risk analysis approach. In T. Klemetti, B. Mishra, H. Lawson, M. Murphy, & K. Perry (Eds.), *39th International Conference on Ground Control in Mining* (pp. 319–326). Society for Mining, Metallurgy & Exploration.

Mortazavi, A., Hassani, F. P., & Shabani, M. (2009). A numerical investigation of rock pillar failure mechanism in underground openings. *Computers and Geotechnics*, *36*(5), 691–697. https://doi.org/10.1016/j.compgeo.2008.11.004

Mushangwe, P. C. (2018). *Analysis of pillar/rockmass failure and propagation dynamics due to mining in hard rock platinum mines* [MSc]. University of the Witwatersrand.

Napier, J. A. L., & Malan, D. F. (2011). Numerical computation of average pillar stress and implications for pillar design. *Journal of the Southern African Institute of Mining and Metallurgy*, *111*(12), 837–846.

Napier, J. A. L., & Malan, D. F. (2018). Simulation of tabular mine face advance rates using a simplified fracture zone model. *International Journal of Rock Mechanics and Mining Sciences*, *109*, 105–114. https://doi.org/10.1016/j.ijrmms.2018.06.024

Napier, J. A. L., & Malan, D. F. (2021). A limit equilibrium model of tabular mine pillar failure. *Rock Mechanics and Rock Engineering*, *54*(1), 71–89. https://doi.org/10.1007/s00603-020-02265-2

Napier, J. A. L., & Malan, D. F. (2023). Numerical simulation of large-scale pillar-layouts. *Journal of the Southern African Institute of Mining and Metallurgy*, *123*(5), 203–210. https://doi.org/10.17159/2411-9717/2451/2023

Oates, T. E., & Malan, D. F. (2023). A study of UG2 pillar strength using a new pillar database. *Journal of the Southern African Institute of Mining and Metallurgy*, *123*(5), 265–273. https://doi.org/10.17159/2411-9717/2656/2023

Ozbay, M. U., Ryder, J. A., & Jager, A. J. (1995). The design of pillar systems as practised in shallow hard-rock tabular mines in South Africa. *Journal of the Southern African Institute of Mining and Metallurgy*, *95*(1), 7–18.

Potvin, Y. (2017). The need for new technology to optimise the engineering design of ground support systems in underground mines. In M. Hudyma & Y. Potvin (Eds.), *Proceedings of the First International Conference on Underground Mining Technology* (pp. 9–22). Australian Centre for Geomechanics, Perth. https://doi.org/10.36487/ACG_rep/1710_0.2_Potvin

Poulsen, B. A. (2010). Coal pillar load calculation by pressure arch theory and near field extraction ratio. *International Journal of Rock Mechanics and Mining Sciences*, *47*(7), 1158–1165. https://doi.org/10.1016/j.ijrmms.2010.06.011

Rafiei-Renani, H., & Martin, C. D. (2018). Modeling the progressive failure of hard rock pillars. *Tunnelling and Underground Space Technology*, *74*, 71–81. https://doi.org/10.1016/j.tust.2018.01.006

Roberts, D. P., Van der Merwe, J. N., Canbulat, I., Sellers, E. J., & Coetzer, S. (2002). *Development of a method to estimate coal pillar loading*.

Roberts, D., Tolfree, D., & McIntyre, H. (2007, May). Using confinement as a means to estimate pillar strength in a room and pillar mine. *First Canada - U.S Rock Mechanics Symposium*.

Ryder, J. A., & Ozbay, M. U. (1990). A methodology for designing pillar layouts for shallow mining. In R. Brummer (Ed.), *Proceedings ISRM International Symposium on Static and*

Dynamic Considerations in Rock Engineering (pp. 273–286). International Society for Rock Mechanics.

Saaty, T. L. (1977). A scaling method for priorities in hierarchical structures. *Journal of Mathematical Psychology*, *15*(3), 234–281. https://doi.org/10.1016/0022-2496(77)90033-5

Saaty, T. L. (1980). *The Analytic Hierarchy Process*. McGraw-Hill.

Sainoki, A., & Mitri, H. S. (2017). Numerical investigation into pillar failure induced by time-dependent skin degradation. *International Journal of Mining Science and Technology*, *27*(4), 591–597. https://doi.org/10.1016/j.ijmst.2017.05.002

Salamon, M. D. (1974). Rock mechanics of underground excavations. *Advances in Rock Mechanics: Proceedings of the Third Congress of the International Society for Rock Mechanics.*, 951–1099.

Salamon, M. D., & Munro, A. H. (1967). A study of the strength of coal pillars. *Journal of the South African Institute of Mining and Metallurgy*, *68*, 55–67.

Sinha, S., & Walton, G. (2018). A progressive S-shaped yield criterion and its application to rock pillar behavior. *International Journal of Rock Mechanics and Mining Sciences*, *105*, 98–109. https://doi.org/10.1016/j.ijrmms.2018.03.014

Sinha, S., & Walton, G. (2019a). Investigation of longwall headgate stress distribution with an emphasis on pillar behavior. *International Journal of Rock Mechanics and Mining Sciences*, *121*, 104049. https://doi.org/10.1016/j.ijrmms.2019.06.008

Sinha, S., & Walton, G. (2019b). Numerical analyses of pillar behavior with variation in yield criterion, dilatancy, rock heterogeneity and length to width ratio. *Journal of Rock Mechanics and Geotechnical Engineering*, *11*(1), 46–60. https://doi.org/10.1016/j.jrmge.2018.07.003

Sinha, S., & Walton, G. (2021). Integration of three-dimensional continuum model and two-dimensional bonded block model for studying the damage process in a granite pillar at the Creighton Mine, Sudbury, Canada. *Journal of Rock Mechanics and Geotechnical Engineering*, *13*(2), 275–288. https://doi.org/10.1016/j.jrmge.2020.06.011

Sinkala, P., Nishihara, M., Fujii, Y., Fukuda, D., Kodama, J., & Chanda, E. (2019, June). Investigation of rockburst in deep underground mines, a case study of Mufulira mine, Copperbelt, Zambia. *53rd U.S. Rock Mechanics/Geomechanics Symposium*.

Sinkala, P., Nishihara, M., Nakayama, Y., Fujii, Y., Kodama, J., Fukuda, D., & Chanda, E. (2022). Creep Damage Model for Rockburst at Mufulira Mine in Zambia. *Mining, Metallurgy & Exploration*, *39*(5), 1983–2000. https://doi.org/10.1007/s42461-022-00668-z

Soni, A., Monsalve, J. J., Bishop, R., & Ripepi, N. (2023). Modified design of pillar based on estimated stresses and strength of pillar in an underground limestone mine. *Mining, Metallurgy & Exploration*, *40*, 529–541. https://doi.org/10.1007/s42461-023-00733-1

Soni, A., Monsalve, J. J., Bishop, R., Ripepi, N., & Baggett, J. G. (2022). Estimating strength of pillars with karst voids in a room-and-pillar limestone mine. *Mining, Metallurgy & Exploration*, *39*(3), 1073–1086. https://doi.org/10.1007/s42461-022-00594-0

Stacey, T. R., & Swart, A. H. (2001). Support. In *Practical rock engineering practice for shallow and opencast mines* (pp. 37–38). The Safety in Mines Research Advisory Committee (SIMRAC).

Sweby, G., Dight, P., & Potvin, Y. (2016). A numerical modelling case study - correlation of ground support instrumentation data with a three dimensional inelastic model. In E. Nordlund, T. H. Jones, & A. Eitzenberger (Eds.), *Proceedings of the 8th International Symposium on Ground Support in Mining and Underground Construction*. Luleå University of Technology.

Theron, W. J., & Malan, D. F. (2024). Pillar design and the associated mining engineering constraints in hard rock bord-and-pillar mines. *Journal of the Southern African Institute of Mining and Metallurgy*, *124*(11), 631–644.

Tuncay, D., Tulu, I. B., & Klemetti, T. (2021). Investigating different methods used for approximating pillar loads in longwall coal mines. *International Journal of Mining Science and Technology*, *31*(1), 23–32. https://doi.org/10.1016/j.ijmst.2020.12.007

Turk, N., & Dearman, W. R. (1986). A correction equation on the influence of length-to diameter ratio on the uniaxial compressive strength of rocks. *Engineering Geology*, *22*(3), 293–300. https://doi.org/10.1016/0013-7952(86)90030-X

Vlachogiannis, I., & Benardos, A. (2024). Proposed formulas for pillar stress estimation in a regular room-and-pillar pattern. *International Journal of Rock Mechanics and Mining Sciences*, *180*, 105826. https://doi.org/10.1016/j.ijrmms.2024.105826

Wagner, H. (1980). Pillar design in coal mines. *Journal of the South African Institute of Mining and Metallurgy*, *80*(1), 37–45.

Wagner, H., Ladinig, T., & Blaha, H. (2016). Design considerations for pillar systems in deep mines. *Geomechanics and Tunnelling*, *9*(5), 524–528. https://doi.org/10.1002/geot.201600045

Walczak, S., & Cerpa, N. (2003). *Encyclopedia of physical science and technology* (3rd ed.). Academic Press.

Walton, G., Diederichs, M., & Punkkinen, A. (2015). The influence of constitutive model selection on predicted stresses and yield in deep mine pillars – A case study at the Creighton mine, Sudbury, Canada. *Geomechanics and Tunnelling*, *8*(5), 441–449. https://doi.org/10.1002/geot.201500023

Wang, M., & Cai, M. (2020). A grain-based time-to-failure creep model for brittle rocks. *Computers and Geotechnics*, *119*, 103344. https://doi.org/10.1016/j.compgeo.2019.103344

Wang, M., & Cai, M. (2021). Numerical modeling of time-dependent spalling of rock pillars. *International Journal of Rock Mechanics and Mining Sciences*, *141*, 104725. https://doi.org/10.1016/j.ijrmms.2021.104725

Watson, B. P., Lamos, R. A., & Roberts, D. P. (2021a). PlatMine pillar strength formula for the UG2 Reef. *Journal of the Southern African Institute of Mining and Metallurgy*, *121*(8), 1–12. https://doi.org/10.17159/2411-9717/1387/2021

Watson, B. P., Ryder, J. A., Kataka, M. O., & Kuijpers, J. S. (2008). Merensky pillar strength formulae based on back-analysis of pillar failures at Impala Platinum. *Journal of the Southern African Institute of Mining and Metallurgy*, *108*(8), 449–461.

Watson, B. P., Theron, W., Fernandes, N., Kekana, W. O., Mahlangu, M. P., Betz, G., & Carpede, A. (2021b). UG2 pillar strength: Verification of the PlatMine formula. *Journal of the Southern*

African Institute of Mining and Metallurgy, *121*(8), 1–8. https://doi.org/10.17159/2411-9717/1491/2021

Wattimena, R. K. (2014). Predicting the stability of hard rock pillars using multinomial logistic regression. *International Journal of Rock Mechanics and Mining Sciences*, *71*, 33–40. https://doi.org/10.1016/j.ijrmms.2014.03.015

Wattimena, R. K., Kramadibrata, S., Sidi, I. D., & Azizi, M. A. (2013). Developing coal pillar stability chart using logistic regression. *International Journal of Rock Mechanics and Mining Sciences*, *58*, 55–60. https://doi.org/10.1016/j.ijrmms.2012.09.004

Wessels, D. G., & Malan, D. F. (2023). A limit equilibrium model to simulate time-dependent pillar scaling in hard rock bord and pillar mines. *Rock Mechanics and Rock Engineering*, *56*(5), 3773–3786. https://doi.org/10.1007/s00603-023-03239-w

Wilson, A. H., & Prendergast, M. D. (1989). The great dyke of Zimbabwe : I- tectonic setting, stratigraphy, petrology, structure, emplacement and crystallization. *Prendergast, M.D., Jones, M.J. (Eds.), Magmatic Sulphides – the Zimbabwe Volume.*, 1–20.

Zhang, L., & Einstein, H. H. (2004). Using RQD to estimate the deformation modulus of rock masses. *International Journal of Rock Mechanics and Mining Sciences*, *41*(2), 337–341. https://doi.org/10.1016/S1365-1609(03)00100-X

Zhang, Y., Ren, F., & Zhao, X. (2017). Characterization of joint set effect on rock pillars using Synthetic Rock Mass numerical method. *International Journal of Geomechanics*, *17*(3). https://doi.org/10.1061/(ASCE)GM.1943-5622.0000756

Zhou, J., Li, X., & Mitri, H. S. (2015). Comparative performance of six supervised learning methods for the development of models of hard rock pillar stability prediction. *Natural Hazards*, *79*(1), 291–316. https://doi.org/10.1007/s11069-015-1842-3

Zhou, Z., Chen, L., Zhao, Y., Zhao, T., Cai, X., & Du, X. (2017). Experimental and numerical investigation on the bearing and failure mechanism of multiple pillars under overburden. *Rock Mechanics and Rock Engineering*, *50*(4), 995–1010. https://doi.org/10.1007/s00603-016-1140-8

Zvarivadza, T., & van der Merwe, J. N. (2017). Reflections on narrow-reef platinum mining pillar design systems as applied to a large platinum exploration feasibility project. *Journal of the Southern African Institute of Mining and Metallurgy*, *117*(2), 169–178. https://doi.org/10.17159/2411-9717/2017/v117n2a8

APPENDICES

Appendix A : Characteristics of rocks at case study mine

This Appendix contains the results of the thin section analysis and laboratory tests of the drill core samples from the case study mine in Zimbabwe. Mechanical testing including uniaxial compression, triaxial compression, Brazilian, P-wave velocity (Vp) and density tests were performed on the drill core samples. All tests were according to the standards specified by the International Society of Rock Mechanics (ISRM).

Appendix A1: Thin section analysis

Tables A.1 and A.2 are a summary of the thin section analysis of the core samples of the orebody from the case study mine. Figure A.1 shows the thin section images of the polarised light micrographs of the rock samples.

Table A.1 The rock type and mineral composition of the orebody at the case study mine.

Rock type	Melanocratic amphibole pyroxene gabbro	
Structure	Holocrystalline and equigranular	
Primary minerals		
Mineral	**Amount (%)**	**Maximum particle size (mm)**
Orthopyroxene	63	4.5
Plagioclase	11	5.5
Amphibole	11	1.8
Clinopyroxene	9	5.0
Biotite	1	1.6
Magnetite	–	0.15
Secondary minerals		
Talc >> Chrolite and Cummingtonite > Chalcopyrite, Pyrrhotite, and Pyrite		
Talc and chrolite are from orthopyroxene and biotite, respectively		

Table A.2 XRD results indicating the significance of the presence of each mineral in the samples.

Mineral	**Intensity peak (presence in sample)**
Talc	++++
Enstatite	++++
Amphibole	+++
Plagioclase	++++
Cummingtonite	++
Micas	++
Chrolite	++

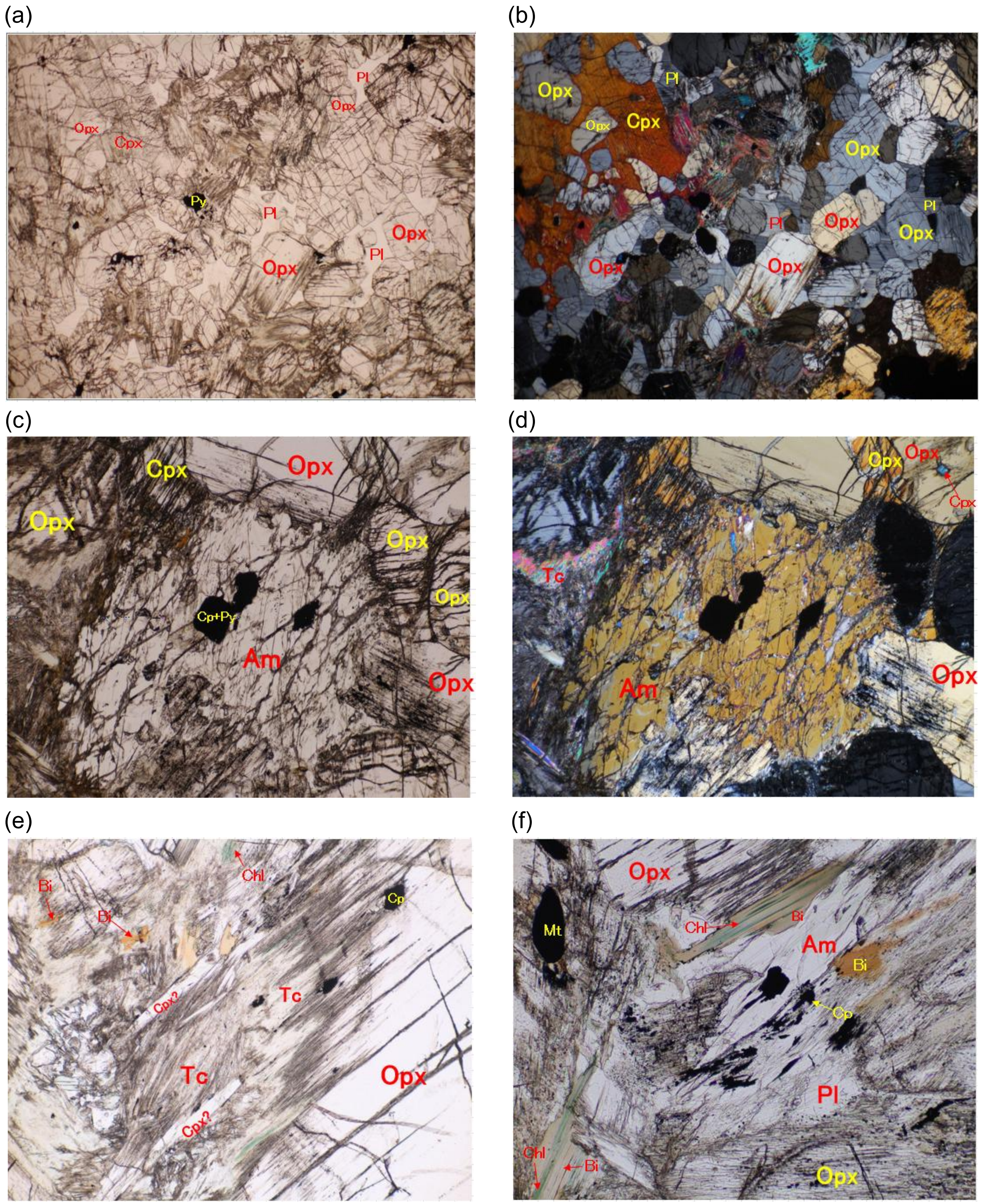

Fig. A.1 Polarised light micrographs of the rock samples from the case study mine. (a) Open Nicol, (b) crossed Nicols, (c) open Nicol, (d) crossed Nicols, (e) open Nicol, and (f) open Nicol. **Notes:**

Orthopyroxene (Opx), Plagioclase (Pl), Amphibole (Am), Clinopyroxene (Cpx), Biotite (Bi), Magnetite (Mt), Talc (Tc), Chrolite (Chl), Cummingtonite (Cum), Chalcopyrite (Cp), Pyrrhotite (Po), and Pyrite (Py).

Appendix A2: Primary wave velocity and density test

Samples UPU1, UPU2, UPU3, UPU4, UPU5 and UPU6 (Fig. A.2) were used for these tests. Table A.3 is a summary of the test results. Young's Modulus (E) was estimated using equations that relate Vp, E and Poisson's ratio (*v*). Poisson's ratio was assumed to be 0.2.

Fig. A.2 Samples UPU1, UPU2, UPU3, UPU4, UPU5 and UPU6.

Table A.3 Summary of Vp and density tests.

Sample	**Length (mm)**	**Diameter (mm)**	**Mass (kg)**	**Density (kg/m^3)**	**Time (μs)**	**Vp (m/s)**	**E (GPa)**
UPU1	87.88	41.76	0.396	3290	19.2	4577	62
UPU2	88.33	41.75	0.398	3291	19.6	4507	60
UPU3	87.71	41.78	0.396	3293	19.2	4568	62
UPU4	88.60	41.65	0.397	3289	20.4	4343	56
UPU5	88.17	41.67	0.396	3293	19.6	4498	60
UPU6	87.32	41.61	0.390	3284	19.2	4548	61

Appendix A3: Brazilian tensile test

Samples UPB1, UPB2, UPB3, UPB4, UPB5 and UPB6 (Fig. A.3) were prepared for the Brazilian test. Table A.4 is a summary of the test results. Figure A.4 shows the stress-strain relationships from the test.

Fig. A.3 Samples UPB1, UPB2, UPB3, UPB4, UPB5 and UPB6.

Table A.4 Summary of Brazilian tests.

Sample	**Thickness (mm)**	**Diameter (mm)**	**Loading Rate (mm/min)**	**Max Load (N)**	**Tensile strength (MPa)**	**Failure Mode**
UPB1	40.16	41.80	0.42	37032.10	14.10	Tensile Failure
UPB2	40.69	41.45	0.42	37632.34	14.21	Tensile Failure
UPB3	40.35	41.42	0.42	34482.20	13.13	Tensile Failure
UPB4	39.97	41.35	0.42	30085.50	11.59	Tensile Failure
UPB5	40.25	41.55	0.42	35585.90	13.55	Tensile Failure
UPB6	39.80	41.50	0.42	33916.30	13.07	Tensile Failure

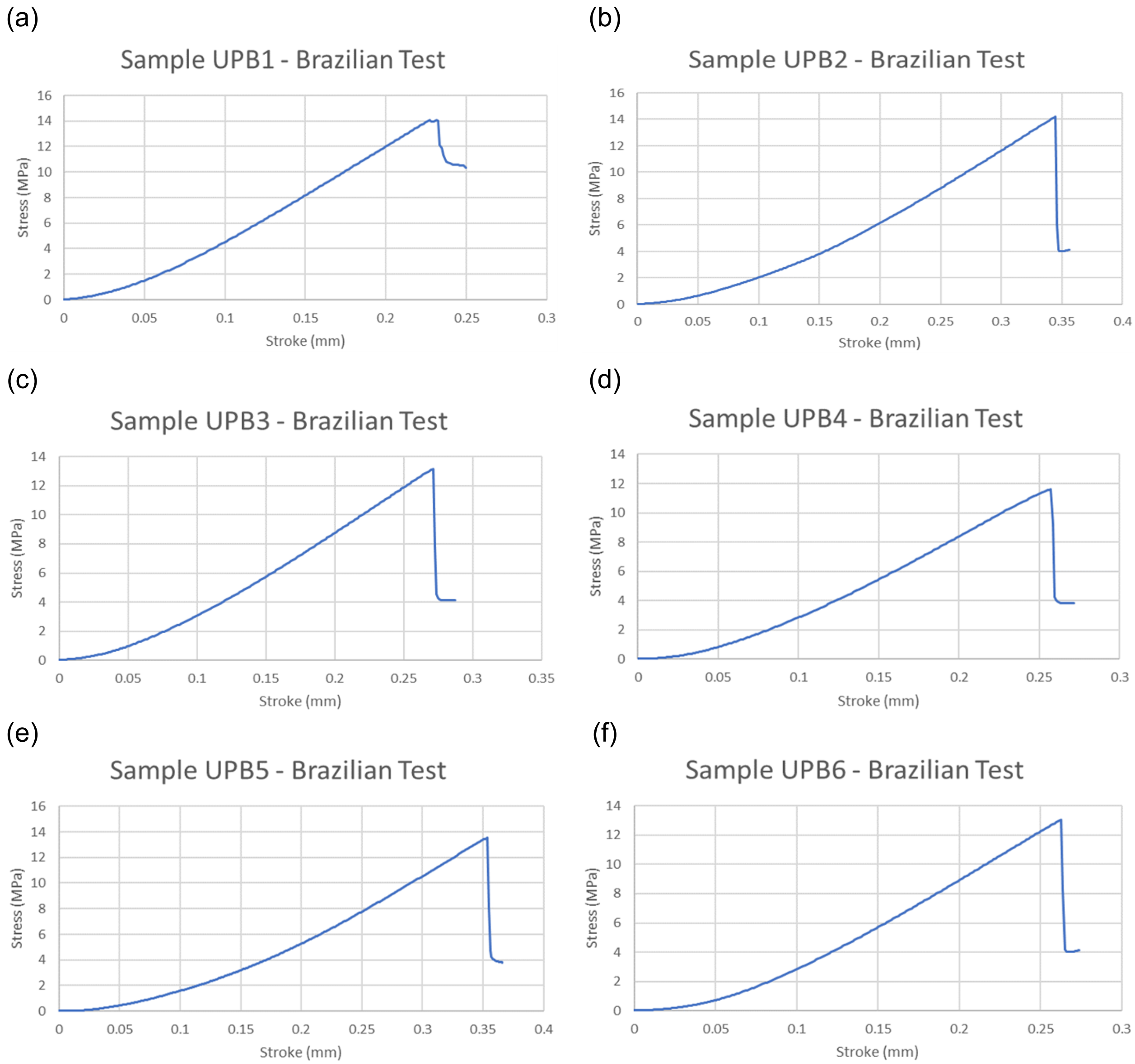

Fig. A.4 Stress vs strain curves for the Brazilian tests.

Appendix A4: Uniaxial compression test

Samples UCS1, UCS2, UCS3, UCS4, UCS5 and UCS6 (Fig. A.5) were prepared to determine UCS E, and Poisson's ratio (ν). The direct uniaxial compression test used three samples UCS1, UCS2, and UCS3 and the stress-strain curves of the tests are indicated in Fig. A.6. Measured UCS and triaxial strengths were corrected to match that of 50 mm diameter samples according to Turk & Dearman, (1986). Table A.5 is a summary of the uniaxial compression test results.

Fig. A.5 Samples UCS1, UCS2, UCS3, UCS4, UCS5 and UCS6.

Table A.5 Summary of uniaxial compression tests.

Sample	**Length (mm)**	**Diameter (mm)**	**Strain rate (s^{-1})**	**UCS (MPa)**	**E (GPa)**	**ν –**
UCS1	59.94	29.95	10^{-4}	237.30	130.40	0.17
UCS2	59.95	29.94	10^{-4}	144.70	113.12	0.13
UCS3	59.90	29.93	10^{-4}	185.87	122.41	0.18

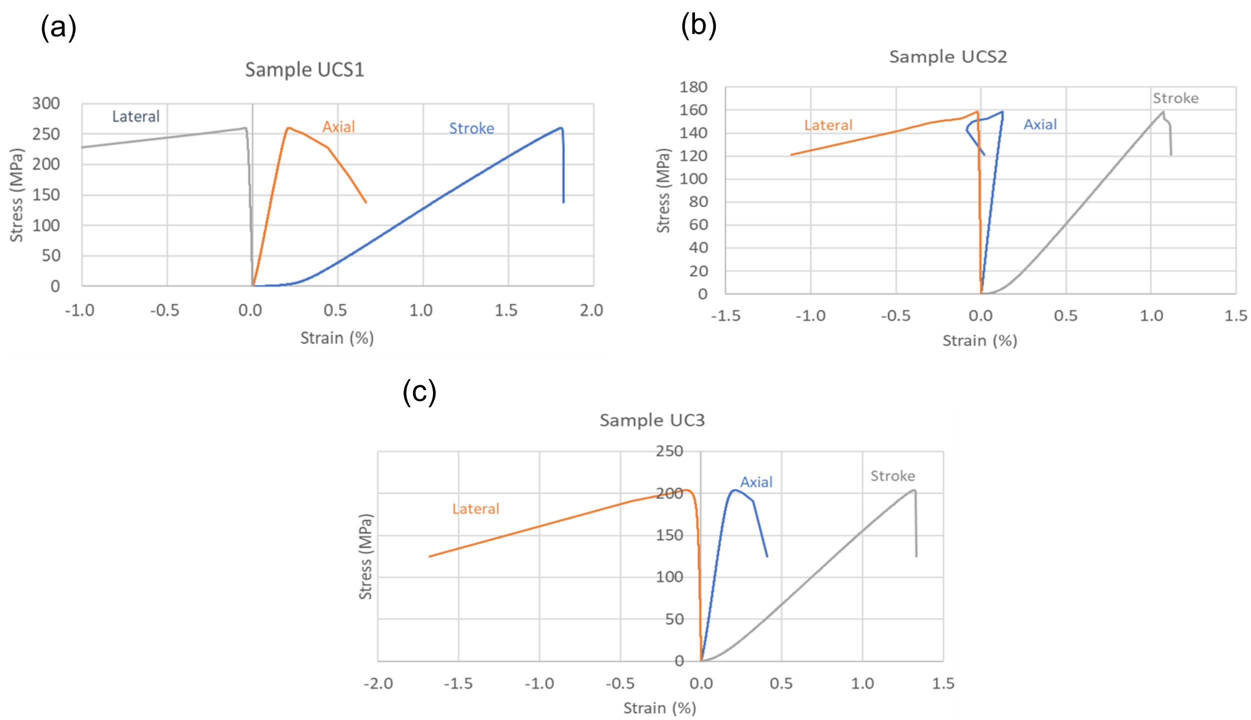

Fig. A.6 Stress vs strain curves for the uniaxial compression tests.

Appendix A5: Triaxial compression test

Three samples UCS4, UCS5 and UCS6 (Fig. A.5) were used in the triaxial tests. Table A.6 summarises the triaxial compression test results and Fig. A.7 shows the stress-strain relationships.

Table A.6 Summary of triaxial results.

Sample	Length (mm)	Diameter (mm)	Strain rate (s^{-1})	σ_3 (MPa)	σ_1 (MPa)	Residual strength (MPa)
UCS4	59.51	29.93	10^{-4}	5	201.10	66.10
UCS5	59.45	29.97	10^{-4}	10	290.40	75.40
UCS6	59.41	29.96	10^{-4}	15	318.40	90.80

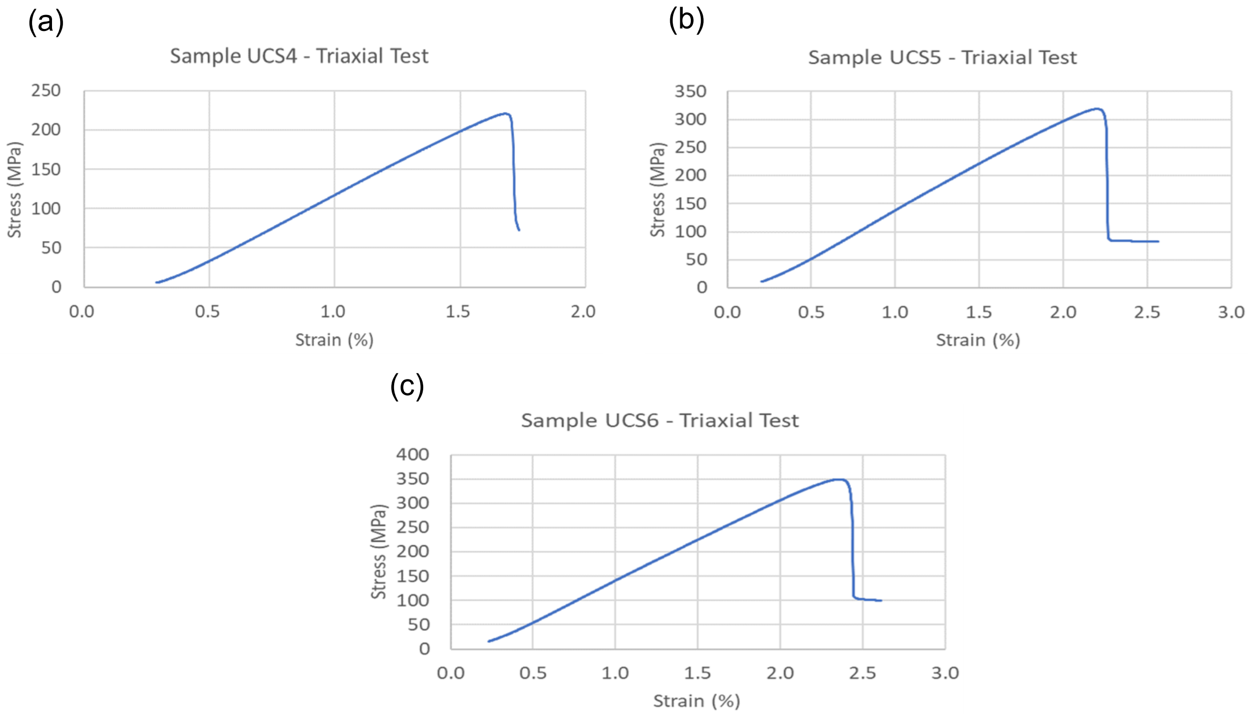

Fig. A.7 Stress vs strain curves for the triaxial compression tests.